FRICTION FACTOR MEASUREMENT, ANALYSIS, AND MODELING FOR FLAT-PLATES WITH 12.15 MM DIAMETER HOLE-PATTERN, TESTED WITH AIR AT DIFFERENT CLEARANCES, INLET PRESSURES, AND PRESSURE RATIOS

A Thesis

by

THANESH DEVA ASIRVATHAM

Submitted to the Office of Graduate Studies of
Texas A&M University
in partial fulfillment of the requirements for the degree of

MASTER OF SCIENCE

December 2010

Major Subject: Mechanical Engineering

FRICTION FACTOR MEASUREMENT, ANALYSIS, AND MODELING FOR FLAT-PLATES WITH 12.15 MM DIAMETER HOLE-PATTERN, TESTED WITH AIR AT DIFFERENT CLEARANCES, INLET PRESSURES, AND PRESSURE RATIOS

A Thesis

by

THANESH DEVA ASIRVATHAM

Submitted to the Office of Graduate Studies of
Texas A&M University
in partial fulfillment of the requirements for the degree of

MASTER OF SCIENCE

Approved by:

Co-Chairs of Committee	Dara Childs
	Gerald Morrison
Committee Member,	Paul Cizmas
Head of Department,	Dennis O'Neal

December 2010

Major Subject: Mechanical Engineering

ABSTRACT

Friction Factor Measurement, Analysis, and Modeling for Flat-Plates with 12.15 mm Diameter Hole-Pattern, Tested with Air at Different Clearances, Inlet Pressures, and Pressure Ratios. (December 2010)

Thanesh Deva Asirvatham, B.E., Government College of Technology, Coimbatore-India

Co-Chairs of Advisory Committee: Dr. Dara Childs
Dr. Gerald Morrison

Friction factor data are important for better prediction of leakage and rotordynamic coefficients of gas annular seals. A flat-plate test rig is used to determine friction factor of hole-pattern/honeycomb flat-plate surfaces representing annular seals. Three flat-plates, having a hole-pattern with hole diameter of 12.15 mm and hole depths of 0.9 mm, 1.9 mm, and 2.9 mm, are tested with air as the working medium. Air flow is produced between two surfaces, one having the hole-pattern roughness representing the hole-pattern seal and the other smooth, at the following three clearances of 0.254, 0.381, and 0.635 mm and three inlet pressures of 56, 70, and 84 bar with all possible pressure ratios at each configuration. The friction factor data are presented for all tested configurations, with description of the test rig and theory behind the calculations. The effect of hole diameter, hole depth, clearance, Reynolds number, and inlet pressure are analyzed, and friction factor models based on these parameters are calculated. Friction factor upset (an undesirable phenomenon making the test data non repeatable) is also explained.

Dynamic pressure data are presented, measured from dynamic pressure probes located at both the hole-pattern plate and the smooth plates at different locations.

DEDICATION

I dedicate this work to my parents, Mr. Deva Asirvatham Thangasamy and Mrs. Tamilarasi Deva Asirvatham, and to my uncle and aunt, Mr. David Manoharan Thangasamy and Mrs. Selvi David Manoharan, for their love and sacrifice.

ACKNOWLEDGMENTS

I express my sincere thanks to Dr. Dara Childs for giving me the opportunity to work under him at the Turbo lab and for his timely guidance. I thank Mr. Stephen Philips for his suggestions at every stage of the project. I thank Dr. Gerald Morrison and Dr. Paul Cizmas for giving their input. I would also like to thank my friends at Turbo Lab, Chris Kulhanek, Michael Vannarsdall and Philip Brown, for their help in setting up the test rig.

TABLE OF CONTENTS

Page

Page

LIST OF FIGURES

Page

Page

Page

Page

Page

LIST OF TABLES

Page

Page

NOMENCLATURE

Roman

A	Cross sectional area [L^2]
A_s	Surface area [L^2]
C, c	Direct and cross-coupled damping coefficients introduced in Eq. (1) [FT/L]
C_{eff}	Effective damping coefficient introduced in Eq. (5) [FT/L]
C_0	Speed of sound [L/T]
C_r	Radial clearance [L]
C_{pl}	Clearance between the plates [L]
dx	Differential length of control volume [L]
D	Direct impedance introduced in Eq. (2) [F/L]
D_h	Hydraulic diameter [L]
E	Cross coupled impedance introduced in Eq. (2) [F/L]
e	Surface roughness height [L]
f_f	Combined friction factor (Fanning)
f_s, f_r	Friction factors for stator and rotor
f_{res}	Resonant frequency [T^{-1}]
F	Force [F]
H	Local clearance [L]
h_d	Hole depth [L]
h_φ	Hole diameter [L]

j $\sqrt{-1}$

K, k Direct and cross-coupled stiffness coefficients introduced in Eq. (1) [F/L]

K_{eff} Effective stiffness coefficient introduced in Eq. (4) [F/L]

L Duct length [L]

M Mach number

$\dot{m}$ Mass flow rate [M/T]

n, m Blasius coefficients introduced in Eq. (24)

P Pressure [F/L^2]

P_c Critical pressure of air [F/L^2]

$P_{flow\_in}, P_{flow\_out}$ Pressures measured at inlet and exit of the flow meter [N/m^2]

P_{in} Inlet pressure [F/L^2]

R Air gas constant [FL/MT]

Re Reynolds number introduced in Eq. (13)

T Static temperature [K]

T_{inlet}, T_{exit} Inlet and exit temperatures at the plates [K]

T_{flow} Flow meter temperature [K]

T_t Stagnation temperature [K]

U Bulk flow circumferential velocity [L/T]

U_m Axial mean velocity relative to the surface [L/T]

V Narrow channel axial velocity introduced in Eq. (14) [L/T]

W Bulk flow axial velocity [L/T]

W_{pl} Plate width or channel width [L]

X Horizontal coordinate [L]

Y Vertical coordinate [L]

Z Seal axial coordinate [L]

ΔP Pressure difference across the plates [F/L^2]

Δx, Δy Components of the relative displacement vector between stator and rotor [L]

Greek

μ Absolute viscosity of air [M/LT]

γ Ratio of specific heats

γ_A Area ratio

ω Rotor rotational frequency [T-1]

ρ Air density [M/L^3]

τ_f Shear stress due to wall friction [F/L^2]

1. INTRODUCTION

1.1. Introduction to annular seals

In industrial high pressure turbo machineries such as turbines and compressors, sealing around the rotor plays an important role to avoid leakage of the working fluid or the lubricant either between the stages of a machine or from the machine to the surrounding. Effective sealing is necessary for efficient operation. Various types of rotary seals exist, like lip seals, alternative elastomer and plastic seals, mechanical seals, annular seals, magnetic fluid seals etc. Each kind of seal has its own advantages and drawbacks with respect to their effective sealing, cost and their possible impact on rotor vibrations, etc.

Annular seals are non-contacting type of seals. Annular seals are cheaper in general, and they don't create any wear to the rotor. But, this type of seals cannot completely arrest the leakage. So, they are effectively utilized in appropriate places where complete sealing may not be necessary.

The clearance between an annular seal and rotor is typically larger than that of a bearing, and normally has a clearance-to-radius ratio on the order of 0.003. Figure 1 shows the locations of annular seals in a compressor.

This thesis follows the style of Journal of Tribology.

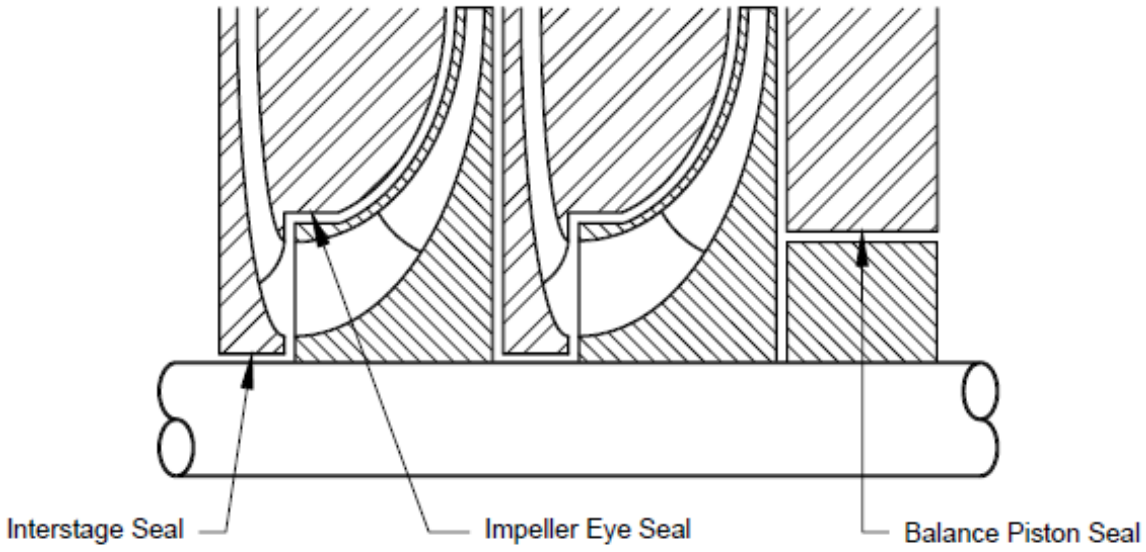

Figure 1. Locations of annular seals in a compressor [1]

Labyrinth annular seals are extensively used because of their low cost. They restrict leakage by providing a tortuous fluid flow path. In spite of their cost effective nature, some improvements were sought, as labyrinth seals are detrimental in causing rotordynamic instabilities. A honeycomb seal which has honeycomb hole-pattern was considered to be an effective alternate for Labyrinth seals both in terms of controlling leakage and reducing rotor vibration. The honeycomb seal was originally introduced in the 1960's as a replacement for aluminum labyrinth seals, which were being consumed by process fluids. This type of seal was able to provide stability to otherwise unstable systems. For example, Childs and Moyer [2] discussed using honeycomb seals to eliminate synchronous and sub-synchronous instabilities experienced by the high-pressure oxygen turbo-pump on the Space Shuttle main engine. Also, Zeidan, Perez, and

Stephenson [3] replaced labyrinth seals in two gas compressors with honeycomb seals, and were able to eliminate the previously experienced rotordynamic instabilities. A third example is by Armstrong and Perricone [4], who replaced labyrinth seals with honeycomb seals in a steam turbine to reduce sub-synchronous whirling. Figure 2 shows the setup of a honeycomb seal around a smooth rotor.

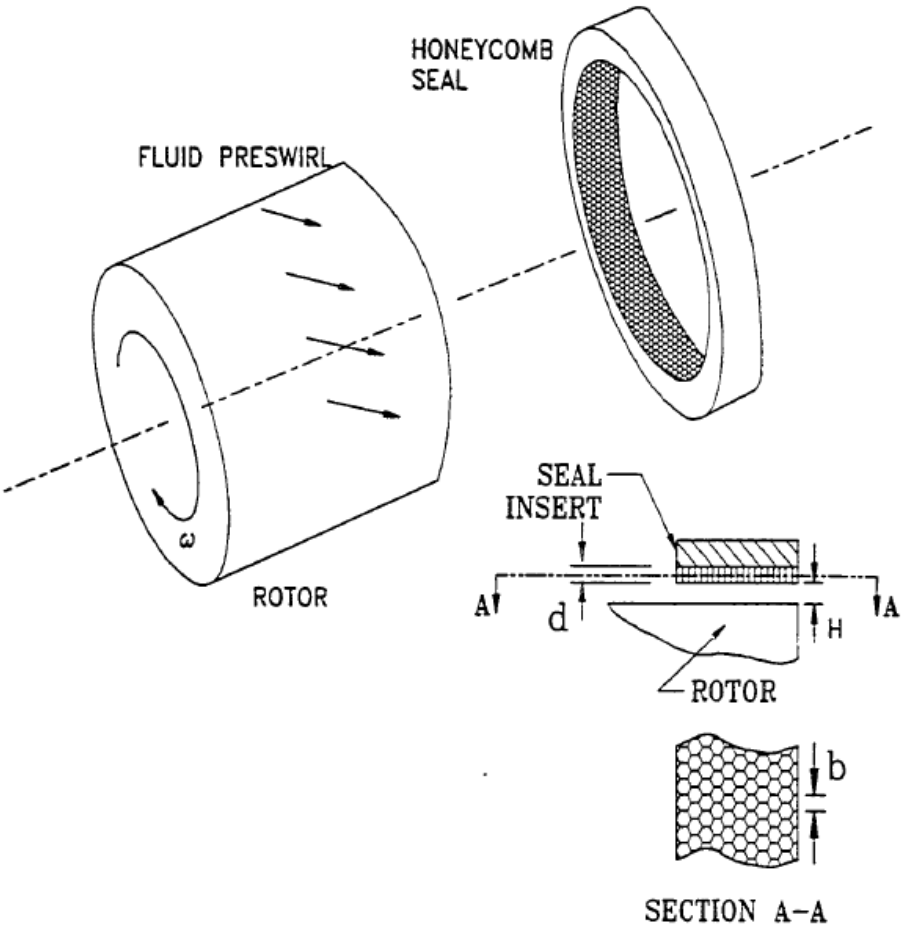

Figure 2. A honeycomb seal around a smooth rotor [5]

1.2. Hole-pattern annular seals

Hole-pattern (HP) annular seals are similar to honeycomb seals, the difference being HP seals have circular holes instead of hexagonal holes. Figure 3 shows an annular seal with circular HP. Childs and Yu [6] first reported test results for HP seals and compared them to those of honeycomb seals.

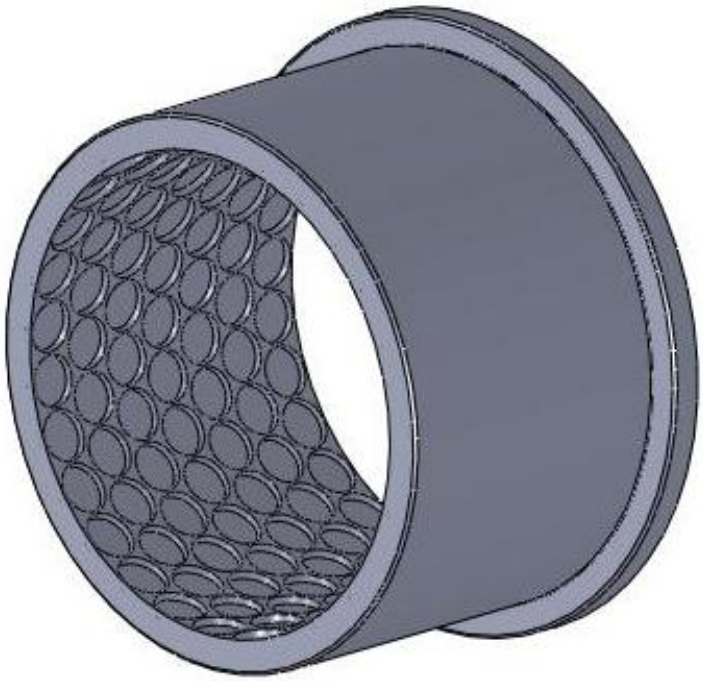

Figure 3. An annular seal with a large diameter circular HP

HP seals are used in place of a honeycomb seal because they are cheaper. Holes in a circumferential area as found in an HP seal can be easily drilled via a CNC machine

tool. Also, this nature of easy machinability enables HP seals to be made of softer materials like aluminium which create less wear to the rotor in case of a contact, unlike a honeycomb seal which is usually made of hard materials making the rotor vulnerable for wear. These advantages make the HP seals preferable over honeycomb seals.

1.3. Rotordynamic analysis of annular seals

Seal rotordynamic coefficients and leakage need to be calculated in operating conditions. Lomakin [7] first demonstrated that liquid annular seals have a direct stiffness which can increase critical speeds.

For a labyrinth seal, for small motions of the rotor about a centered position, the rotor-to-seal interaction force is described by

$$-\begin{Bmatrix} F_X \\ F_Y \end{Bmatrix} = \begin{bmatrix} K & k \\ -k & K \end{bmatrix} \begin{Bmatrix} X \\ Y \end{Bmatrix} + \begin{bmatrix} C & c \\ -c & C \end{bmatrix} \begin{Bmatrix} \dot{X} \\ \dot{Y} \end{Bmatrix} \tag{1}$$

where X and Y are the displacements of the rotor relative to the seal, and F_x and F_y are the components of the reaction forces acting on the rotor in the X and Y directions, respectively. K is the direct stiffness, k is the cross-coupled stiffness, C is the direct damping and c is the cross-coupled damping. K, k, C, and c are referred to as the rotordynamic coefficients [8]. The direct stiffness represents a centering force opposed to the rotor's displacement, a behavior known as the "Lomakin" effect. The cross-coupled stiffness creates a tangential force that can destabilize the rotor. The bulk-flow theory is the most widely used method to evaluate the rotordynamic coefficients of annular seals. Originally developed by Hirs [9], this theory uses averaged pressure, averaged flow velocity across the clearance and an empirical friction factor data

correlation to help determine the coefficients. Bulk-flow models require no definition of shear stress variation for the fluid within the clearance and only account for shear stress at boundaries of the model, and they also assume a homogeneous friction factor for both axial and circumferential flow.

A full analysis of gas annular seal was first presented by Nelson [10]. Nelson's governing equations are applied to a single-control-volume and are (a) a continuity equation, (b) an axial momentum equation, (c) a circumferential momentum equation, (d) an energy equation, and (e) an equation of state for a perfect gas. Nelson's bulk flow, one-control-volume model gave reasonable predictions for smooth-stator/smooth-rotor seals. However, for honeycomb stator/smooth rotor seals, the honeycomb surface was regarded as a 'rough surface', and the prediction was poor.

A two-control-volume method using the Bulk flow theory was then proposed by Ha and Childs [5] which includes an additional control volume adjacent to the main flow-control volume in the clearance, to simulate the honeycomb cell depth and allow the gas to enter and exit the honeycomb in the radial direction during perturbed rotor motion as shown in Figure 4. Figure 5 shows a two-control-volume model.

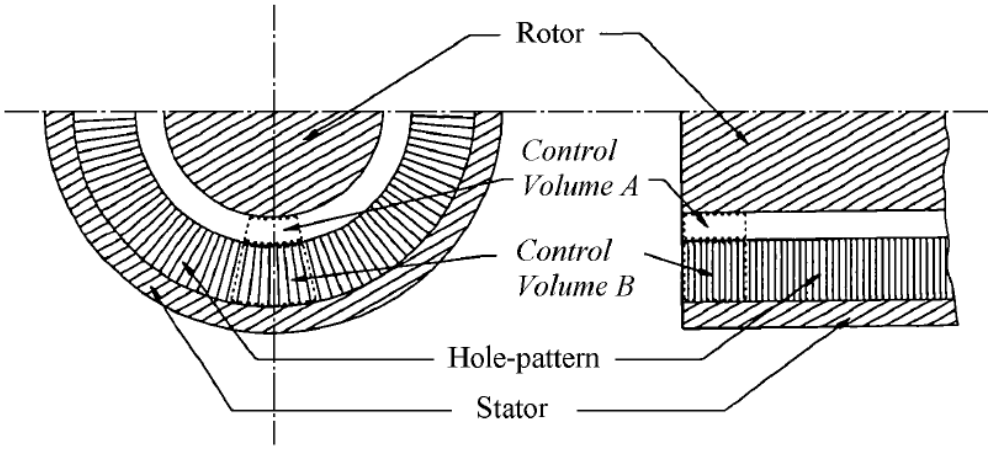

Figure 4. Two-control-volume method [5]

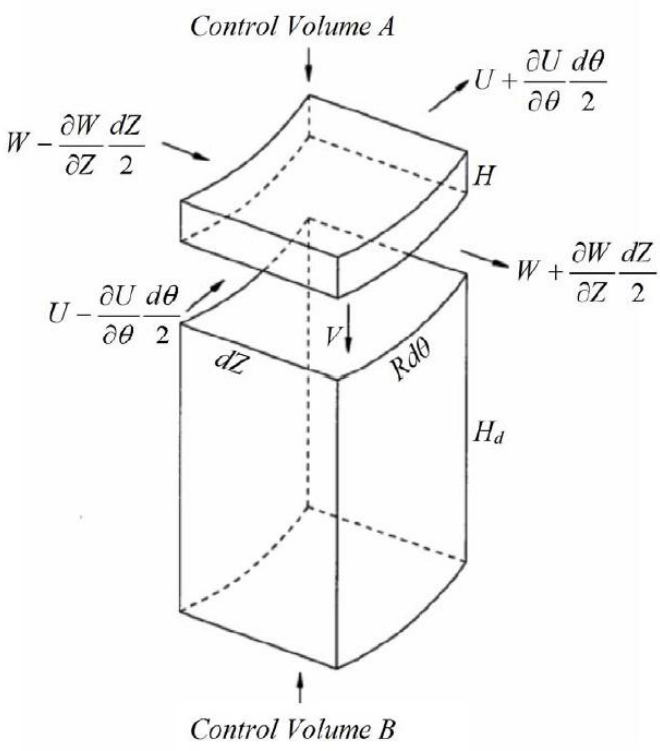

Figure 5. Two-control-volume model [5]

For the two-control-volume model, Ha and Childs developed the following governing equations. (a) Continuity equation for the two control volumes, (b) an axial momentum equation, (c) a circumferential momentum equation, and (d) an energy equation.

Numerical solution to the above model is presented in Kleynhans and Childs [11]. The two-control-volume analysis demonstrates that the frequency independent model of Eq. (1) is generally not valid for hole-pattern seals. The two-control-volume analysis yielded a general transfer function

$$-\begin{Bmatrix} F_X(i\Omega) \\ F_Y(i\Omega) \end{Bmatrix} = \begin{bmatrix} D((i\Omega) & E(i\Omega) \\ -E(i\Omega) & D(i\Omega) \end{bmatrix} \begin{Bmatrix} \Delta x(i\Omega) \\ \Delta y(i\Omega) \end{Bmatrix} \tag{2}$$

which requires the forms of D and E to be defined from curve fits of the radial and tangential impedance solutions. For a given processional frequency, the rotordynamic coefficients are obtained from the general transfer function by the following relationship

$$-\begin{Bmatrix} F_X(i\Omega) \\ F_Y(i\Omega) \end{Bmatrix} = \begin{bmatrix} K + jC\Omega & k + jc\Omega \\ -(k + jc\Omega) & K + jC\Omega \end{bmatrix} \begin{Bmatrix} \Delta x(i\Omega) \\ \Delta y(i\Omega) \end{Bmatrix} \tag{3}$$

The effective stiffness K_{eff} and effective damping C_{eff} are calculated as follows,

$$K_{eff} = K + c\,\Omega \tag{4}$$

$$C_{eff} = C - (K/\Omega) \tag{5}$$

Note: *the K, C, k, c, K_{eff} and C_{eff}* values in the above equations are frequency dependent.

A FORTRAN computer program (ISOTSEAL) incorporating the new analytical model for annular gas seals was developed by Kleynhans and Childs [10]. ISOTSEAL is used to predict the static and dynamic properties of annular gas seals. The two-control-volume model better predicts the rotordynamic coefficients of honeycomb and HP seals and has been verified by past and ongoing tests at the Turbomachinery Laboratory. The solution showed a very good match with test results by Childs and Wade [12].

1.4. Importance of friction factor in predicting seal leakage and rotordynamic coefficients

Shear stresses appearing in the governing equations of the two-control-volume method are generally defined as

$$\tau = f_f(\frac{1}{2}\rho\ U_m^2) \tag{6}$$

Here τ is the wall shear stress, f_f is the friction factor of the surface upon which the shear stress is acting and U_m is the mean velocity relative to the surface and ρ is the density of the fluid.

Specific shear stress are defined as

$$\tau_{sz} = \frac{1}{2}\rho\ W\ U_s\ f_s \tag{7}$$

$$\tau_{rz} = \frac{1}{2}\rho\ W\ U_r\ f_r \tag{8}$$

$$\tau_{s\theta} = \frac{1}{2}\rho\ U\ U_s\ f_s \tag{9}$$

$$\tau_{r\theta} = \frac{1}{2}\rho\,(U - R\omega)\,U_r\,f_r \tag{10}$$

where

$$Us = \sqrt{W^2 + U^2} \tag{11}$$

$$U_r = \sqrt{W^2 + (U - R\omega)^2} \tag{12}$$

The suffixes *r, s* in Eqs. (7) to (12) represent rotor and stator respectively and *z* and θ represent seal axial and circumferential directions respectively.

In determining the numerical solution from the governing equations, a perturbation of the variables pressure *P*, local clearance *H*, axial velocity *W* and circumferential velocity *U* is employed. The resulting equations are separated into zeroth and first order equations. The leakage of the seal is predicted using the zeroth order equations for which the friction factor is needed as an input. The first order equations are solved to find the dynamic coefficients and they need partial derivatives of the friction factor with respect to the perturbation variables as inputs to define shear stresses at the boundaries, $\frac{\partial f}{\partial P}, \frac{\partial f}{\partial H}, \frac{\partial f}{\partial W}, \frac{\partial f}{\partial U}$. So, friction factor values must be established for leakage determination and the partial derivatives for better prediction of dynamic coefficients. To establish these derivatives and friction factor values, friction factor needs to be modeled through experimental data.

1.5. Past work done related to experimental friction factor calculation

Lewis F. Moody developed the widely used Moody diagram for commercial circular pipes [13]. The Moody diagram has been used to predict friction factors at

certain flow conditions. Moody proposed the friction factor as a function of Reynolds number and surface roughness. For increasing Reynolds number, as per Moody diagram, the friction factor decreases asymptotically in the turbulent regime. But, the Moody diagram does not predict the friction factor in case of flow between closely spaced surfaces. There exists little information on friction factor data for closely spaced parallel plates (i.e. channel flow). Ha [14] presented friction factor data using a flat-plate tester with air as the working fluid. Ha tested air passing between honeycomb surfaces at different clearances and inlet pressures. Figure 6 shows the honeycomb pattern used in Ha's study. In general, Ha's results show that the honeycomb surfaces yield larger friction factor values than smooth surfaces. In most of the test cases, the friction factor remains nearly constant or decreases slightly with increasing Reynolds numbers as in the case of the Moody diagram. In about 34% of the test cases, Ha observed a friction-factor jump phenomenon when testing opposed honeycomb surfaces. The friction-factor jump is a significant increase in the friction factor over small changes in the Reynolds numbers. When the friction-factor jump was present, Ha detected high pressure oscillations that were believed to be the result of a normal mode resonance [14] accompanied by harmonics of the Helmholtz frequency. In the non-friction-factor jump cases, Ha detected two dominant frequencies: normal mode resonance and feedback mode resonance. He concluded that the absence of harmonics in the Helmholtz frequencies is a characteristic of the non-friction-factor jump cases. Friction-factor jump phenomenon can create rotordynamic instabilities. Seals are expected to produce a positive direct stiffness through Lomakin effect given that the friction factor decreases

with increasing Reynolds number. If the friction factor increases with increasing Reynolds number or clearance or inlet pressure, the seal can produce a negative stiffness. ISOTSEAL predicts that a negative stiffness can be produced for the friction-factor jump cases.

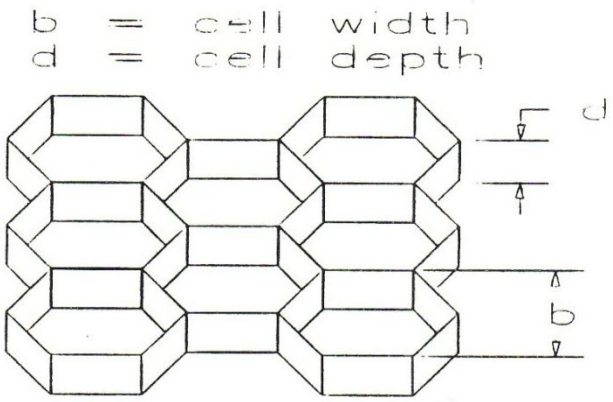

Figure 6. Honeycomb cell pattern used in Ha's investigation [14]

Thomas [15] used a different flat-plate tester for tests with water, investigating, smooth-on smooth, smooth-on-knurl (small and large knurls), and smooth-on-hole configurations. Figure 7 shows the patterns used in Thomas' investigation. Thomas observed that the friction factor decreases with increasing Reynolds numbers. He found that the smooth-on-hole configuration provides the lowest friction factor data. But, most studies show that the smooth-on-smooth configuration yields minimum friction factor. He also found that the friction factor increases with increasing clearance and also

observed that there exists a clearance, referred to as a plateau clearance, beyond which the friction factor does not increase.

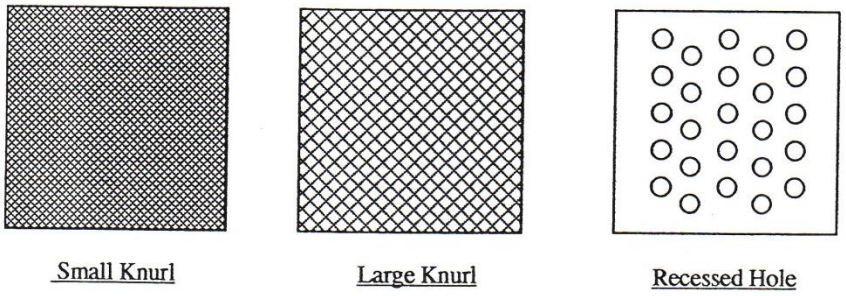

Figure 7. Patterns used in Thomas' investigation

Nava [16] used the same flat-plate tester to further investigate Thomas' results. She examined configurations such as small and large knurls and small and large recessed holes and tested them in combination with a smooth plate. Figure 8-Figure 9 show patterns used in Nava's investigations. She found that the small and large knurls had a plateau clearance of 0.508 mm, whereas the small and large recessed holes had a plateau clearance of 0.762 mm. Highest friction factor was observed with large knurl size, and the lowest friction factor was observed in smooth-on-smooth cases.

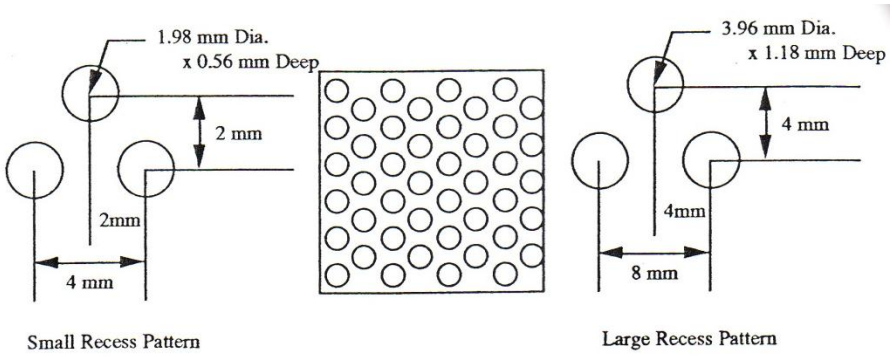

Figure 8. Recess patterns used in Nava's investigation

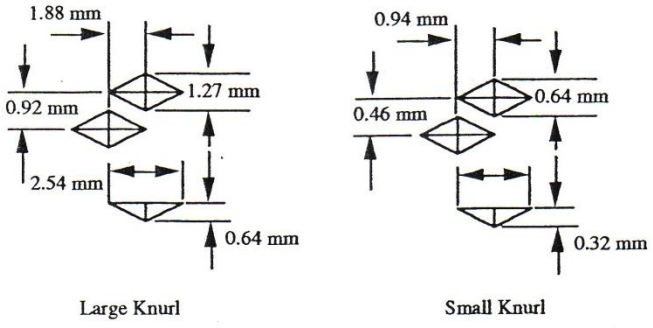

Figure 9. Knurl patterns used in Nava's investigation

Villasmil [17] used a commercial CFD code to simulate the results obtained by Nava. Although the trends in the experimental and numerical results were very similar, the numerical simulation overestimated friction factors. Moreover, the numerical simulations reproduced the plateau phenomena for the small knurl pattern only. For the large knurl and large recessed holes, for the larger clearances the curves lay almost on

top of each other leading to the belief that the plateau phenomena might occur. However, in a certain Reynolds number range, there is little dependence of the friction factor on the clearance in what Villasmil [18] referred to as the friction factor-to-clearance indifference behavior.

This increase in the friction factor with increasing clearance conflicts with Moody's friction factor diagram for pipe flow. From the Moody diagram, for a constant Reynolds number and a fixed roughness value, the friction factor decreases with increasing clearance which reduces the relative roughness. Results by Ha and Childs [14] for air flow between honeycomb surfaces show that the friction factor increases with increasing clearances. Similar results were obtained by DeOtte et al. [19] for water flow between closely spaced parallel plates. Fayolle and Childs [20] conducted tests for two identical liquid hole-pattern seals with different hole depths. Their results show an increase in the friction factor with increasing clearance and a major loss in the direct stiffness. Arghir et al. [21] numerically predicted friction factor for the same configuration as tested by Fayolle and Childs and concluded that friction factor increases with increasing clearance.

Kheireddin [22] tested HP seal configurations with holes of diameter 3.175 mm facing smooth plates in flat-plate test rig with air as the medium. Figure 10 shows typical plate used by Kheireddin. Plates with different hole depths were tested in different clearances (0.254, 0.381, and 0.635 mm) and inlet pressures (55, 70, and 84 bar). The test results showed that friction factor was increasing considerably with respect to increasing clearance, and friction-factor jump as faced by Ha was not observed in any of

the tests. Kheireddin also tested an HP plate facing an HP plate and observed the friction-factor jump phenomenon. Similar to Ha's observations, Kheireddin also observed presence of Helmholtz frequencies in the dynamic pressure of the tests with an HP plate facing an HP plate.

1.6. Objectives of this research

This study focuses on HP gas annular seals. Hole diameter could be an important parameter that affects the leakage characteristics of a HP seal. There are minimal friction factor test data available related to annular HP gas seals. To optimize dimensions such as hole diameter, hole depth, etc, which would produce better leakage control, more seals with different geometries need to be tested.

HP seals with larger diameter holes could have an advantage of not getting clogged easily over the operation and might be cheaper to manufacture. This project will test flat-plates having HP of hole diameter 12.15 mm. Three flat-plates will be tested having the same hole diameter but different depths of 0.9, 1.9, and 2.9 mm. Each plate will be tested at three clearances of 0.254, 0.38, and 0.635 mm (these values actually represent 10, 15, and 25 mils respectively) and three inlet pressures of 56, 70, and 84 bar (representing gauge pressures of 800, 1000, and 1200 psi respectively). These nine combinations of clearance and inlet pressure will give a range of friction factor. The following objectives are considered.

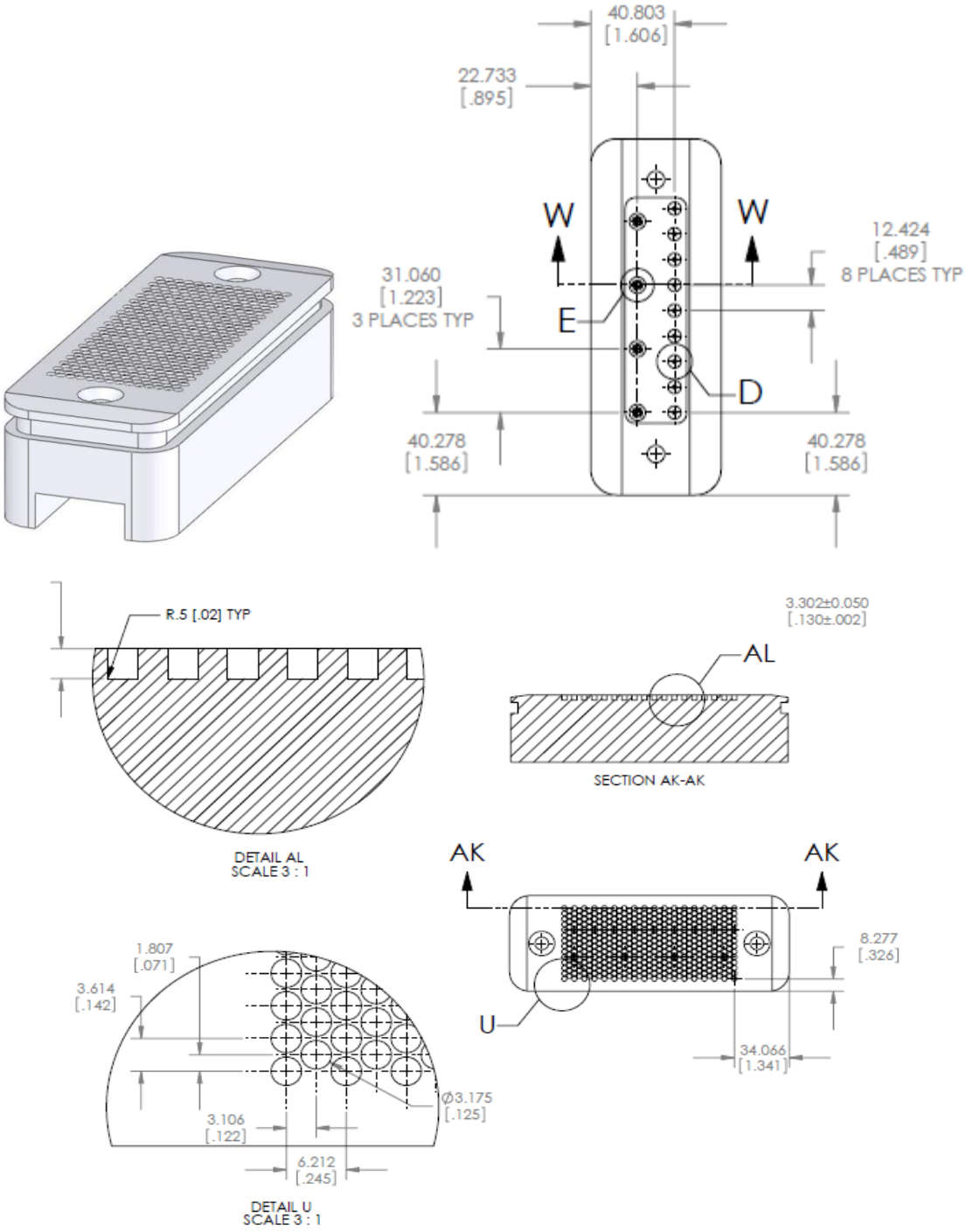

Figure 10. Detailed view of a 3.175 mm diameter hole-pattern plate [22]

(All dimensions are in mm)

1.6.1. Friction factor data

Friction factors will be calculated from test data at all tested configurations. At each clearance and inlet pressure combination, friction factor data will be produced for all possible Reynolds numbers.

1.6.2. Effect of various parameters on friction factor

The effect of hole diameter will be studied by comparing these data with Kheireddin's data for plates with holes of diameter 3.175 mm. The effect of hole depth among the three tested plated will be studied. Effect of other parameters such as clearance, Reynolds number, and inlet pressure will also be studied.

1.6.3. Friction-factor jump and dynamic pressure data

The dynamic pressure data will be studied to look for the presence or absence of Helmholtz frequencies or normal mode frequencies or feedback-mode frequencies as observed by Ha, to extend his explanations for the presence or absence of friction-factor jump.

1.6.4. Friction factor modeling

Empirical parameters for Blasius friction factor model will be estimated from the data, and an attempt will be made to model a custom friction factor model.

This document, also explains 'Friction-factor upset' phenomenon that was faced during the tests, making the measurements non-repeatable and how it was eliminated to assure test-data integrity.

2. CONCEPT AND THEORY OF FLAT-PLATE TESTING

2.1. Flat-plate testing concept

Flat-plate testing has long been used to experimentally determine friction factors. The test configuration uses an HP roughened plate that represents the seal surface facing a smooth plate that represents the rotor surface. Air flow is produced between the plates through a clearance representing the seal radial clearance. The friction factor is measured in a fully developed flow region where the axial velocity U_m can be considered to be one dimensional, and the Reynolds number is,

$$\mathrm{Re} = \frac{\rho\,(2\mathrm{H})\,\mathrm{U_m}}{\mu} \tag{13}$$

The velocity gradient is calculated by measuring the pressure drop across the plate and the stagnation temperature of the flow. Then considering the flow as Fanno flow, f_f is evaluated across an axial segment of the plate.

ISOTSEAL also requires entrance loss coefficient and exit recovery factors for considering inlet and exit effects, as the flow is not fully developed in the entry and exit of the actual conditions. This flat-plate test facility is not intended to find these entrance and exit variations, as the inlet and exit in the actual condition and in the test rig are different. Instead, it finds f_f for the fully developed region. The two-control-volume model also requires different friction factors for stator and rotor surfaces. However, this test rig produces a combined (stator + rotor) friction factor for the two surfaces.

2.2. Theory of flow between narrow channels

The derivation of the f_f formula based on the Fanno line flow for compressible flow in rectangular channels is the subject of this section. The test section represents a rectangular channel that can be modeled by the control volume shown in Figure 11. The following derivation is obtained from Dr. G. Morrison's class notes [23] and John and Keith [24]. Substantial portion of the text of this section is taken from Kheireddin [22].

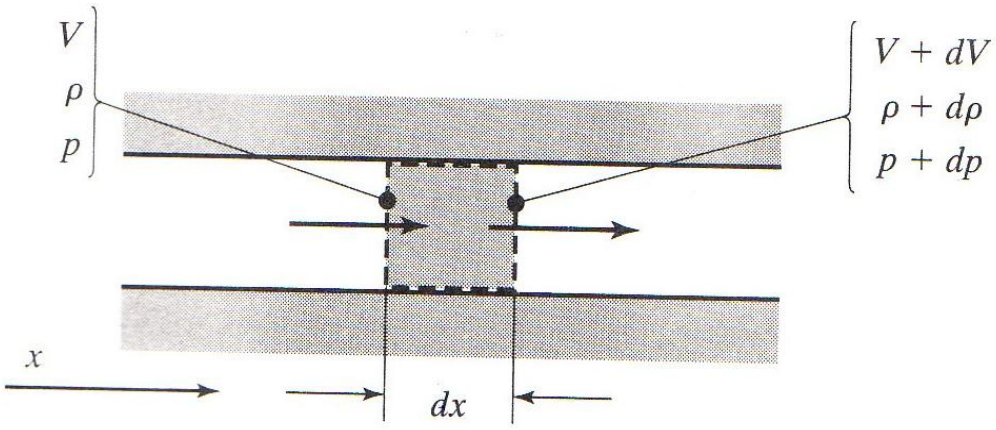

Figure 11. Control volume for adiabatic, constant area channel flow

One dimensional flow is assumed since the width-to-height ratio is large (i.e. $W_{pl}/C_{pl} >> 1$). To simplify the analysis of this section further, air is assumed to be an ideal gas with constant specific heats. The effects of area change as well as the body forces and work crossing the control surface can be neglected. The air flow is assumed to be steady and adiabatic. The aforementioned assumptions constitute what is called the

Fanno line flow. The momentum equation in the *x*-direction for the control volume shown in Figure 11 yields:

$$-\tau_f A_s - AdP = \rho AVdV \tag{14}$$

where τ_f is the shear stress due to wall friction, A_s is the surface over which the frictional forces act, A is the cross-sectional are of the rectangular channel, and V is the one dimensional axial velocity considered only in this section.

The hydraulic diameter is defined by:

$$D_h = 4\frac{Cross\_Sectional\_Area}{Wetted\_Perimeter} \tag{15}$$

For a rectangular channel,

$$D_h = 4\frac{W_{pl} * C_{pl}}{2(W_{pl} + C_{pl})} \tag{16}$$

where W_{pl} and C_{pl} are the width and height of the rectangular channel, respectively.

In this specific case, since the width is very large compared to the height of the channel, D_h reduces to:

$$D_h = 2C_{pl} \tag{17}$$

Defining the Fanning friction factor as:

$$f_f = \frac{\tau_f}{0.5\rho V^2} \tag{18}$$

And substituting the f_f definition into the momentum equation yields:

$$-dP-\frac{1}{2}\rho V^2 f_f \frac{dx}{D_h}=\rho V dV \tag{19}$$

The Mach number M is related to the velocity of the fluid by the following formula:

$$M=\frac{V}{\sqrt{\gamma RT}} \tag{20}$$

where γ is the ratio of specific heats and R is the gas constant for air.

The stagnation temperature and the static temperature are related by:

$$T_t=T(1+\frac{\gamma-1}{2}M^2) \tag{21}$$

This derivation aims to arrive at a relationship between the f_f, M and the Mach number gradient dM/dx. The following equation for the M is derived from conservation of mass, the ideal gas law, and the M and T_t definitions.

$$M=\left(\frac{-1+\sqrt{1+2(\gamma-1)(\frac{\dot{m}}{PA})^2(\frac{RT_t}{\gamma})}}{(\gamma-1)}\right)^{\frac{1}{2}} \tag{22}$$

where $\dot{m}$ is the mass flow rate through the test section.

In Eq. (22), $\dot{m}$, P, and T_t are measured quantities, whereas, R, γ and A are known quantities. Hence, the calculation of the M becomes fairly simple.

Using the equations above:

$$f_f = \frac{C_{pl}(1-M^2)}{\gamma M^3\left(1+\frac{\gamma-1}{2}M^2\right)}\frac{dM}{dx} \tag{23}$$

dM/dx is evaluated by curve fitting the Mach number along x and finding the local derivative of the curve. Therefore, with knowledge of M and the evaluation of dM/dx, f_f can be readily calculated.

3. DESCRIPTION OF THE TEST RIG

This test rig utilizes high-pressure air as the working fluid. Figure 12 below depicts a simplified schematic of the test facility flow. This section uses the description referred from Kheireddin [22].

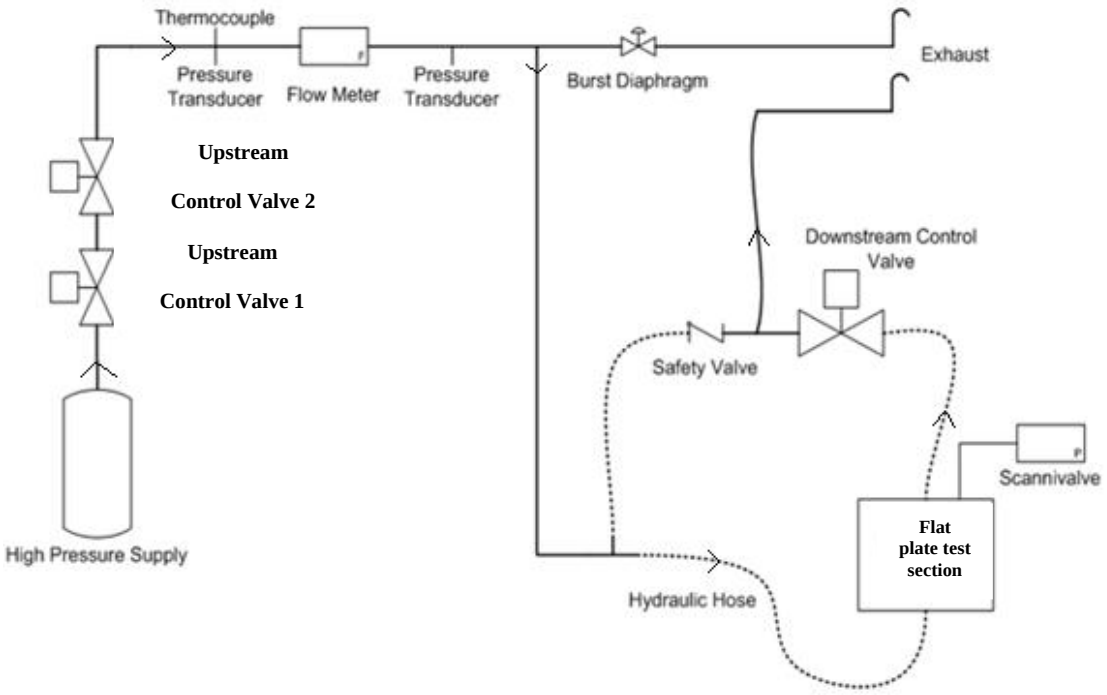

Figure 12. Flow loop in flat-plate test rig [22]

The test specimens consist of stainless steel plates that can easily be mounted on the backup plates through the use of screws. High-pressure air is stored in a tank at a

nearby facility. The flow loop is rated for 104 bar, and a safety valve is used to ensure that the pressure in the test section does not exceed this value. Two inlet control valves are used to allow passage of air into the system. The reason for using two inlet control valves is to adjust the pressure smoothly to get an upset free reading (Please refer the Appendix D for further explanation on this). Downstream of the test section is a backpressure valve that is used to control the exit pressure.

As illustrated in Figure 13 the flat-plate test section consists of backup plates, a boundary vessel, and the test specimens.

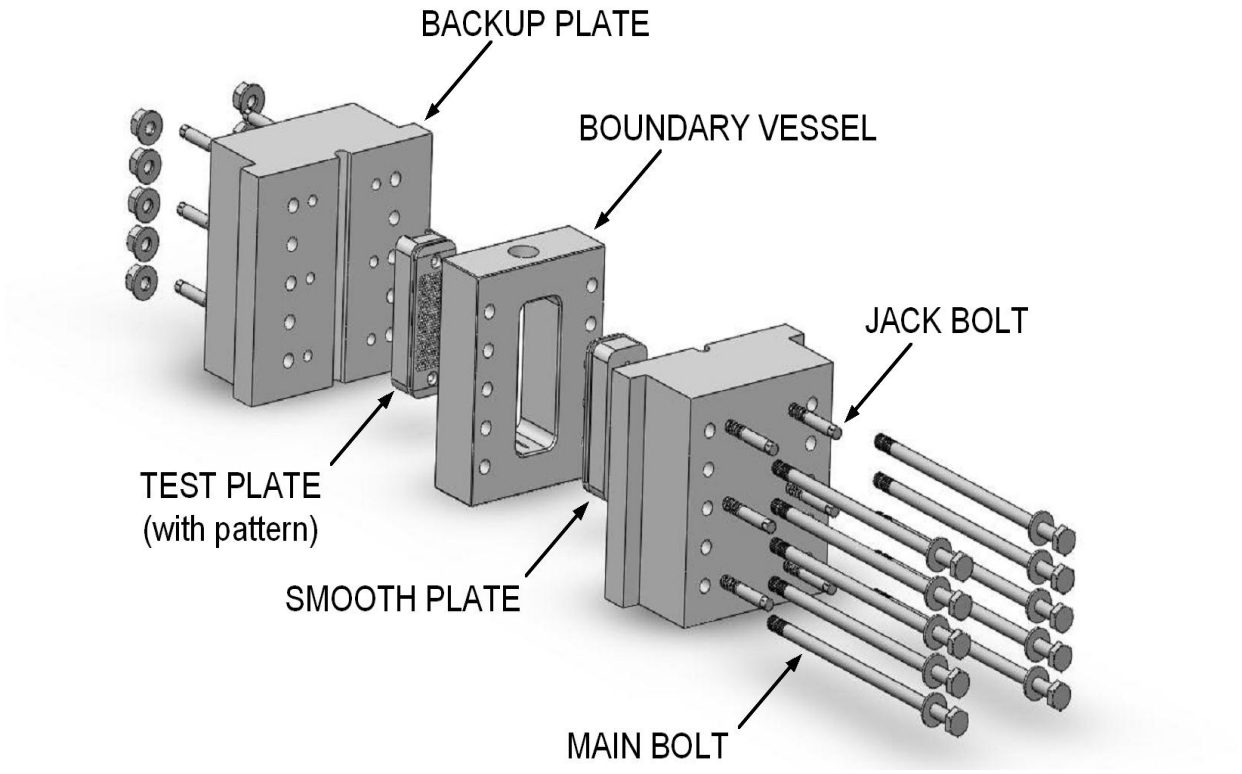

Figure 13. Detailed view of the flat-plate tester [22]

3.1. Description of the test plates

The test plates have two distinct surfaces: smooth and rough. The smooth plate is made from 410 annealed stainless steel with a very high yield strength to withstand stresses induced by the high-pressure air. Figure 14 shows a typical smooth plate. The dimensions of the plate are 4.45 cm x 6.35 cm x 15.24 cm. A groove runs around plate periphery and serves as a seat for a 352 O-ring and two backup rings to insure that air does not escape. The plate has two countersunk holes to allow its attachment to the backup plates.

The plate is instrumented with four subminiature dynamic pressure sensors located along its length. The dynamic pressure sensors are installed flush with the smooth surface. Miniature holes at the inlet and exit of the smooth plate serve as locations for temperature and pressure measurements. The HP plate has the same dimensions as the smooth plate and is made from the same material. For HP plates, circular flat-bottom holes with a specified hole depth (h_d) are drilled into the smooth surface as shown in Figure 15. HP plates are equipped with nine static pressure probes and four dynamic pressure sensors located along the length of the plate. The dynamic pressure sensors are mounted flush with the bottom of the holes.

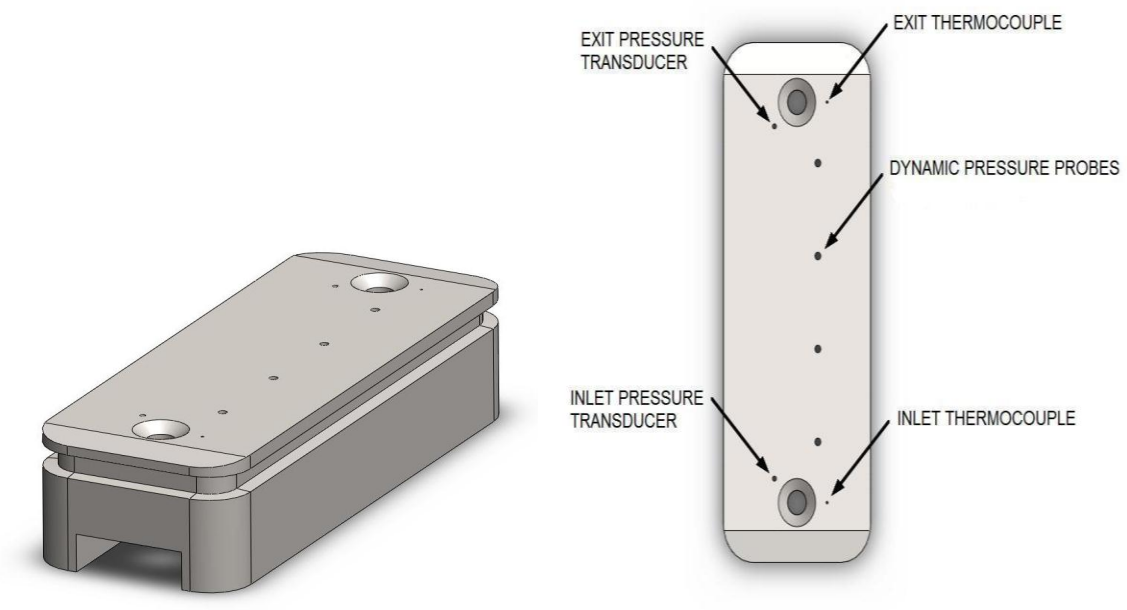

Figure 14. A typical smooth plate

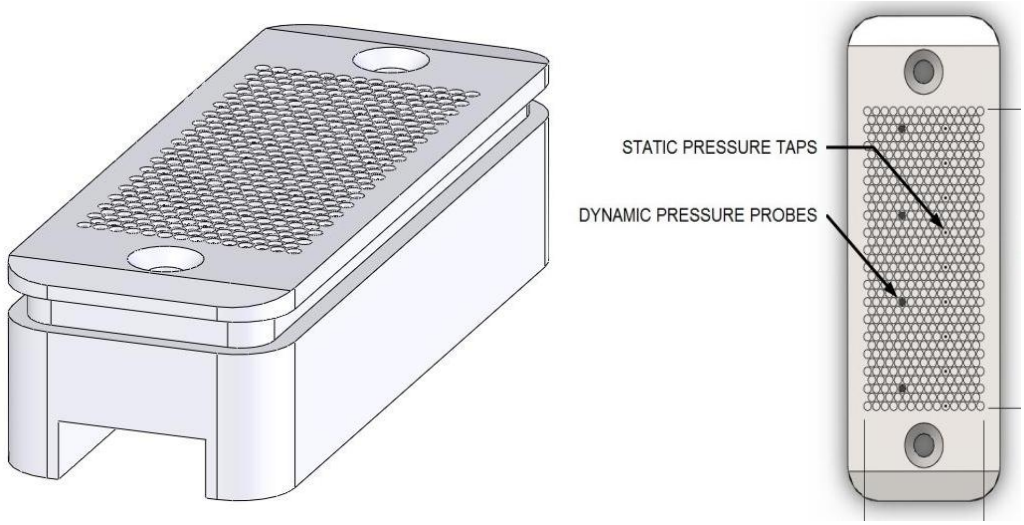

Figure 15. A typical HP plate

Figure 16 is a detailed drawing of one of the three tested plates. Gamma ratio γ_A is defined as the ratio of area occupied by holes in an HP seal to the total seal inner

surface area. For the plates tested, γ_A = 75.4 %. Plates tested by Kheireddin had γ_A = 68.1 %.

Figure 17 shows detailed drawing of the smooth plate. The dynamic-pressure probe locations in a smooth plate are the same as that of its rough plate such that the pressure probes oppose each other at each location after assembly.

3.2. Boundary vessel

The boundary vessel (Figure 18) is the center piece of the assembly. It has a doughnut shape and contains a rectangular window where the test plates are inserted from both sides and come together. At the inlet and exit of the boundary vessel, an aperture of rectangular shape allows air flow in and out of the test section. Ten holes on each side of the vessel allow it to be aligned and assembled with the cover plates with the use of 5/8 x 16 UNF carbon steel bolts.

3.3. Backup plates

The backup plates (Figure 19) consist of heavy blocks of 316 stainless steel. Ten outer holes on both sides of each cover plate are aligned with the holes in the boundary vessel. Six inner holes on each cover plate contain brass pins that are used to disassemble the test rig and to adjust C_{pl}. The entire assembly is pulled together by using 5/8 x 16 UNF carbon steel bolts. The test specimens are rigidly bolted onto the cover plates through the use of flat head screws.

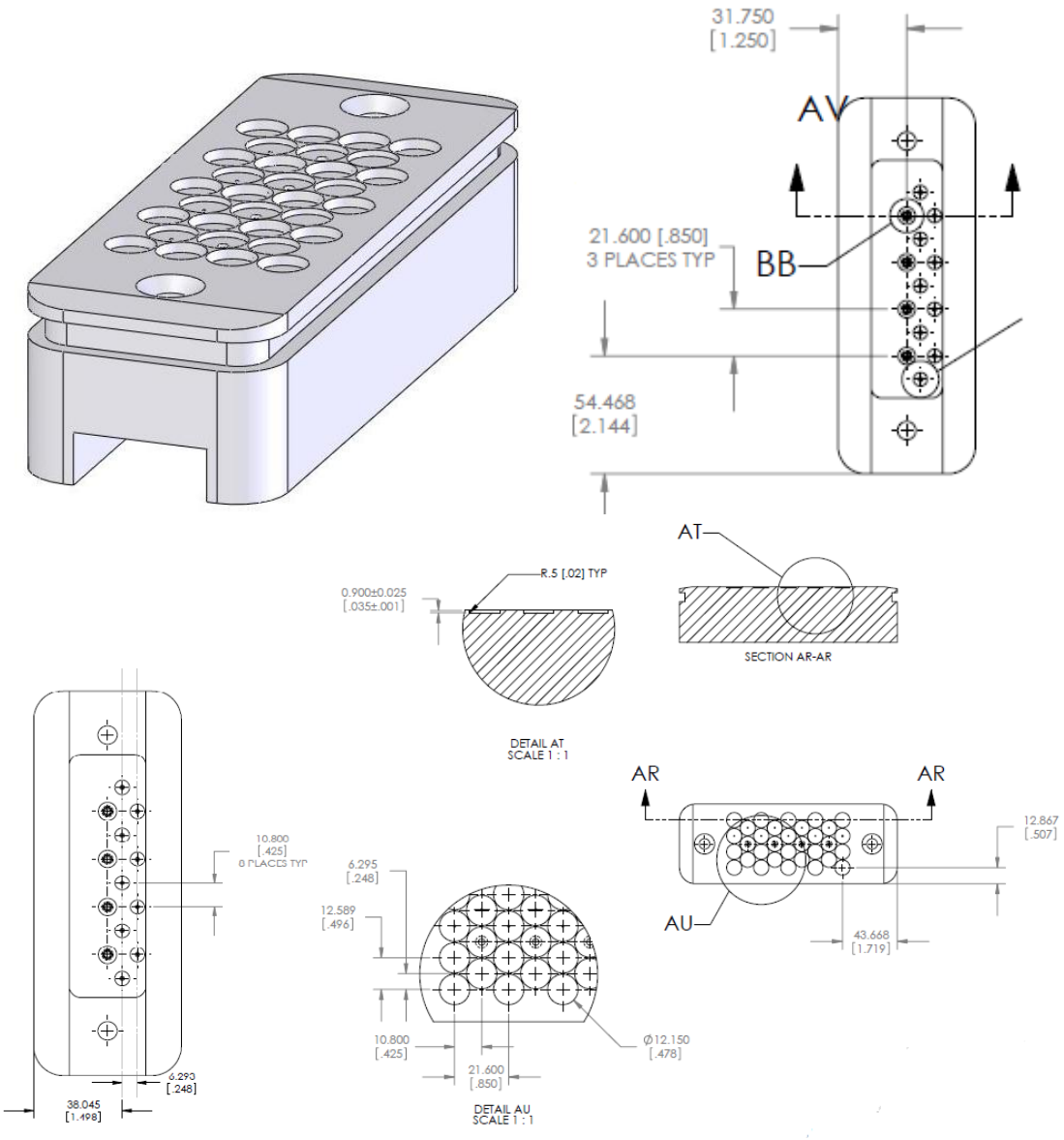

Figure 16. Detailed view of a 12.15 mm diameter HP plate

(All dimensions are in mm)

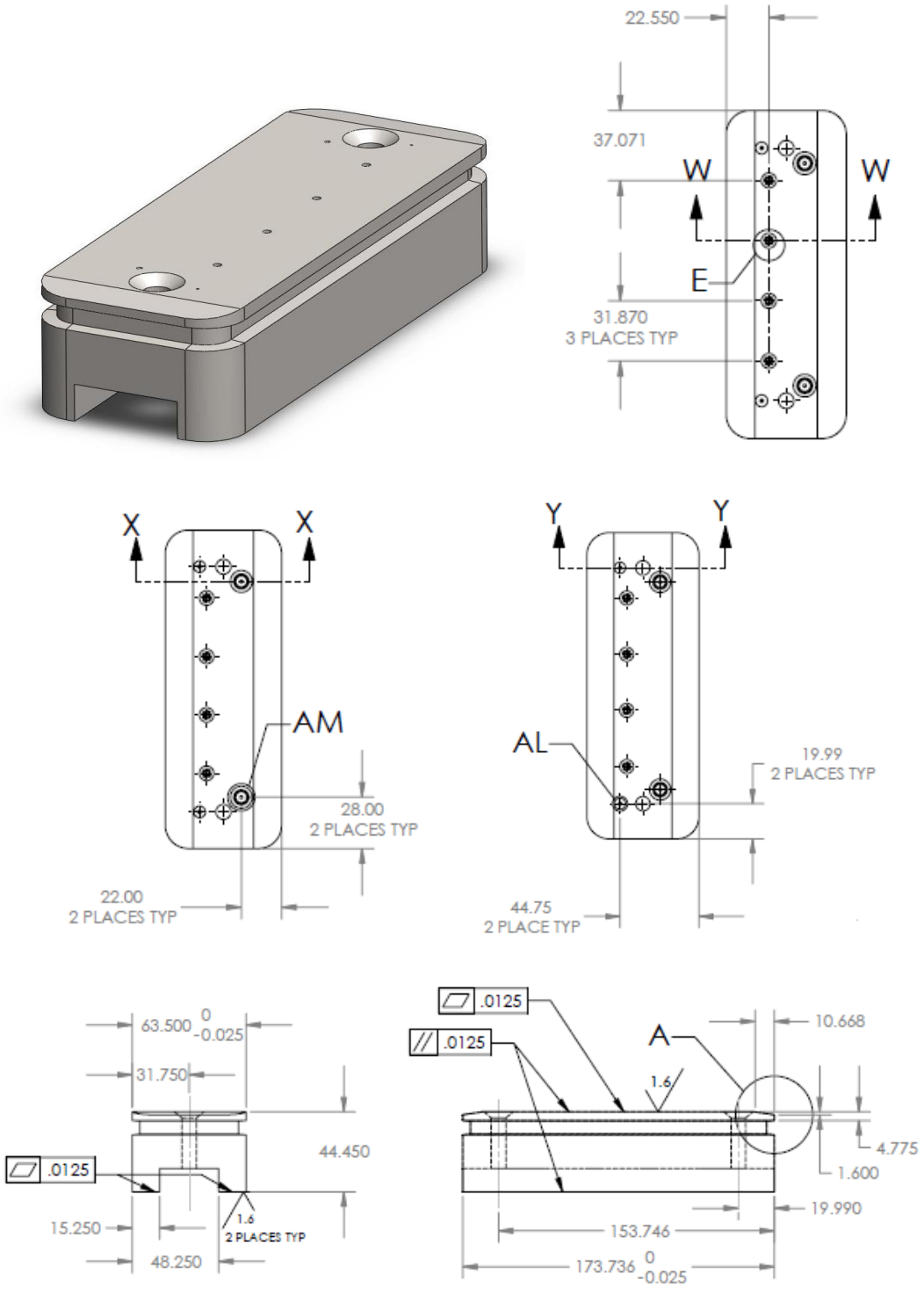

Figure 17. View of smooth plate to be used with 3.175 mm diameter HP plates

(All dimensions are in mm)

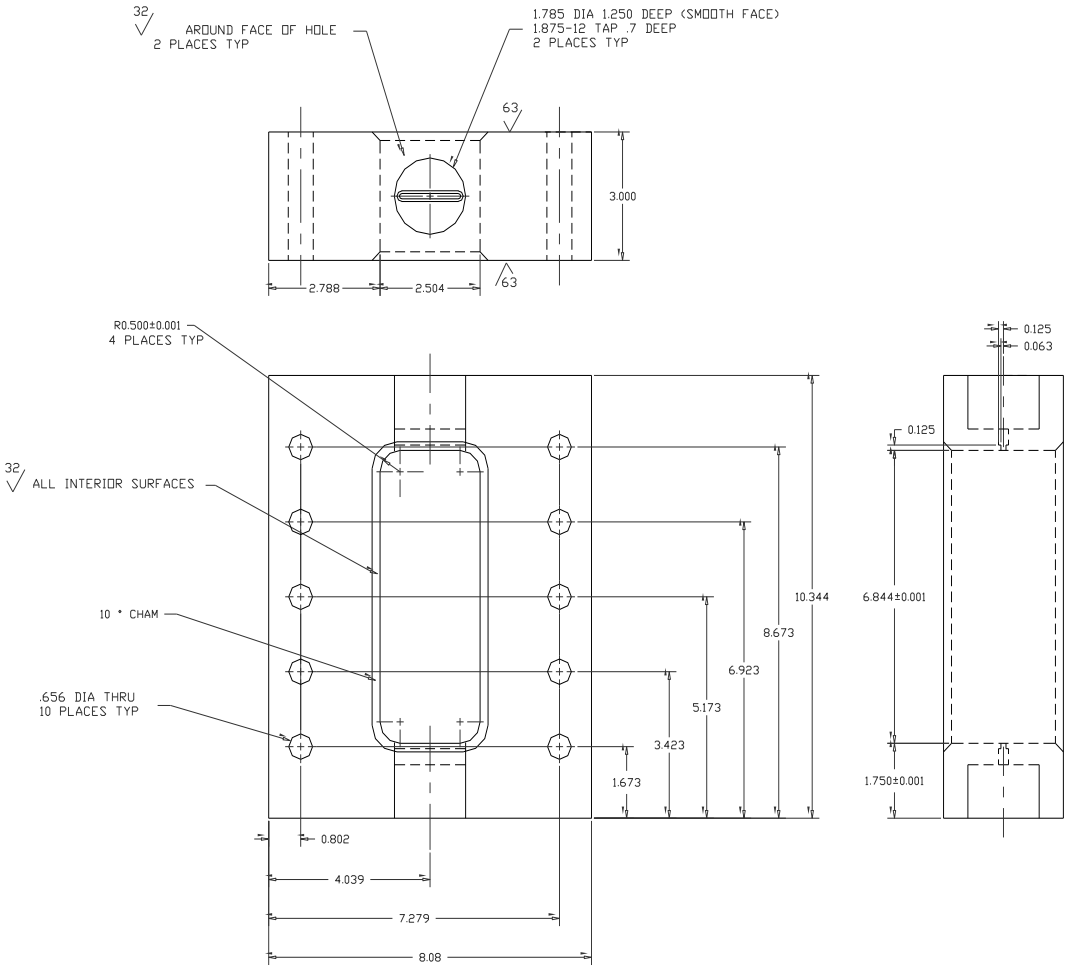

Figure 18. Detailed drawing of the boundary vessel [25]

(All dimensions are in inches)

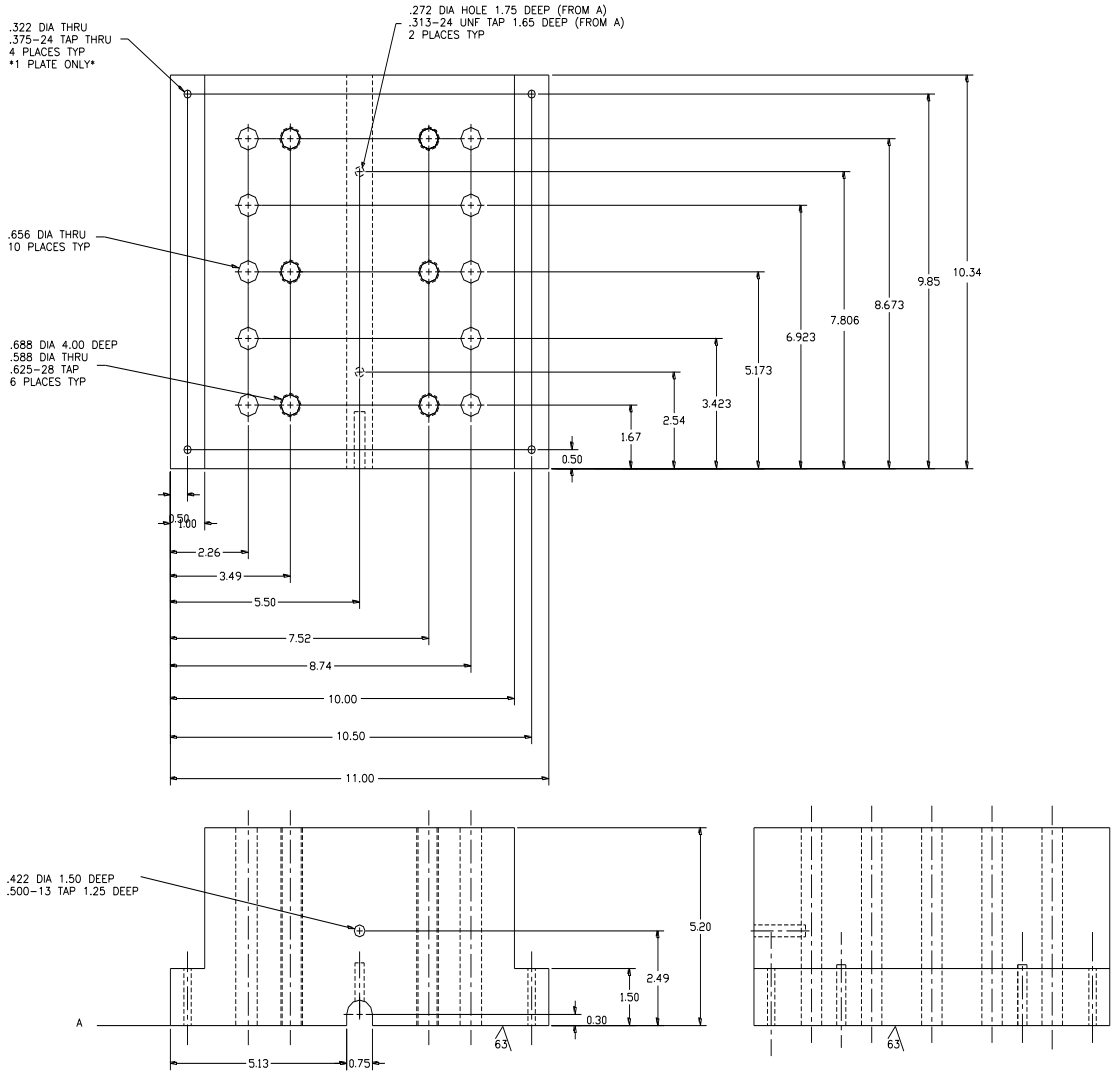

Figure 19. Detailed drawing of backup plates [25]

(All dimensions are in inches)

3.3.1. Clearance definition

Two stainless steel shims of known thicknesses are used to set the plate clearance C_{pl}. The shims are 0.635 cm x 15.24 cm in dimensions and are greased to adhere to the

plates. Clearance tests were conducted using the method of fuse wires. Three fuse wires of known thickness were placed along the length of the plate. After the plates come together, measurements are taken at six points along the length of the wire. The results indicate that the C_{pl} error percentage is within ± 3% for C_{pl} = 0.381 mm as shown in Figure 20 and ± 4% when extrapolated to C_{pl} = 0.254 mm.

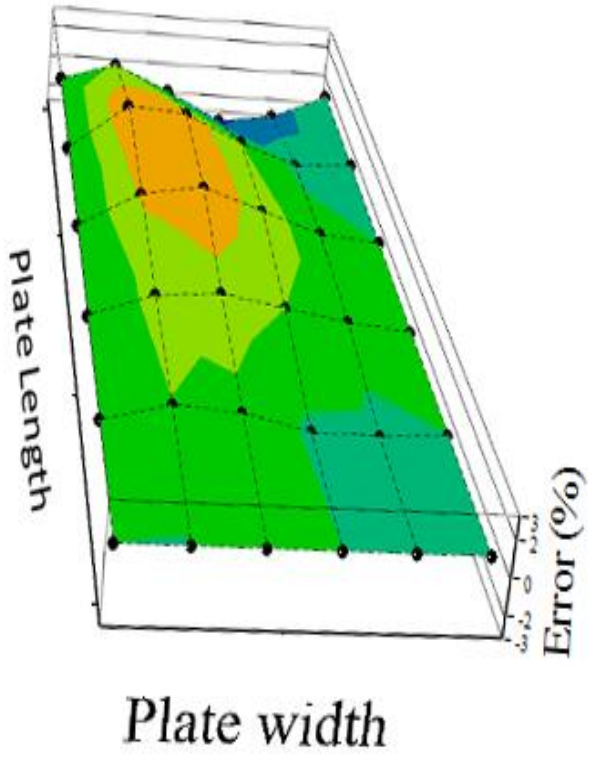

Figure 20. Error distribution for C_{pl} = 0.381 mm [22]

3.4. Instrumentation

Measurements of pressure, temperature, and flow rate are required to define f_f. The inlet control and backpressure valves are controlled via an electronic circuit that sends a 4-20 mA signal. Downstream of the inlet control valve is a Flow Technology® turbine flow meter. It has been calibrated at a pressure of 84 bar and a temperature of 295 °K. It is connected to a digital readout which displays readings in acfm (actual cubic foot per minute) and has an accuracy of ± 0.25% of the target value. Two Omega Engineering® pressure transducers are positioned upstream and downstream of the turbine meter. These pressure transducers are made out of stainless steel and are accurate to within ± 0.25% of the actual pressure. Two additional pressure transducers are located at the inlet and exit of the flat-plate tester. Prior to their use, the pressure transducers are calibrated in-situ with a dead weight tester. They are also connected to a digital readout that converts voltages to pressure readings. A type K thermocouple is located upstream of the flow meter, and two additional thermocouples are located at the inlet and exit of the smooth plate to measure the inlet and exit temperatures. They are accurate to within ± 1° K, and are connected to a digital readout that converts voltages to temperature readings. The pressure, temperature and flow rate digital displays are connected to a NI ®Data Acquisition Board, and a Labview program is used to collect the data. A 32-V power supply is used to power all the instruments.

The static pressure tubes connecting the probes along the test plate are made from stainless steel. The tubes are attached with extreme care to the back of the test plates via epoxy to insure that the tubes do not kink or bend. The epoxy is allowed to

cure for 24 hours before use. Stainless steel tubes and compression fittings are used to connect the static pressure probes to a Scanivalve®. This particular module has 16 ports that allow multiple-point measurements of the static pressures along the plate. It contains a RAM, 16 bit A/D converter and a microprocessor and communicates with a PC through an Ethernet TCP/IP Protocol. Also mounted on the back face of the plates are the dynamic pressure sensors; four of these sensors were mounted flush with the surface of the smooth plate and the remaining four were mounted flush with the bottom of the holes of the HP plate. The dynamic pressure sensors are connected to a Dynamic Data Acquisition Board through a BNC to SMB cables. This NI PCI 4472 DAQ board is also used to power these subminiature ICP pressure sensors. Figure 21 shows photograph of assembled smooth plate showing the air passage

Test plates are mounted on the cover plates and secured in position. The assembly process begins by inserting the plates into the rectangular window of the boundary vessel. Using a torque wrench, the bolts are tightened evenly back and forth until the plates come in contact and a constant tightening torque is maintained across all the bolts.

Figure 22 shows a photograph of HP plate before assembly. Figure 23 shows the photograph of both the plates assembled.

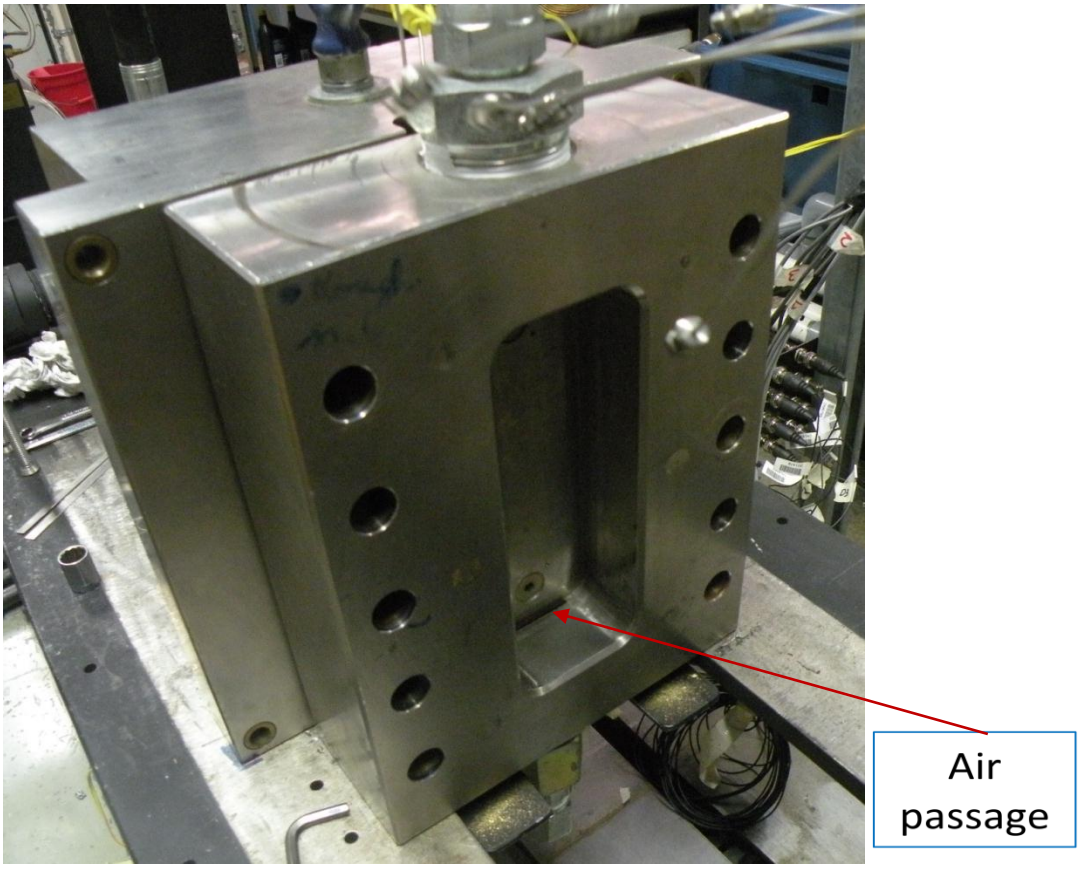

Figure 21. Photograph of assembled smooth plate showing the air passage

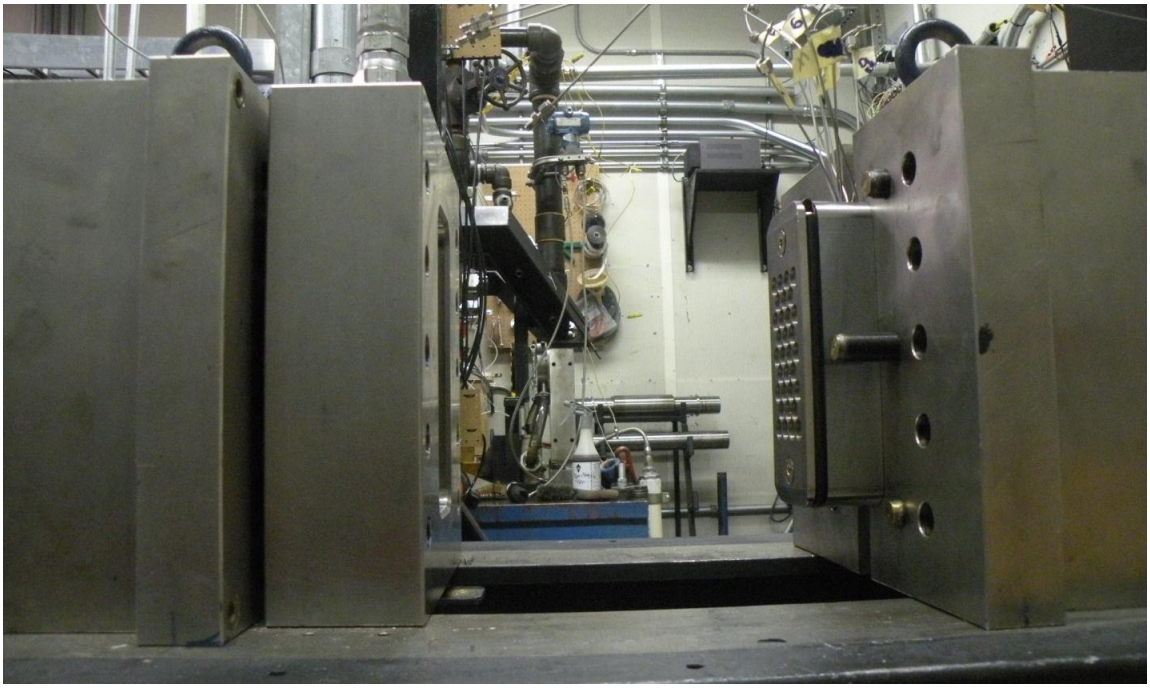

Figure 22. Photograph of HP plate before assembling

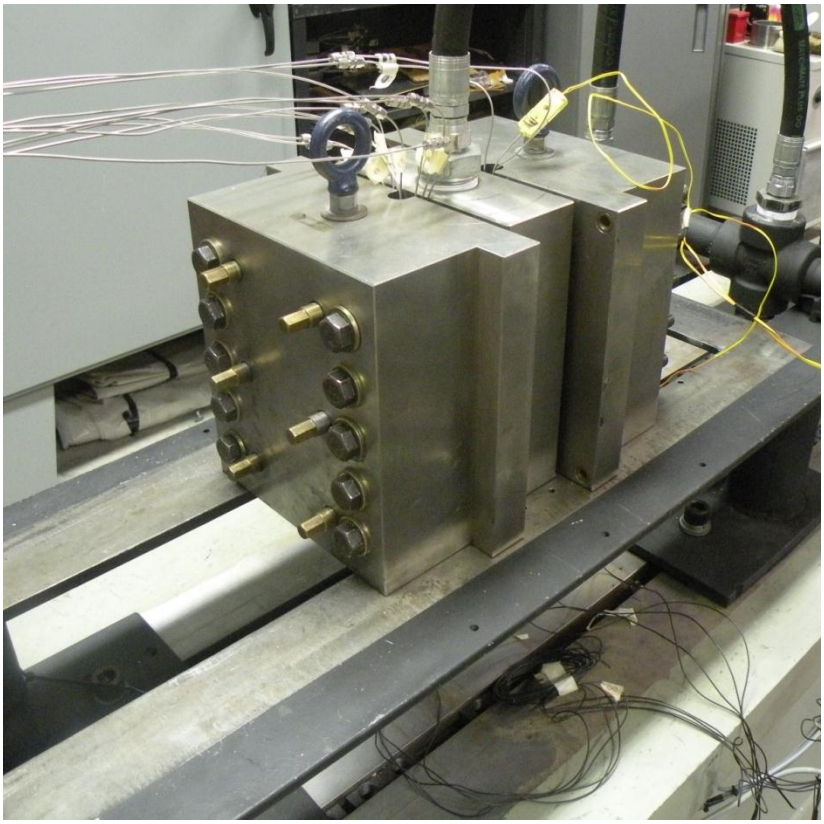

Figure 23. Photograph of both the plates assembled

4. TESTING PROCEDURE

Reference from Kheireddin [22] is taken for most of the portion of the text of this section.

4.1. Testing

A high-pressure air tank is located at the low speed wind tunnel facility and is pressurized using two air compressors. Once the pressure in the tank reaches 104 bar, the compressors are turned off. Each day of testing begins by verifying that all instrumentation is working properly. Before the data acquisition process begins, the entire system is checked for unwanted leakage by opening the inlet control valves while keeping the backpressure valve closed. Once the pressure in the system reaches 84 bar, the inlet control valves are closed, and the pressure in the system is monitored. If no detectable leaks are found, testing begins. To avoid malfunction of the flow meter, the inlet control valves are opened slowly while the backpressure valve is in the closed position. Once the entire system is pressurized to the desired pressure (this is achieved by opening the two inlet valves in the needed proportion based on the required pressure and the available tank pressure), the backpressure valve is slowly opened until a maximum pressure differential is established. Specified pressure drops are then achieved by closing the backpressure valve (Closing the back pressure valve increases the inlet pressure for the same inlet valves' openings. Inlet valve 2 as seen in Figure 12 is adjusted to maintain the constant inlet pressure). Once steady state flow conditions are established, data are collected through a Labview program. This procedure is repeated for inlet pressure values of 56, 70, and 84 bar. At the end of the test day, the flow meter

is disconnected from the flow loop and flushed with denatured alcohol to remove any moisture that could cause erratic readings in future testing.

4.2. Data reduction

Static data including pressures, temperatures, and flow rate are collected with a Labview program. The Labview program collects 100 samples per measurement for a period of 10 seconds, and an EXCEL program is used to reduce the data.

A Labview program is set up to acquire the time signal of the pressure oscillations detected by the dynamic pressure probes sampled at 100k Hz. The same program performs a Fast Fourier Transform (FFT) to locate and analyze the peaks on the frequency spectra. Finally, frequency spectra of the eight channels are obtained by plotting the RMS Amplitude vs. Frequency.

5. CALCULATION PROCEDURE

5.1. Typical data from a test

A typical test will have the following data measured at a run.

a) Volumetric flow rate as measured by the flow meter, $\dot{q}$

b) Stagnation temperature at the flow meter measured by the thermocouple at the entry of the flow meter, T_{flow}

c) Inlet and exit pressures of the flow meter, P_{flow_in}, P_{flow_out}

d) Inlet and exit pressures of the test section measured at the smooth plate, P_{inlet}, P_{exit}

e) Inlet and exit stagnation temperatures of the test section measured at the smooth plate, T_{inet}, T_{exit}

f) Static pressure drop across the HP plate at 9 locations, *P1*,*P2*, *P3,…P9*

g) Dynamic pressure data measured at 4 locations at the smooth plate and 4 locations at the HP plate.

The above test results correspond to a particular plate with a particular C_{pl} with a particular P_{in} and a ΔP which in turn defines the *Re* (The difference between the terms 'pressure difference' and 'pressure ratio' is that they are difference and ratios between the inlet and exit pressures respectively). The same data will again be recorded for different ΔP across the test section, i.e., for a range of Reynolds numbers. The test with HP plate with h_d = 0.9 mm, C_{pl} = 0.635 mm and P_{in} = 84 bar is considered to explain the calculations. This test has the ΔP values of, 49.7, 44.9, 41.2, 37.5, 34.4, 31.0, 27.0, 24.4,

21.2, 17.3, 14.0, 10.9, 7.7, and 4.0 bar which correspond to Reynolds numbers , 790000, 783000, 764000, 746000, 732000, 708000, 675000, 656000, 620000, 571000, 521000, and 468000 respectively (Calculation of *Re* from ΔP is explained below).

5.2. Reynolds number calculation

Density at the flow meter is calculated from a formula derived from ideal-gas relation, $\rho_{flow} = (\frac{P_{flow}}{R * T_{flow}})$ (kg/m^3), where P_{flow} (N/m^2) is the static pressure at the flow meter (which is calculated by taking the average of pressures measured at the inlet and exit of the flow meter), R is specific heat constant for air (= 287 J/kg K) and T_{flow} (K) is the static temperature at flow meter. The temperature measured using a thermocouple in the flow will be the stagnation temperature. As M across the flow meter is of the order of 0.1, this temperature is approximately equal to the static temperature.

$\dot{m}$ is calculated using , $\dot{m} = \dot{q} * \rho_{flow}$ (kg/s) where $\dot{q}$ is the volumetric flow measured by the flow meter (m^3/s) and ρ_{flow} is calculated as seen previously.

Figure 24 shows $\dot{m}$ versus ΔP for the considered test case. $\dot{m}$ proportionally increases as ΔP increases.

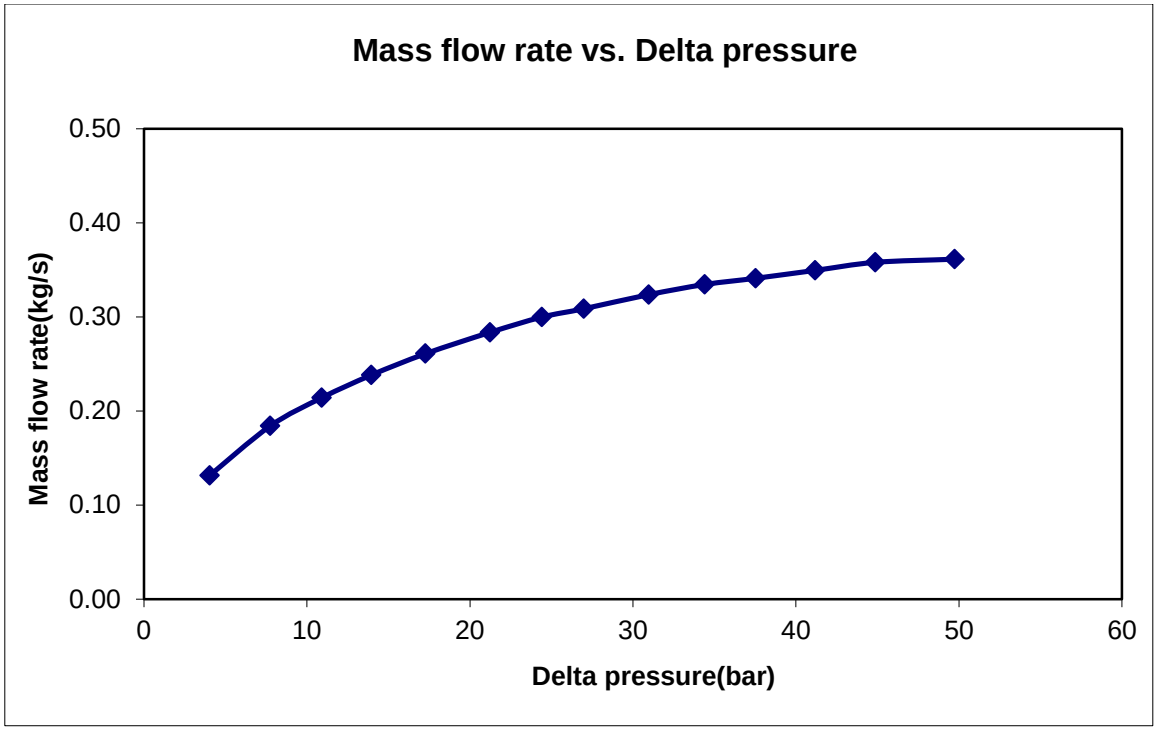

Figure 24. Mass flow rate vs. delta pressure (h_d = 0.9 mm, C_{pl} = 0.635 mm, P_{in} = 84 bar)

Re is calculated by the formula, $\mathrm{Re} = \frac{\rho\,(2\mathrm{H})\,\mathrm{U_m}}{\mu} = \frac{2 * \dot{m}}{C_{pl} * \mu}$

where $\dot{m}$ is calculated as seen earlier (kg/s), C_{pl} is the width of the plate contributing in flow (m) and μ is the absolute viscosity of air (Pa s). *Re* increases with increasing ΔP and a typical plot for the current test is given in Figure 25.

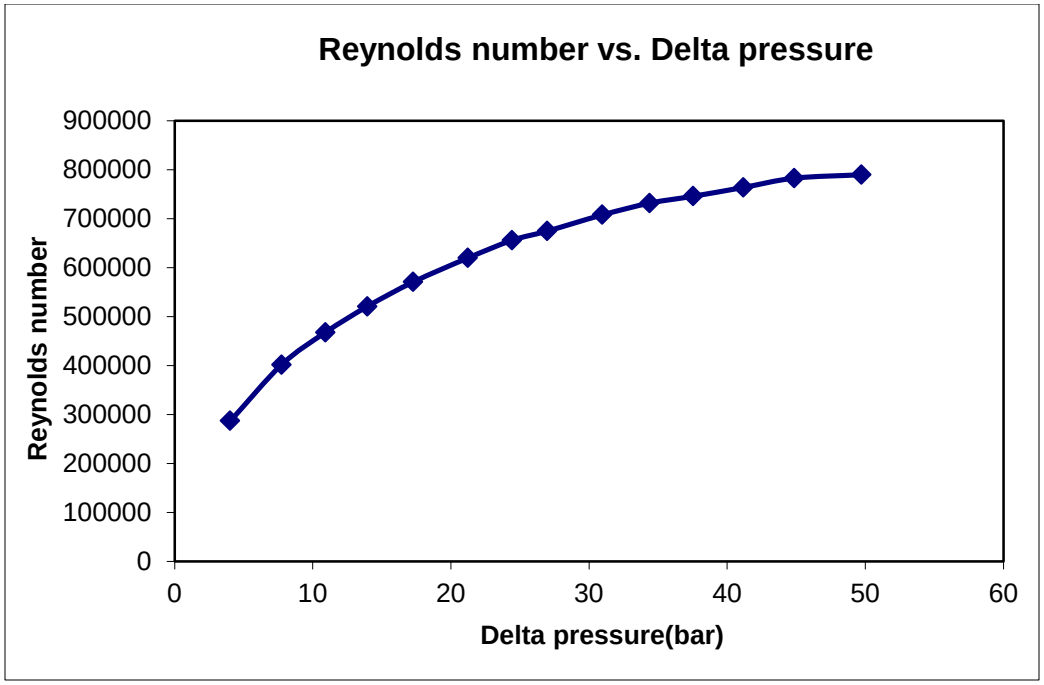

Figure 25. Reynolds number vs. delta pressure (h_d = 0.9 mm, C_{pl} = 0.635 mm, P_{in} = 84 bar)

5.3. Friction factor calculation

Assuming that the change in viscosity is negligible, the *Re* is constant along the flow path. The f_f varies throughout the length of the plate. Hence, f_f is calculated at all nine points of pressure measurement through the following steps.

5.3.1. Mach number calculation at each point

M is calculated at the inlet point, exit point and the nine pressure measurement points using the static pressure values measured at the respective locations and T_t of the flow. Ideally, as per Fanno flow assumptions, T_t of the flow should remain constant, as no heat transfer is assumed. In the actual condition, there is a little drop of T_t from inlet to exit of the plate. But, the maximum measured variation of 3^0K has hardly any effect in

the calculation. Hence an average of the inlet and exit temperatures is used as the T_t of the flow, and the Fanno flow assumption of adiabatic flow is maintained.

Figure 26 shows the measured static pressure values across the plate for all *Re* values. The first data point and the last data point correspond to the inlet and exit pressures measured at the smooth plate and the nine points in between correspond to the nine pressure measurement points on the HP plate.

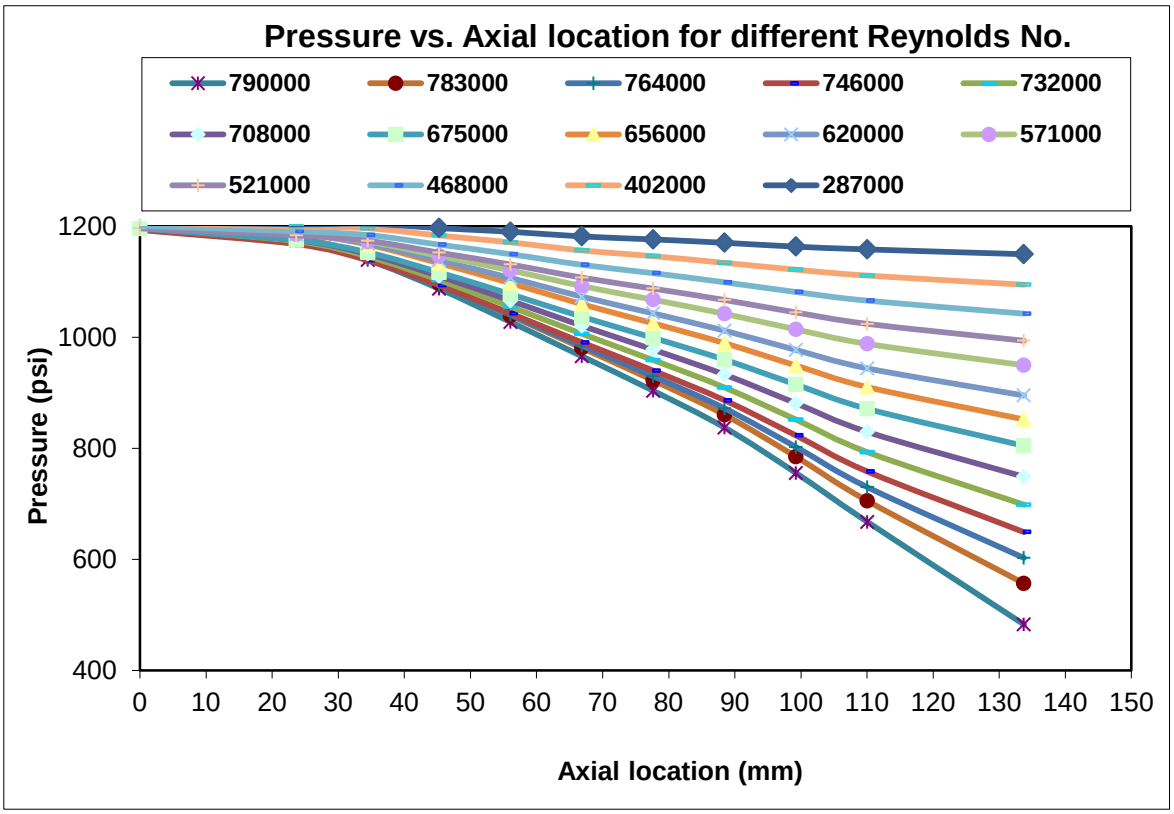

Figure 26. Pressure drop across the plate (h_d = 0.9 mm, C_{pl} = 0.635 mm, P_{in} = 84 bar)

M is calculated using Eq. (22).

For the considered test, calculated M values across the plate are represented in Figure 27.

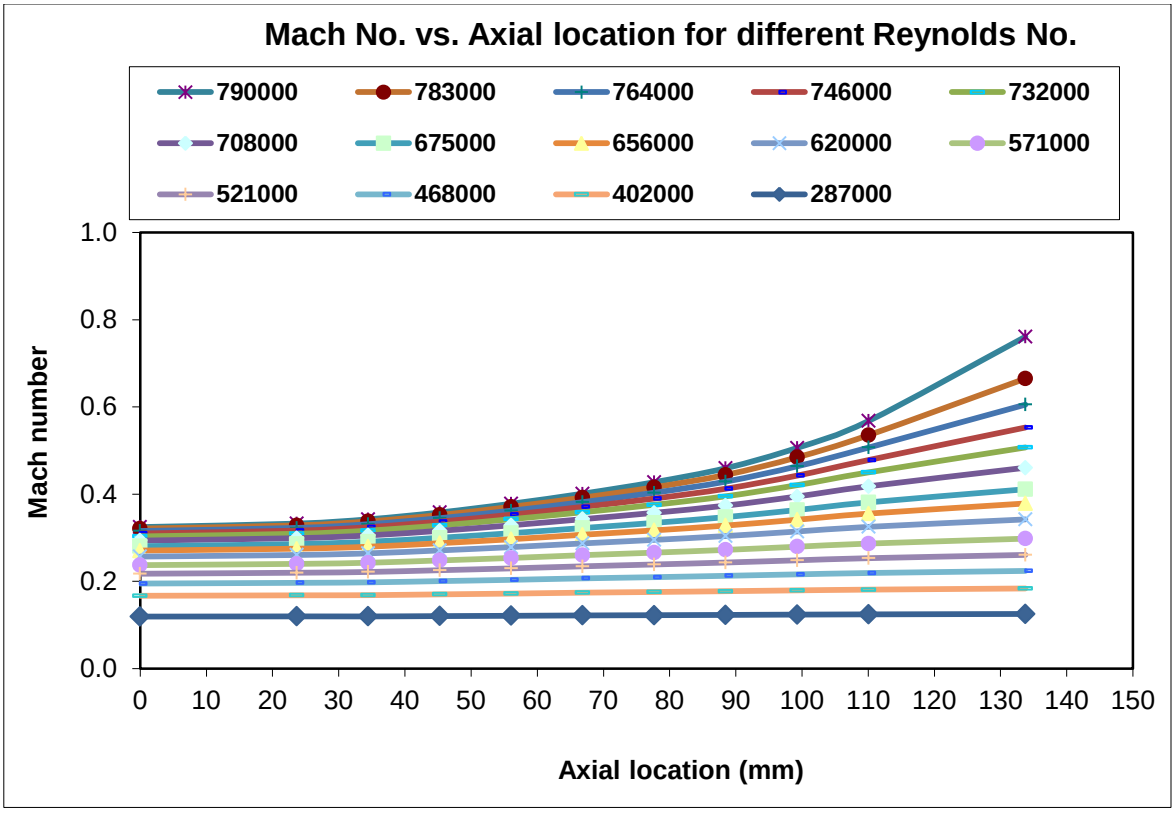

Figure 27. Mach number distribution along the length of the plate

(h_d = 0.9 mm, C_{pl} = 0.635 mm, P_{in} = 84 bar)

Figure 27 shows that M does not reach unity even in the highest Re case at the exit point. But, the exit point referred here is the last pressure measurement point, not exactly the exit of the plate. There is some flow beyond the exit pressure measurement

point along the plate. At higher values of *Re*, the flow chokes at the (actual) exit of the plate. This was confirmed by taking pressure measurement outside the test section that indicated a supersonic flow beyond the test section. For the non-choked cases, the pressure measured close to the exit valve (somewhere away from the exit of the plate in the flow path) is close to the value of the exit point pressure of the plate. In case of choking, the pressure beyond the test section drops considerably which is possible only if *M* reaches the value of 1 in between. This choking has no effect on the measurement or the calculations.

5.3.2. Mach number gradient calculation

To calculate f_f along the plate, the Mach number gradient dM/dx is needed at each point. M calculated across the length of the plate is curve fit with a suitable polynomial as a function of plate location. The derivative of this polynomial with respect to the length is then calculated at the points wherever f_f needs to be found.

dM/dx is calculated at the nine points on the HP plate. Figure 28 shows the curve fit of M versus the axial location for the highest *Re* case. The R^2 value is an indication of how close the data lies to the fit curve. An R^2 value close to 1 indicates a close fit. A fifth order polynomial was selected, as it gave an excellent fit (R^2 value close to 1) for all the cases.

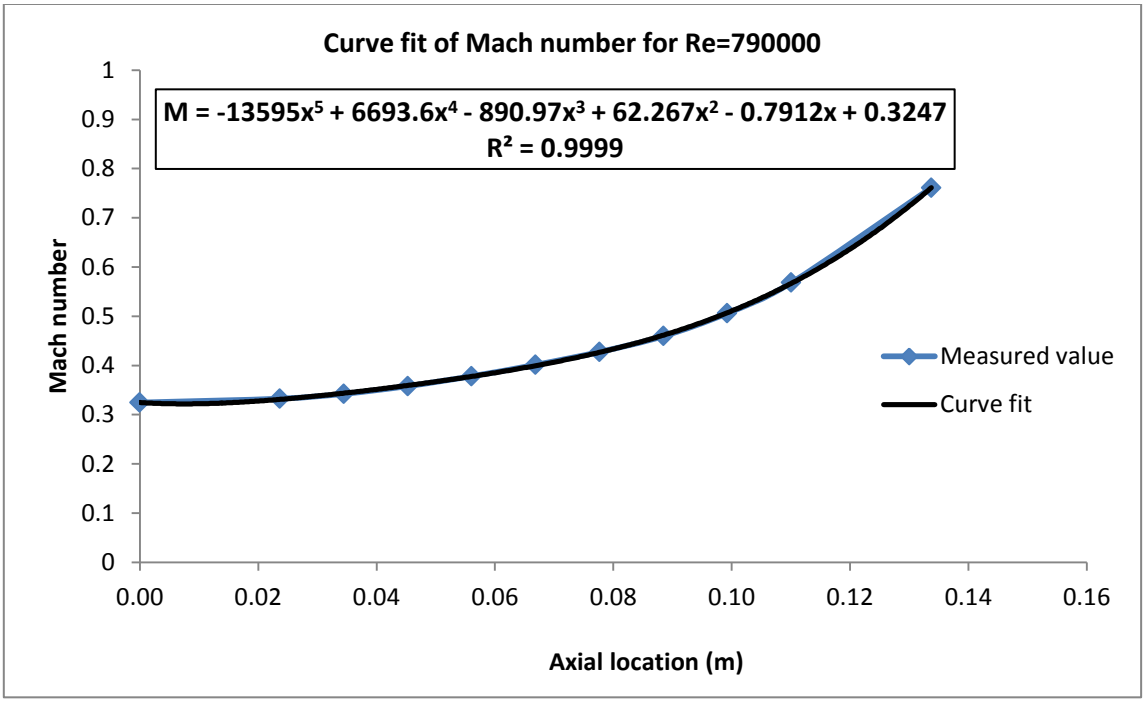

Figure 28. Curve fit for Mach number against axial location of the plate

(h_d = 0.9 mm, C_{pl} = 0.635 mm, P_{in} = 84 bar, *Re* = 790000)

The equation in the figure is differentiated with respect to x and the result is used to find dM/dx at the required location.

For *Re*=790000, the dM/dx is given by,

$$\frac{dM}{dx} = -67975\,x^4 + 26774.4\,x^3 - 2672.91x^2 + 124.534\,x - 0.7912$$

The axial locations of the pressure points of the HP plate are given in the following Table 1.

Table 1. Axial locations of the pressure measurement points

Pressure measurement point on the HP plate	1	2	3	4	5	6	7	8	9
Axial location (m)	0.02368	0.03448	0.04528	0.05608	0.06688	0.07768	0.08848	0.09928	0.11008

Substituting the above values in equation, dM/dx is found for *Re*= 790000 and is shown in Figure 29.

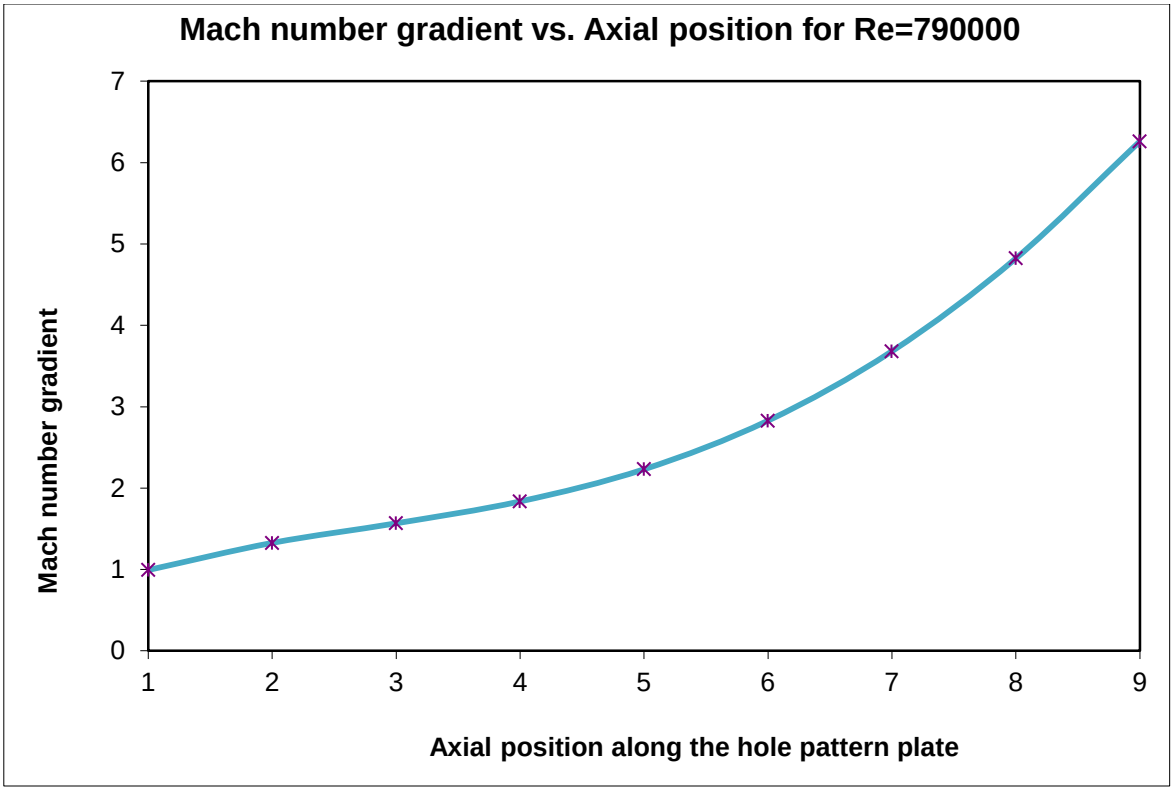

Figure 29. Mach number gradient along length of the plate

(h_d = 0.9 mm, C_{pl} = 0.635 mm, P_{in} = 84 bar, Re = 790000)

5.3.3. Fanning friction factor calculation

Friction factor is calculated using Eq. (23). In the considered test case, for Re = 79000, f_f is calculated at the pressure measurement locations and is plotted in Figure 30.

Figure 31 shows the calculated f_f values for all the Re of this test.

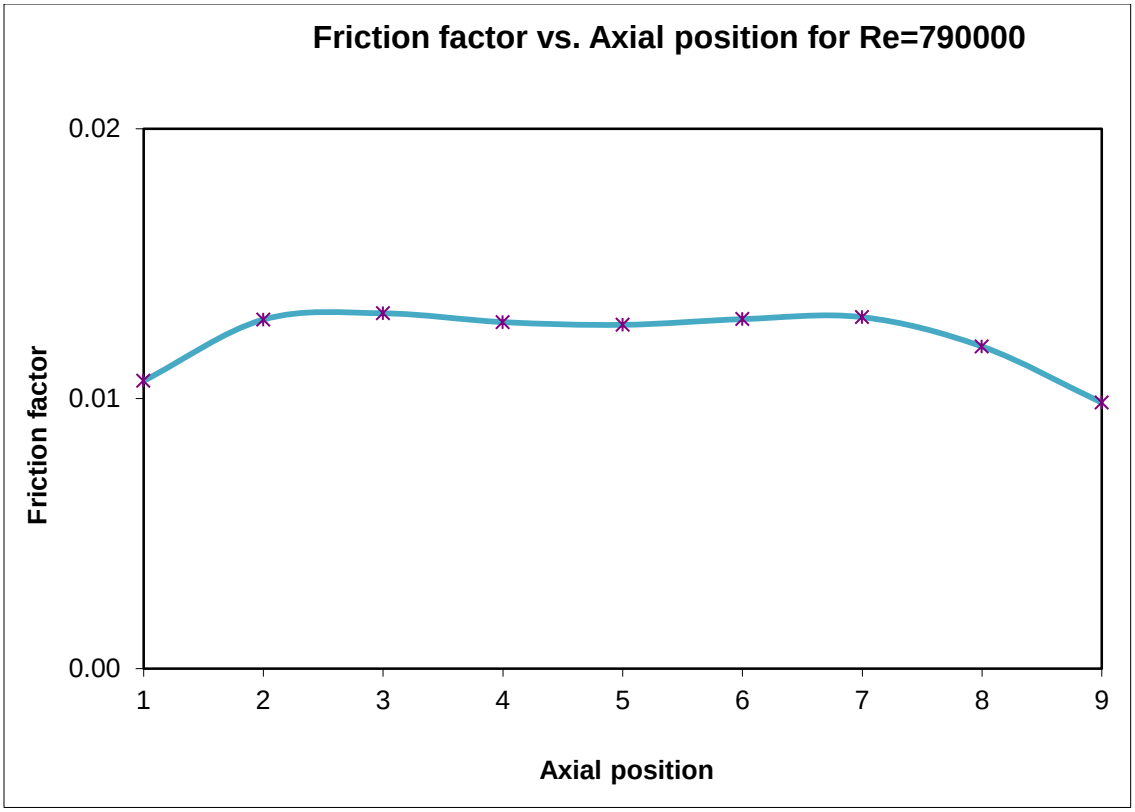

Figure 30. Friction factor along the axial position of the plate

(h_d = 0.9 mm, C_{pl} = 0.635 mm, P_{in} = 84 bar, Re = 790000)

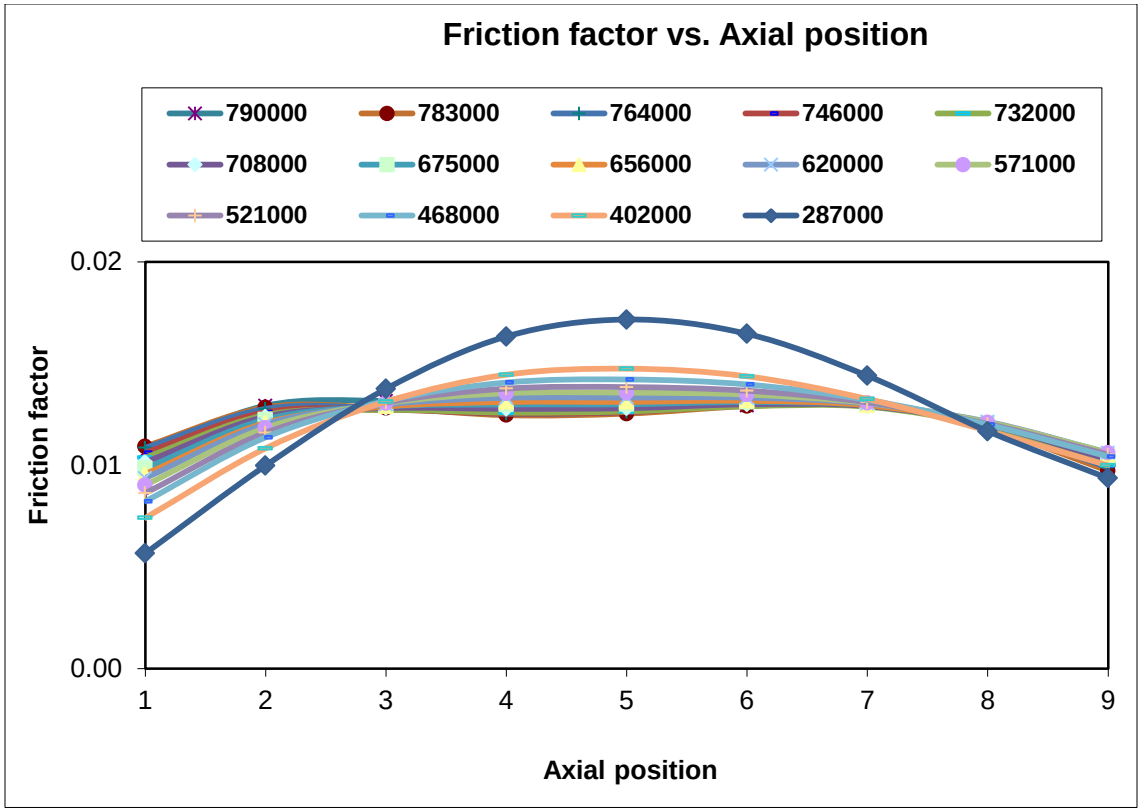

Figure 31. Friction factor along the axial position of the plate for all *Re*

(h_d = 0.9 mm, C_{pl} = 0.635 mm, P_{in} = 84 bar)

These two graphs show that f_f varies axially dropping near the plate's inlet and exit. For all the tested configurations, the inlet and exit effects are ignored, and an average f_f of the values from locations 2,3,4,5,6 and 7 is calculated. Hence a single *Re* will have a single f_f value. Hence forth in this report, f_f means this averaged f_f. Figure 32 shows the averaged f_f versus the *Re* for each test point. The uncertainty in f_f calculation is explained in Appendix C.

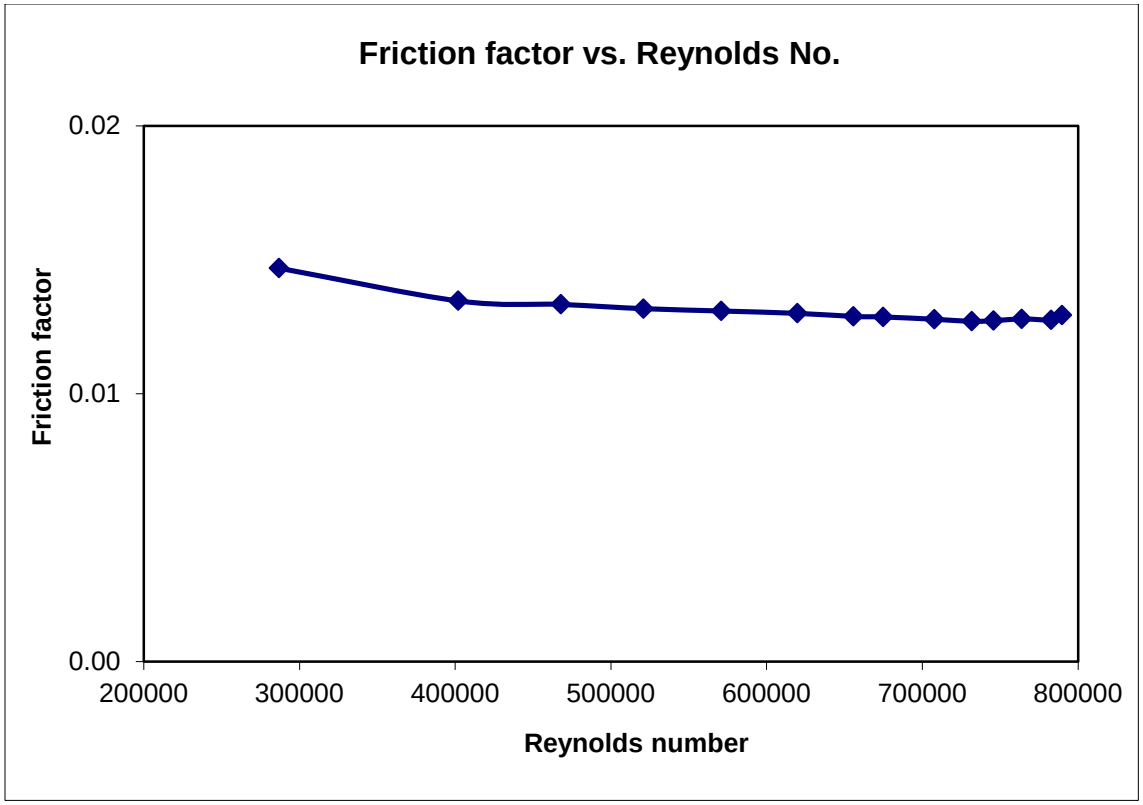

Figure 32. Friction factor vs. Reynolds number

(h_d = 0.9 mm, C_{pl} = 0.635 mm, P_{in} = 84 bar)

For a given plate, there are nine such plots (combination of 3 clearances and 3 inlet pressures).

6. LIST OF TESTS

Totally, 27 tests were done as found in Table 2. At each test, f_f will be calculated against all possible *Re* of that configuration.

Table 2. List of tests

Sl.No.	Hole depth (mm)	Clearance (mm)	Inlet pressure (bar)
1	0.9	0.254	56
2			70
3			84
4		0.381	56
5			70
6			84
7		0.635	56
8			70
9			84
10	1.9	0.254	56
11			70
12			84
13		0.381	56
14			70
15			84
16		0.635	56
17			70
18			84
19	2.9	0.254	56
20			70
21			84
22		0.381	56
23			70
24			84
25		0.635	56
26			70
27			84

7. TEST RESULTS AND DISCUSSION: FRICTION FACTOR DATA

7.1. Friction factor data

Figure 33- Figure 35 represent the f_f data for the three tested plates with h_d = 0.9, 1.9, and 2.9 mm, respectively. Appendix A presents all the calculated values for each test case in tabular form.

7.2. Effect of various parameters

7.2.1. Reynolds number

The following observations can be made from Figure 33-Figure 35:

a) For h_d = 0.9 mm, f_f decreases with increasing *Re*.

b) For h_d = 1.9 mm, at low clearances, f_f decreases with increasing *Re*. At the maximum tested C_{pl} of 0.635 mm, f_f is almost constant with respect to *Re*.

c) For h_d = 2.9 mm plate, f_f is almost constant with varying *Re*.

In general, f_f is a weak function of *Re*.

One objective of this study was to see if f_f jump occurs. Kheireddin [22] tested plates with 3.175 mm diameter holes of different depths and did not see any f_f jump with any of his test of an HP plate against a smooth plate. Figure 36 shows a typical plot of f_f versus *Re* from Kheireddin's tests (Kheireddin has reported Darcy–Weisbach's friction factor which is 4 times higher than Fanning f_f) showing no friction-factor jump. He also tested two HP plates apposing each other and observed friction-factor jump. Figure 37 shows the test results of a typical test of apposing HP plates showing friction –factor jump.

In the current study with h_d = 12.15 mm also, friction-factor jump was not observed for all the tests that featured rough plate facing a smooth plate.

7.2.2. Clearance

Friction factor considerably increases with increasing C_{pl} in all test cases. Previous studies have reported the existence of a plateau clearance where f_f ceases to increase with increasing C_{pl}. The results from the current experiments show a continuing increase in the f_f with increasing C_{pl} in the tested C_{pl} range. Kheireddin [22] observed the same trend of continuously increasing f_f with increasing C_{pl} in all his tests. Note that the plateau clearance value reported by Nava [16] on plates with circular recess tested with water was 0.762 mm (30 mils), but the maximum tested clearance in the current study as well as in Kheireddin's study was 0.635 mm (25 mils).

Friction factor data are plotted against C_{pl} for all h_d and P_{in} combinations in Figure 38.

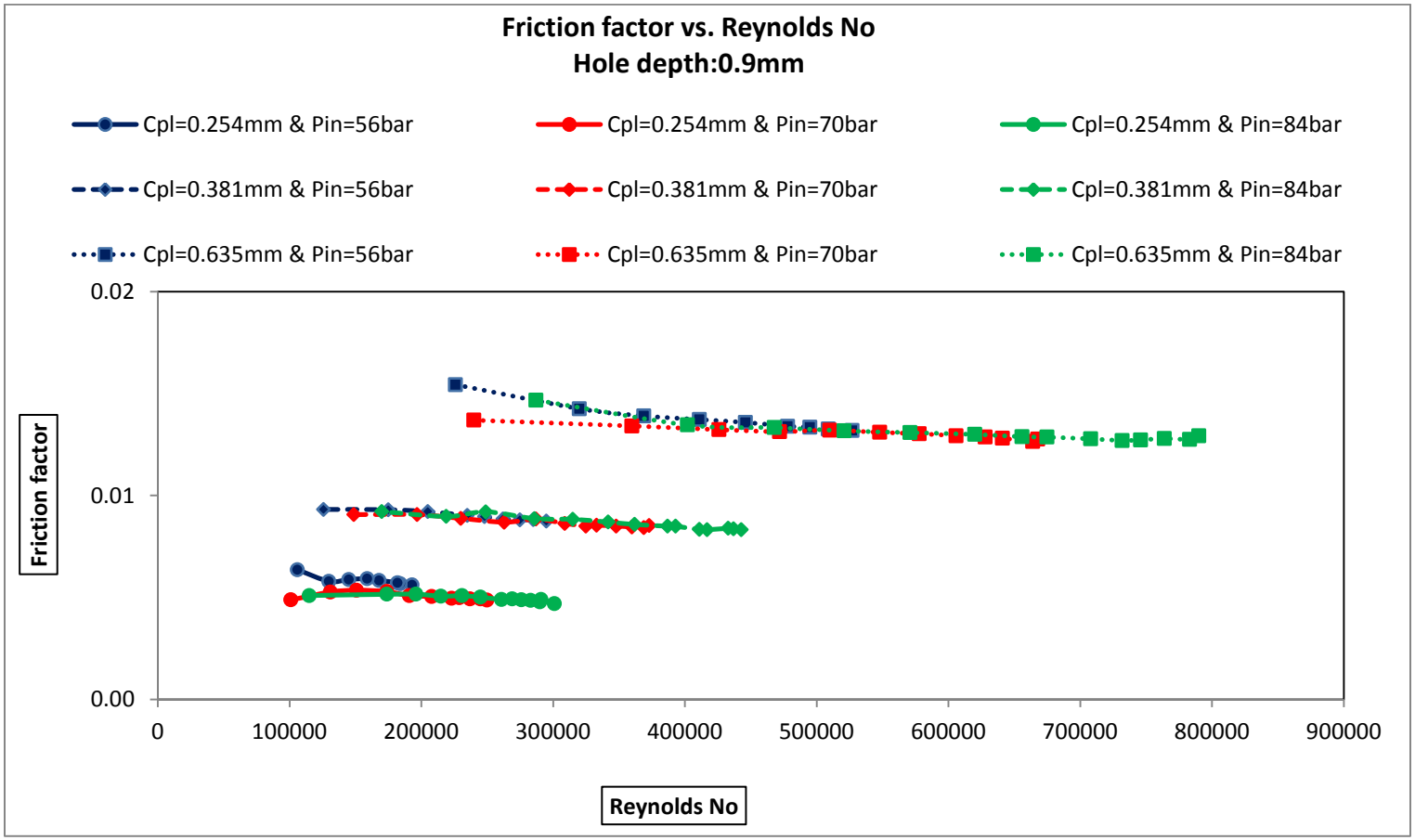

Figure 33. Friction factor data for plate with h_d = 0.9 mm

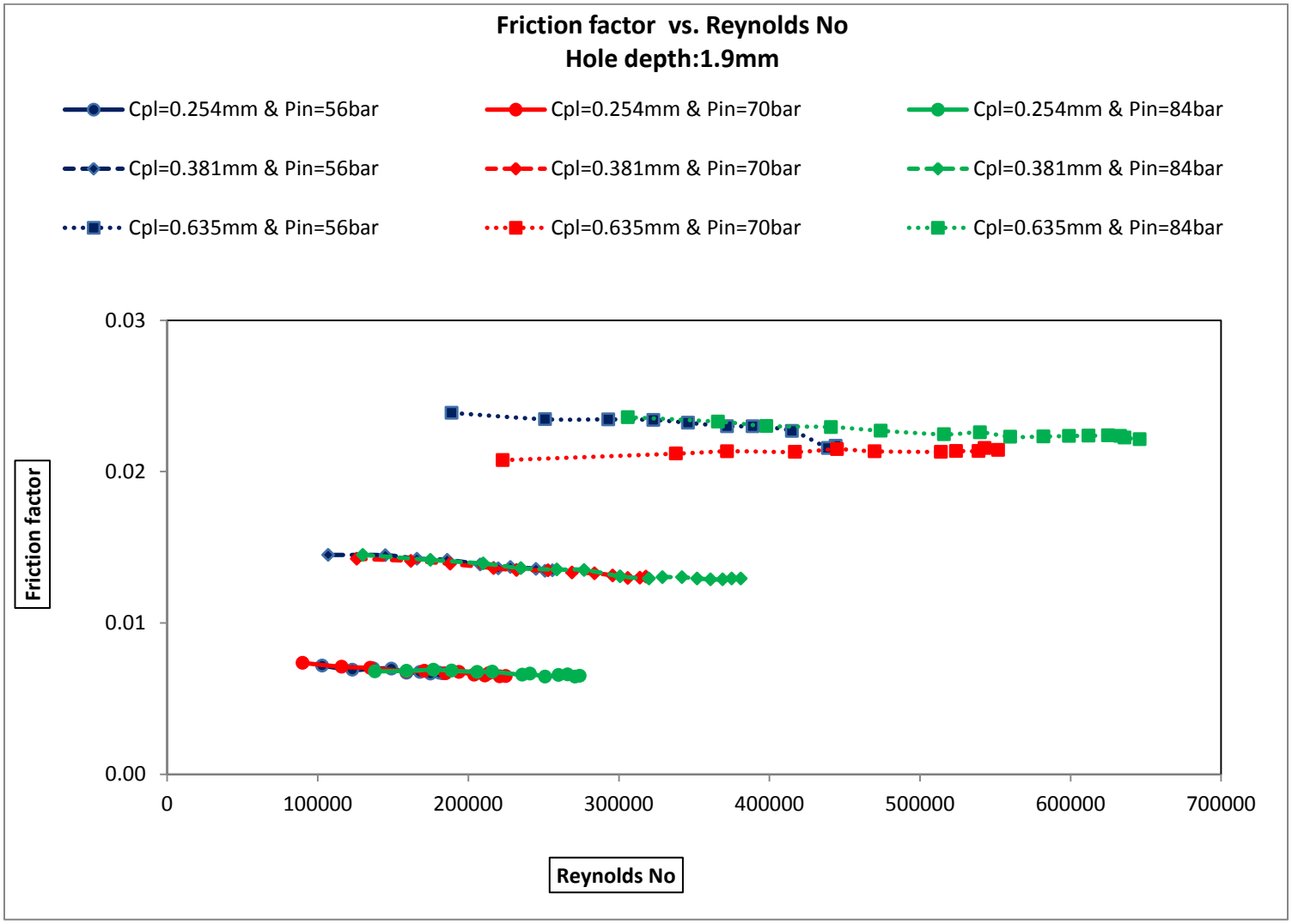

Figure 34. Friction factor data for plate with h_d = 1.9 mm

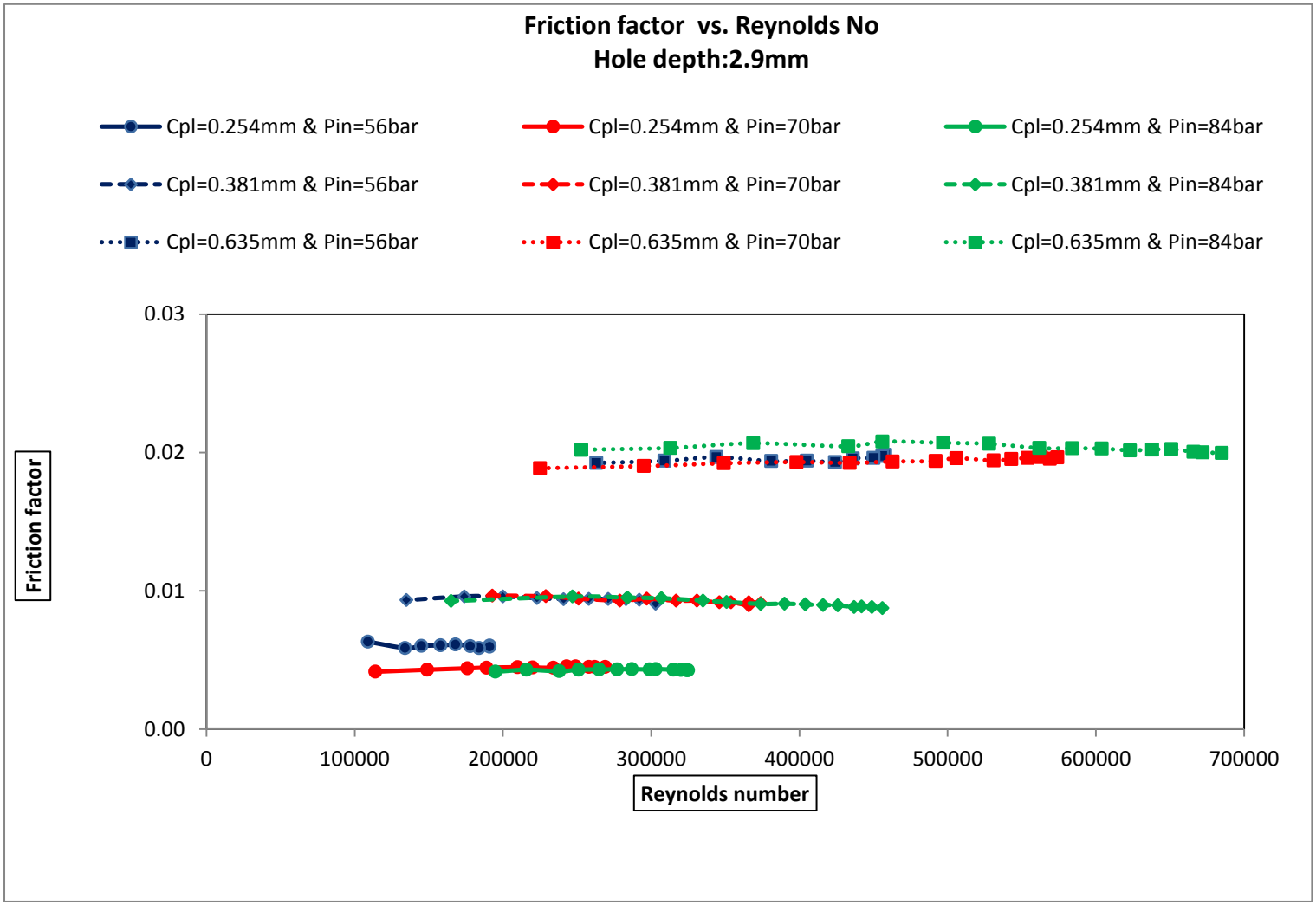

Figure 35. Friction factor data for plate with h_d = 2.9 mm

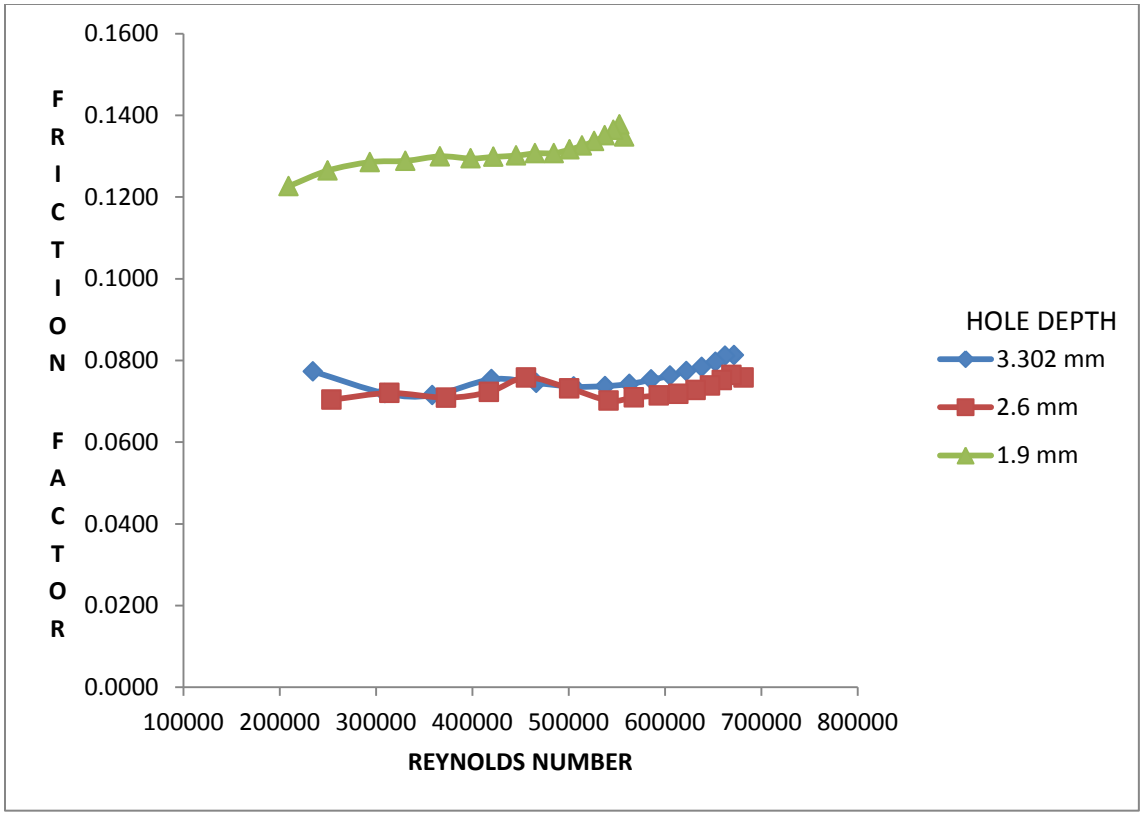

Figure 36. Darcy–Weisbach's friction factor vs. Reynolds number from Kheireddins's tests [22] (h_{φ} = 3.175 mm, C_{pl} = 0.635 mm, P_{in} = 84 bar)

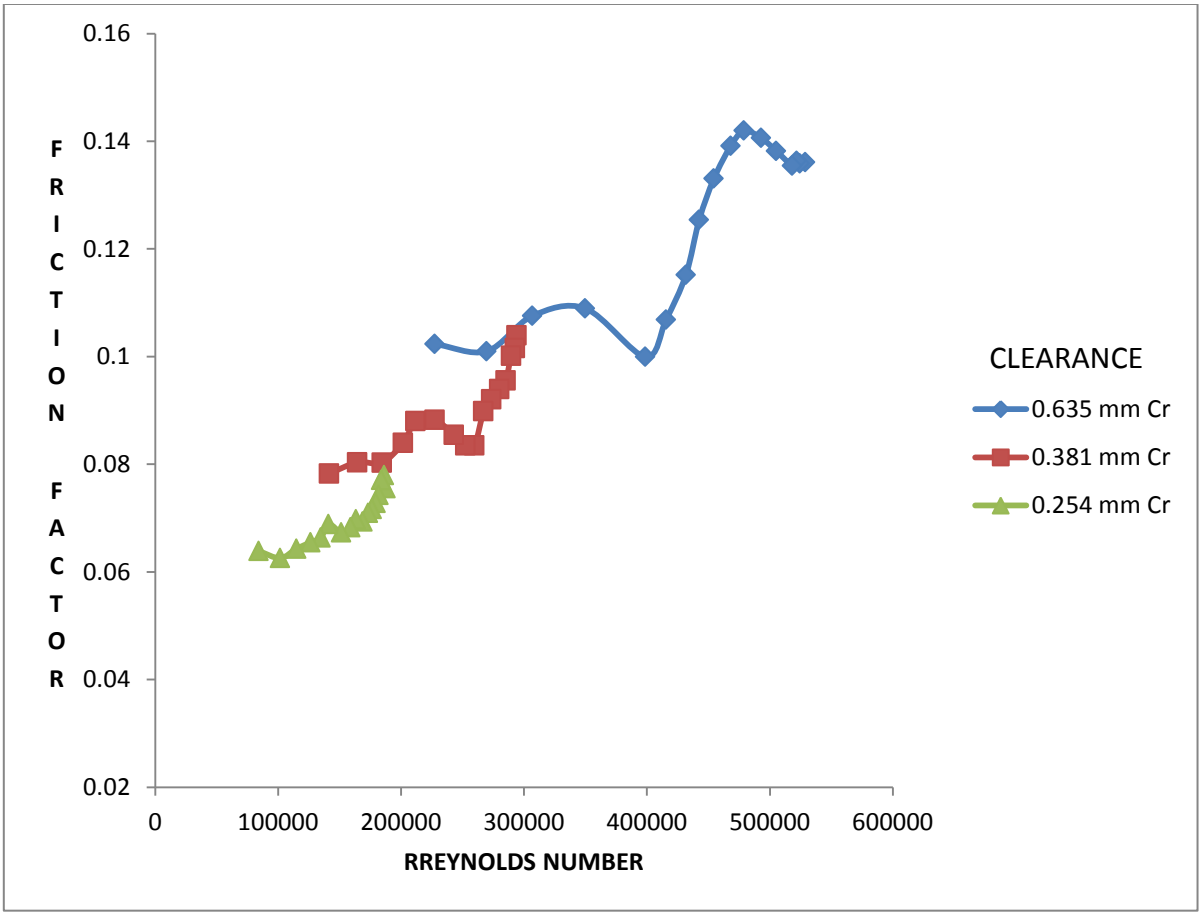

Figure 37. Darcy–Weisbach's friction factor vs. Reynolds number from Kheireddins's tests for HP facing HP configuration showing friction-factor jump [22]

(h_{φ} = 3.175 mm, h_d = 3.302 mm, C_{pl} = 0.635 mm, P_{in} = 84 bar)

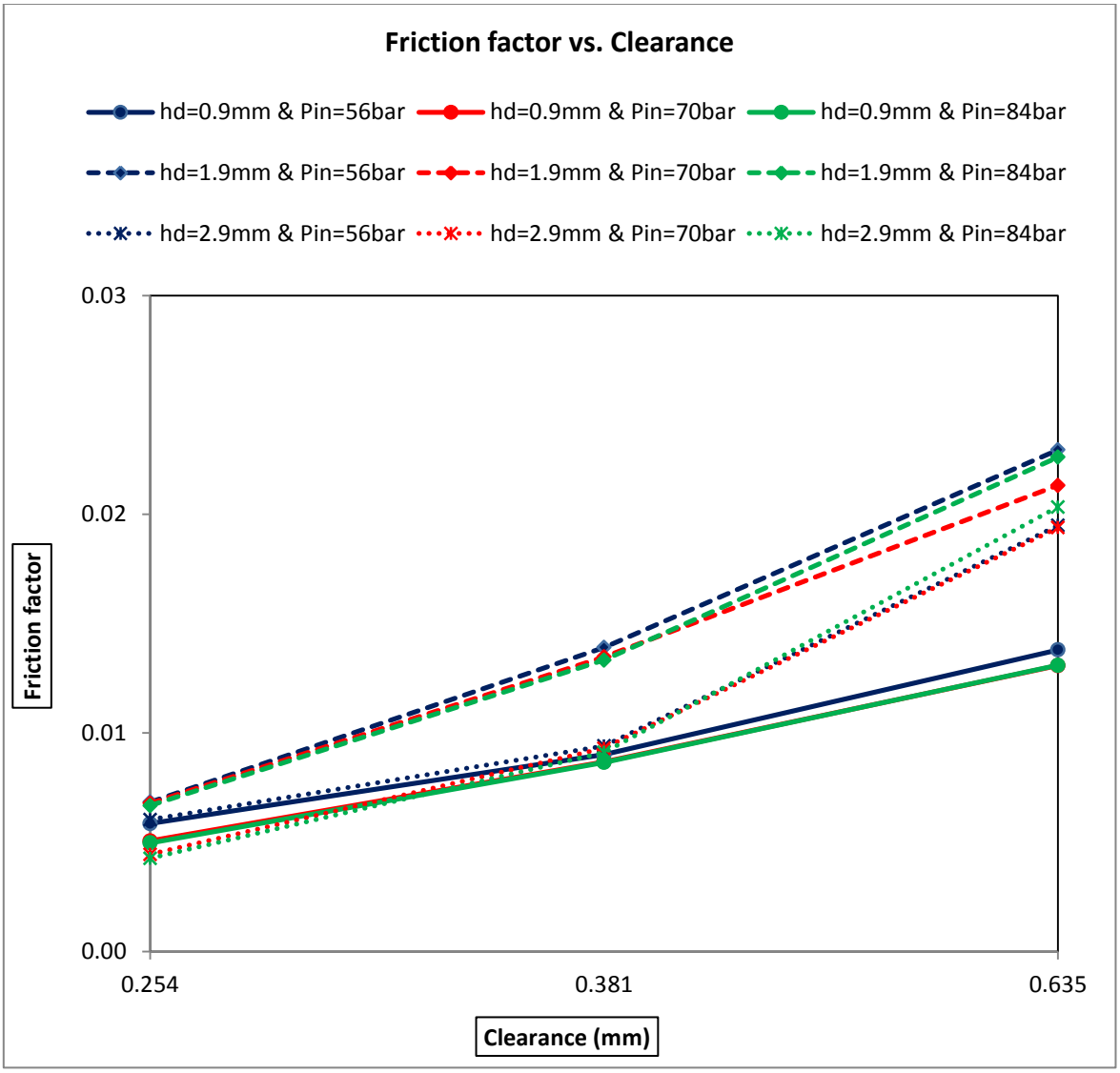

Figure 38. Effect of C_{pl} on f_f (*Re* based averaged f_f vs. C_{pl}) for all tests

Figure 39 is a representative graph from Kheireddin' tests showing f_f variation versus C_{pl}.

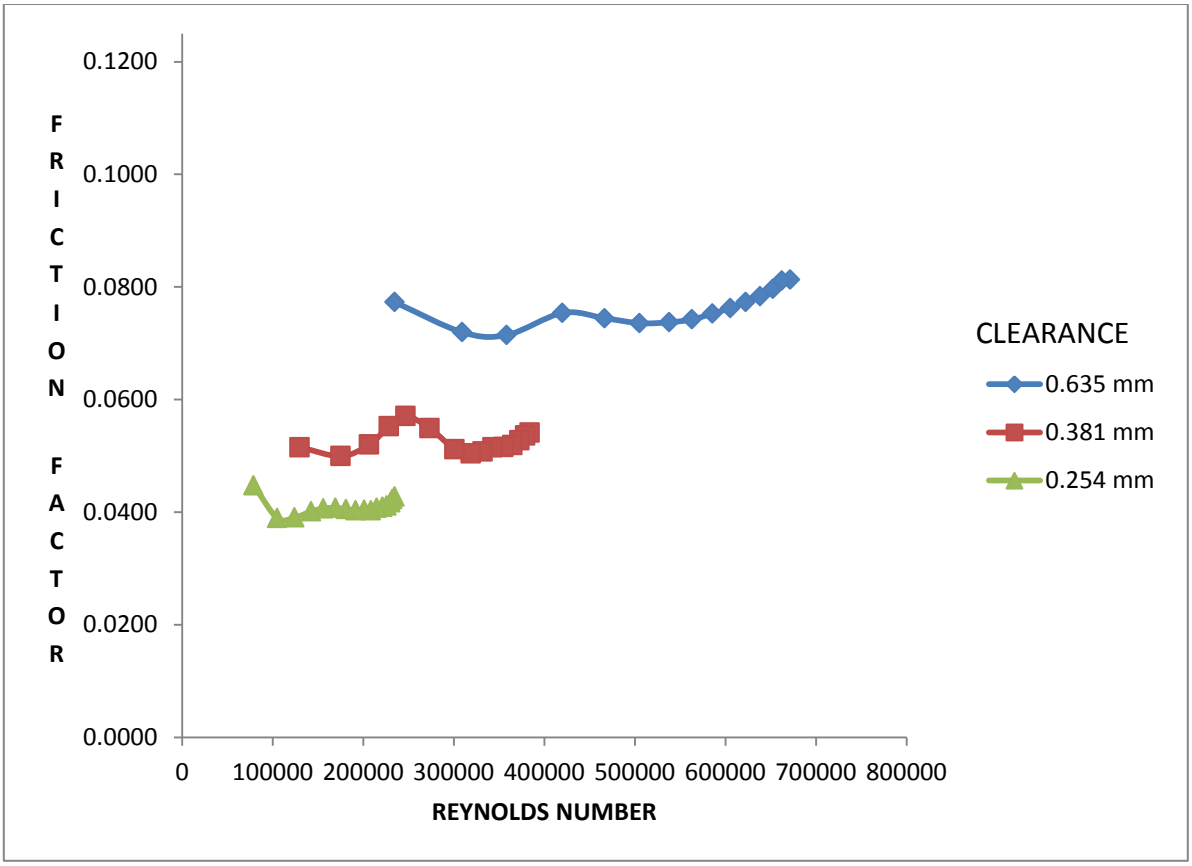

Figure 39.Typical plot for the effect of C_{pl} on the f_f from Kheireddin's test [22]

(h_φ = 3.175 mm, h_d = 3.302 mm, P_{in} = 84 bar)

7.2.3. Inlet pressure

P_{in} has minimal effect on f_f in the plates with h_d = 0.9 mm and 1.9 mm. In most of the cases, f_f decreases slightly with increase in P_{in}. For h_d = 2.9 mm and C_{pl} = 0.254 mm, f_f is considerably affected by changes in P_{in}. The test with P_{in} = 56 bar gives higher values of f_f than the tests with P_{in} = 84 bar and 70 bar.

In Figure 40, f_f data is plotted against P_{in} for different hole depths and clearances to understand the effect of inlet pressure.

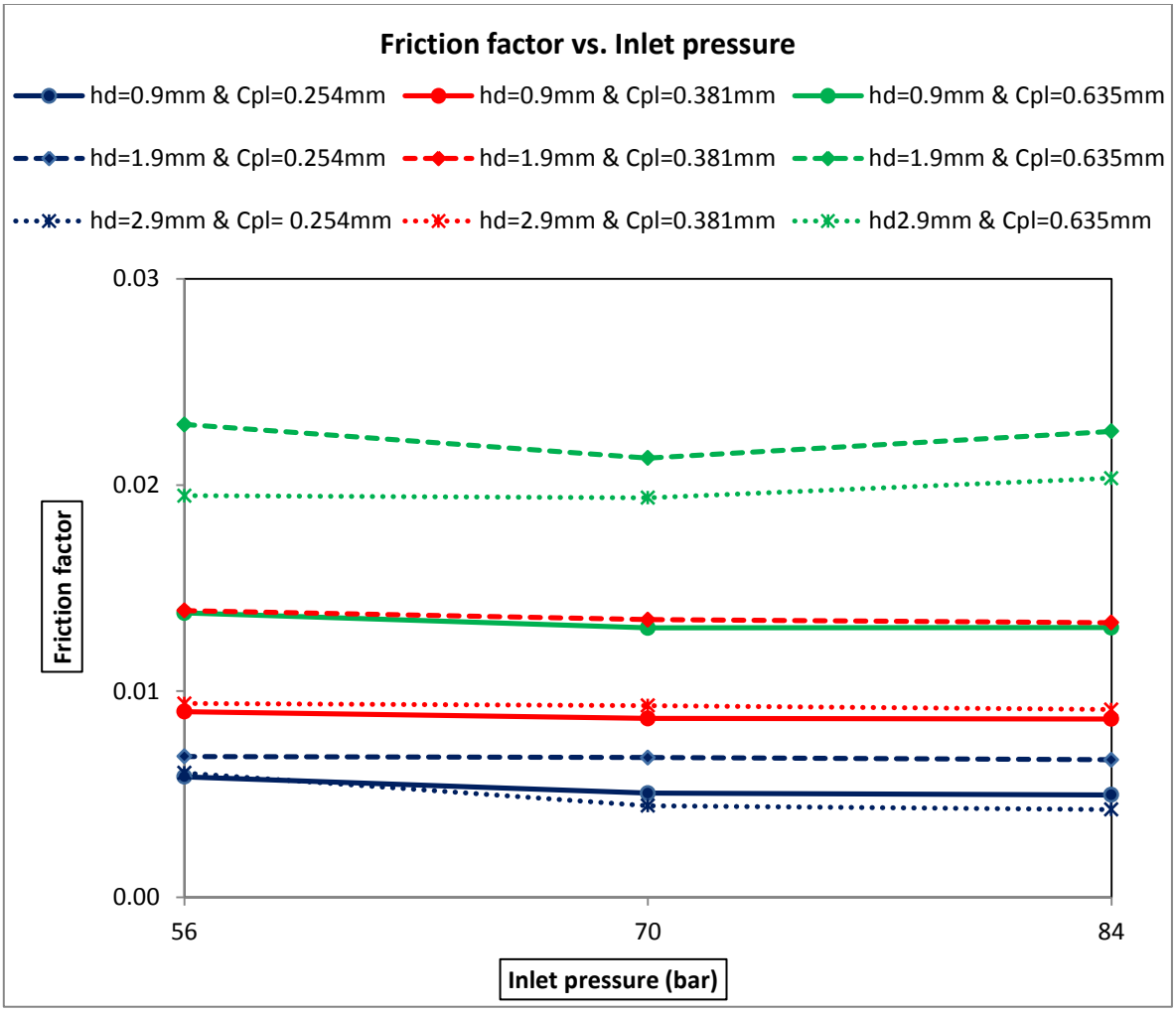

Figure 40. Effect of P_{in} on f_f (Re based averaged f_f vs. P_{in}) for all tests

The lines are almost straight, but have some variation observed at some C_{pl} and h_d. Figure 41 shows variation of f_f versus P_{in} in Kheireddin's test.

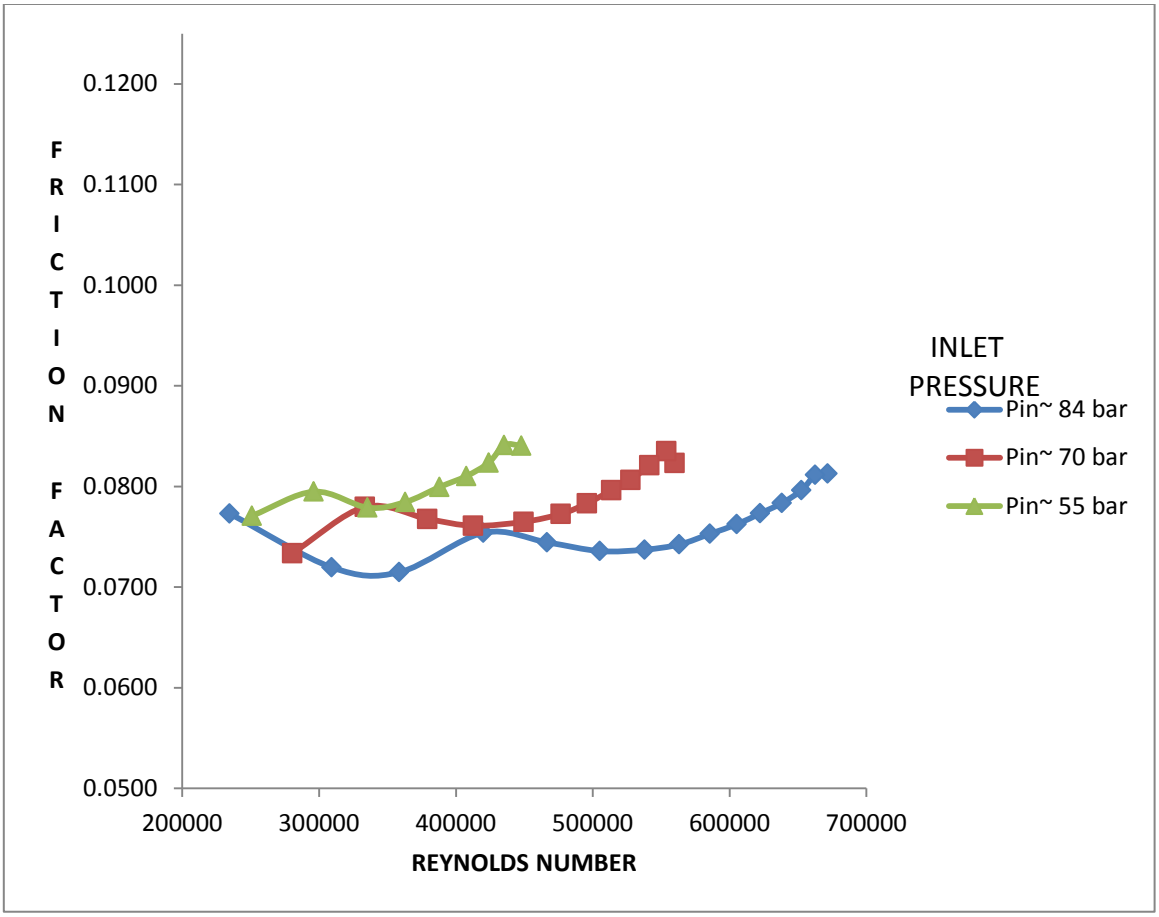

Figure 41. Typical plot for the effect of P_{in} on f_f from Kheireddin's test [22]

(h_φ = 3.175 mm, h_d = 3.302 mm, C_{pl} = 0.635 mm)

7.2.4. Hole depth

Figure 42 shows f_f versus h_d. From 0.9 mm deep plates to 1.9 mm deep plates, f_f increases, and the increase gets steeper with increasing C_{pl}. From 1.9 mm to 2.9 mm, f_f decreases, leaving the situation hard to predict for other hole depths.

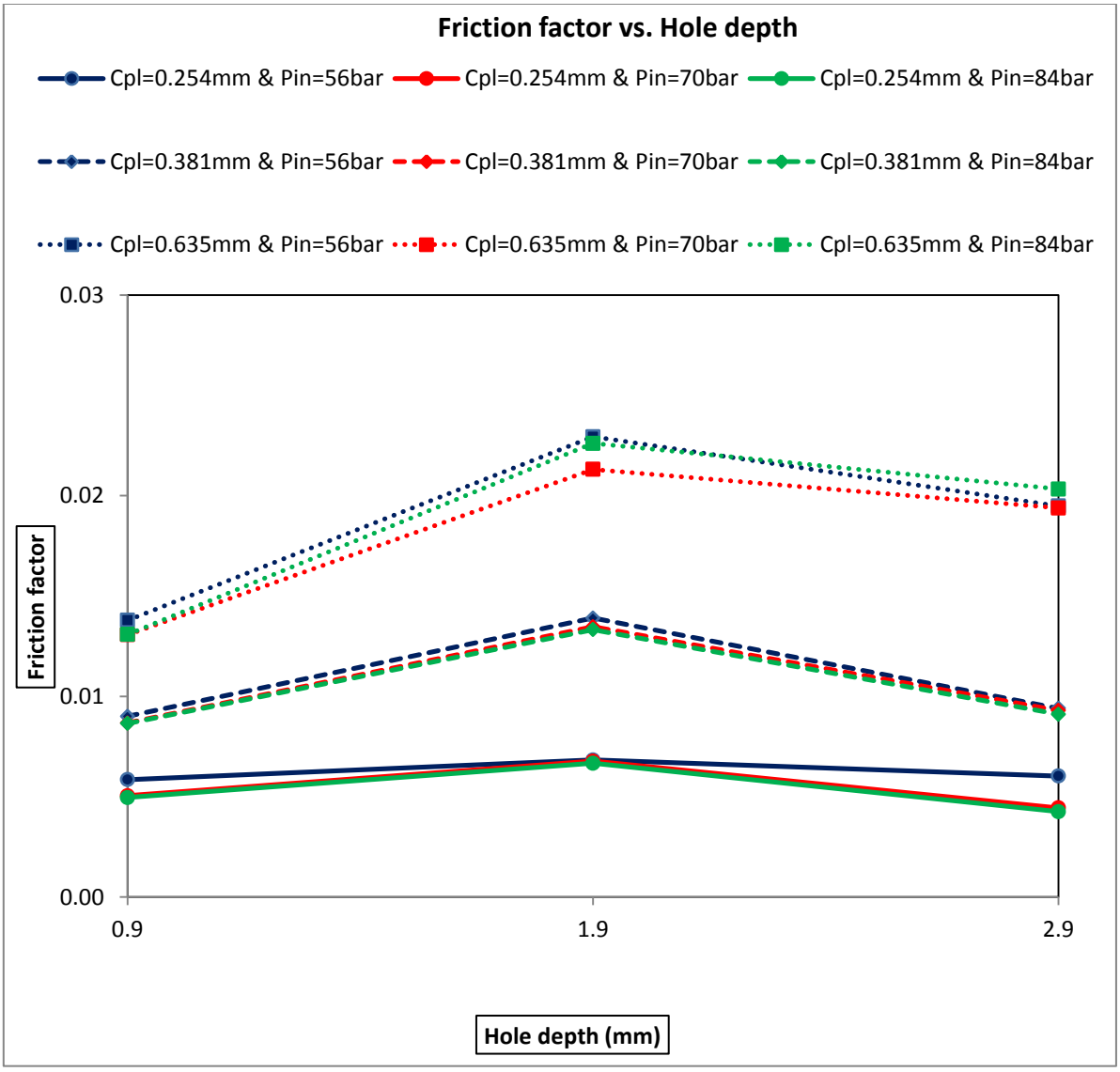

Figure 42. Effect of h_d on f_f (Re based averaged f_f vs. h_d) for all tests

Figure 43 shows f_f versus h_d from Kheireddin's tests, and Figure 44 shows results from Ha's tests.

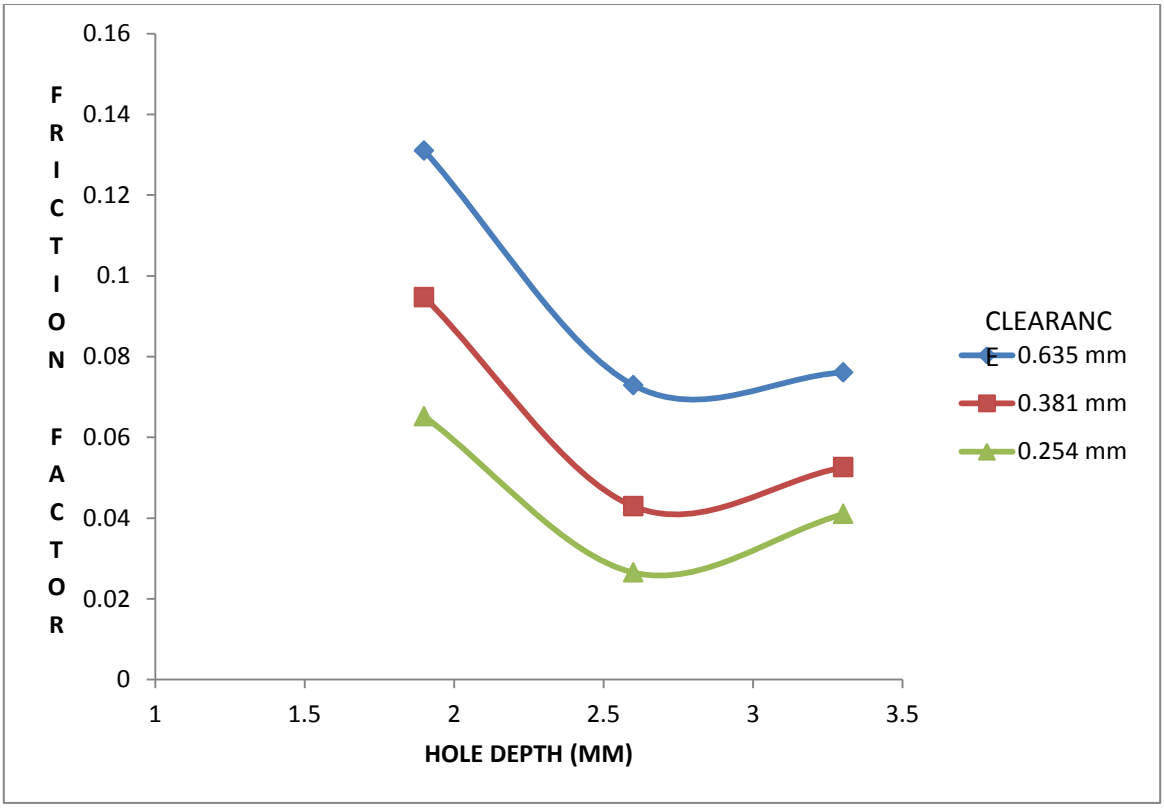

Figure 43. Friction factor vs. h_d for three clearances from Kheireddin's test [22]

(h_φ = 3.175 mm, P_{in} = 84 bar)

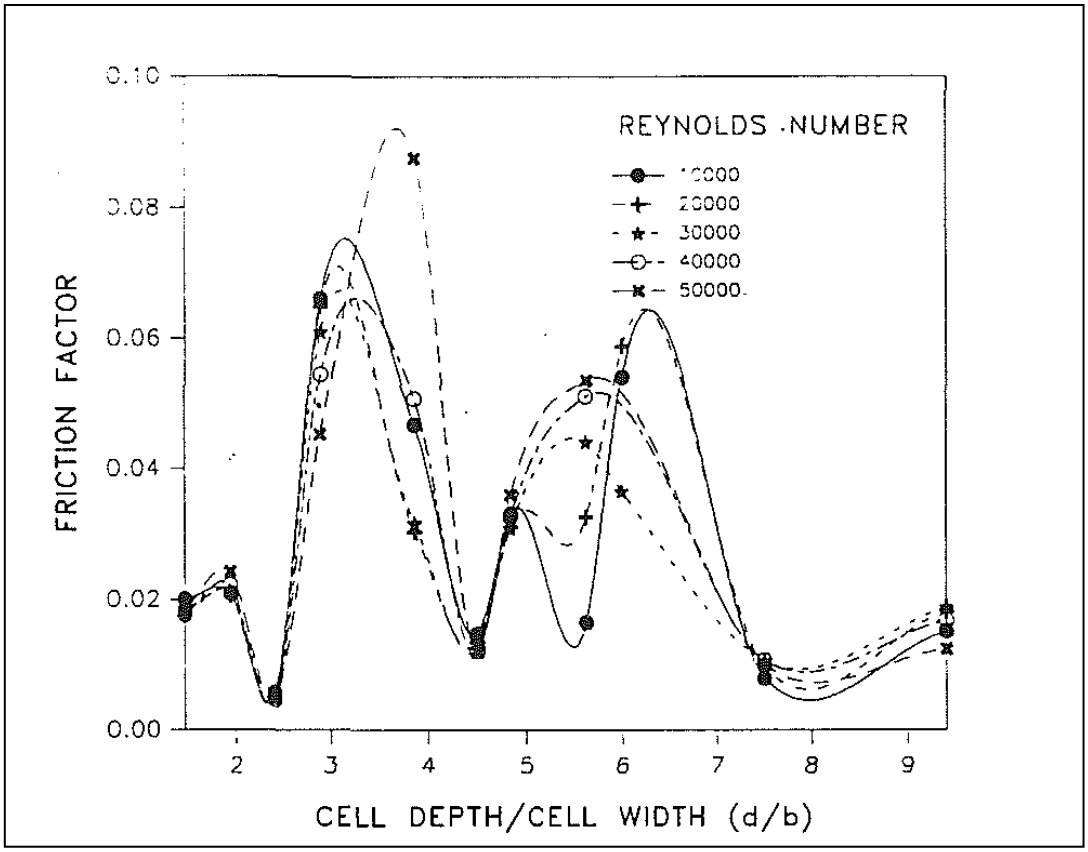

Figure 44. Ha's result for f_f vs. cell depth to cell width ratio [14]

Ha's test results were comparable to data from Schlichting [26] for flow over rough surfaces with an unbounded clearance.

7.2.5. Hole diameter

This research mainly aims at how hole diameter influences f_f. The data obtained from these tests are compared with tests of plates with h_φ = 3.175 mm. One on one comparison cannot be made on these data, as h_d on these plates affects f_f in different ways in addition to the effect of diameter. So, it cannot be concluded if the change in f_f is

because of the effect of h_φ or h_d. The following effort is made to generalize the variation of f_f with h_φ.

$\dot{m}$ measured at each test is a direct representative value of the leakage. Figure 45- Figure 47 show $\dot{m}$ versus ΔP from plates with 3.175 mm diameter holes and 12.15 mm diameter holes at P_{in} = 84 bar and respectively at C_{pl} = 0.635, 0.381, and 0.254 mm.

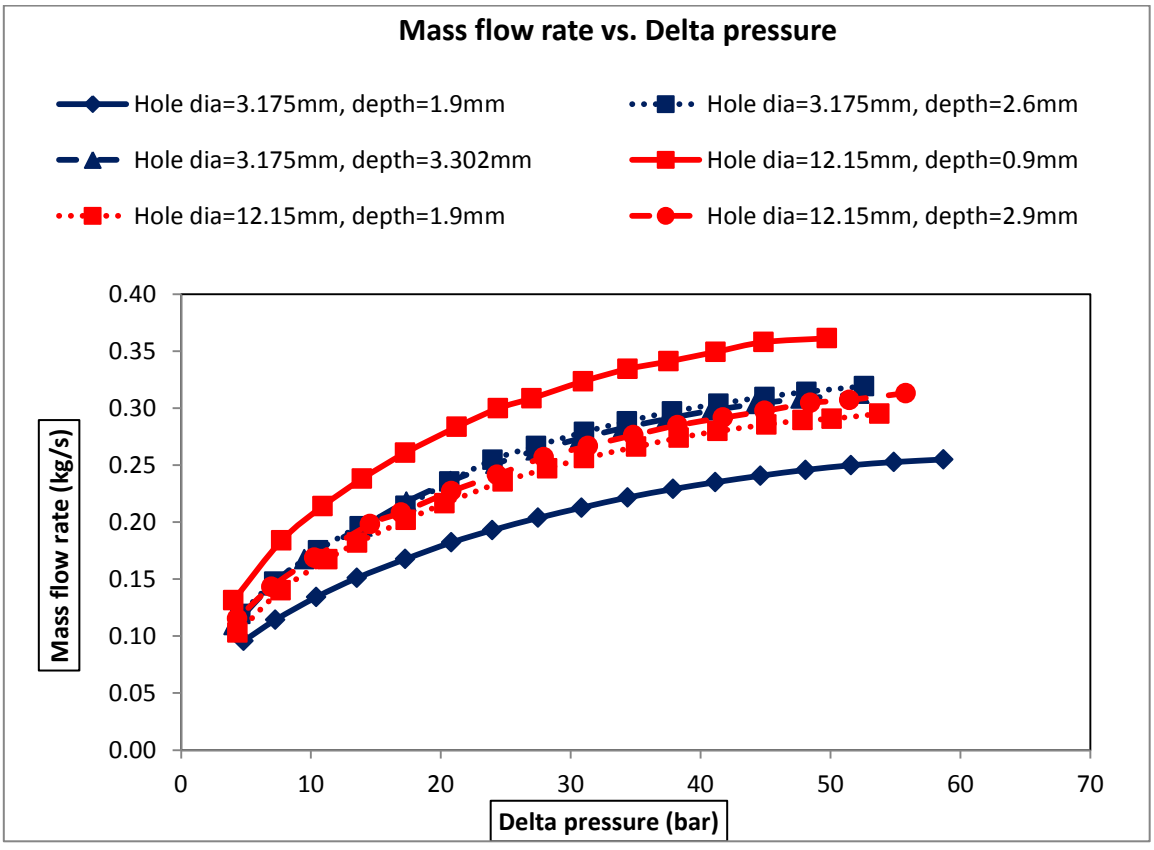

Figure 45. Mass flow rate vs. delta pressure for plates with h_φ = 3.175 mm &12.15 mm (C_{pl} = 0.635 mm and P_{in} = 84 bar)

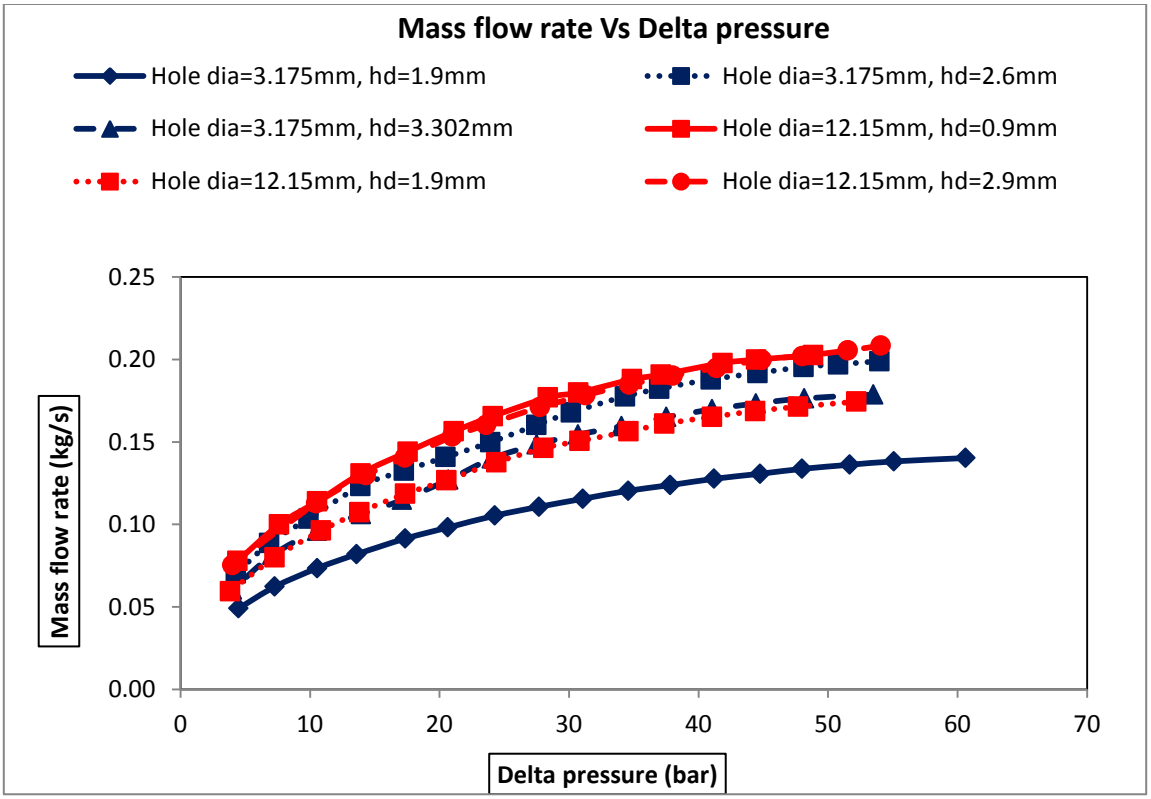

Figure 46. Mass flow rate vs. delta pressure for plates with h_{φ} = 3.175 mm &12.15 mm (C_{pl} = 0.381 mm and P_{in} = 84 bar)

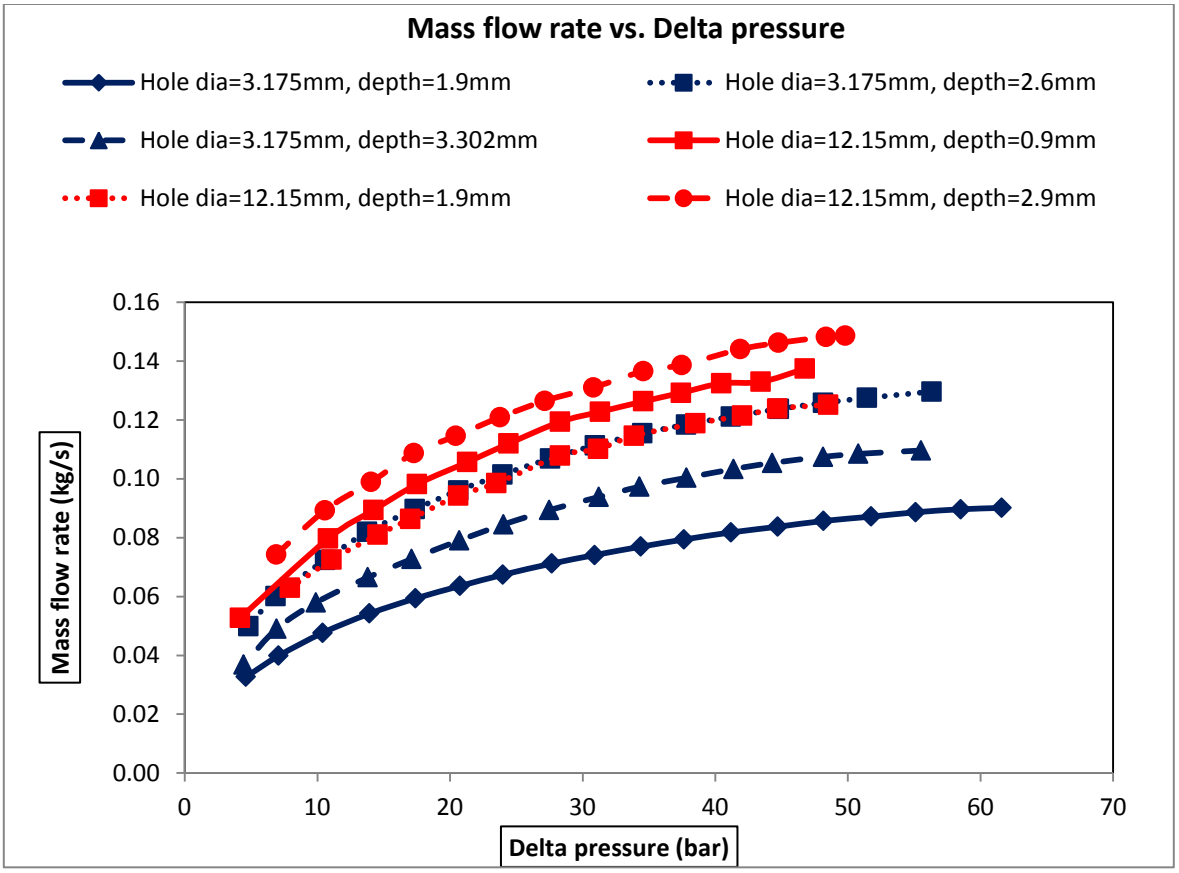

Figure 47. Mass flow rate vs. delta pressure for plates with h_{φ} = 3.175 mm &12.15 mm (C_{pl} = 0.254 mm and P_{in} = 84 bar)

a) At all tested clearances, the highest leakage corresponds to 12.15 mm plate, and the lowest leakage corresponds to 3.175 mm plate.

b) At C_{pl} = 0.254 mm, plates with 3.175 mm hole diameter leak lesser than plates with 12.15 mm hole diameter.

c) At C_{pl} = 0.381 mm and 0.635 mm, the plates have comparable leakage-control performance.

d) Hence, at minimum clearance, plates with smaller hole-pattern leak lesser than plates with larger hole size. When the clearance increases, this effect diminishes, and their leakage control is comparable.

Villasmil [17] used CFD simulations to find friction factor behavior with plates similar to Nava's experiments [16] having circular recesses, using water as the medium. Surfaces with four different kinds of recesses were simulated viz., (a) Tiny with h_φ = 0.99 mm, h_d = 0.28 mm, (b) Small with h_φ = 1.98 mm, h_d = 0.56 mm, (c) Large with h_φ = 3.96 mm, h_d = 1.18 mm, and (d) Big with h_φ = 7.92 mm, h_d = 2.36 mm, each at different clearances. His predictions are shown in Figure 48.

His conclusions based on CFD simulation results are given below with the comparison of conclusions from current test results.

a) *"The tiny recess (TR) emerges as the pattern with the highest friction factor in every clearance, with the exception of the 50 mils (1.270 mm)"* –Exactly the same is observed with the current results. The plate with h_φ = 3.175 mm has minimum leakage at all the tested clearances. (Tests were not done with 1.27 mm clearance).

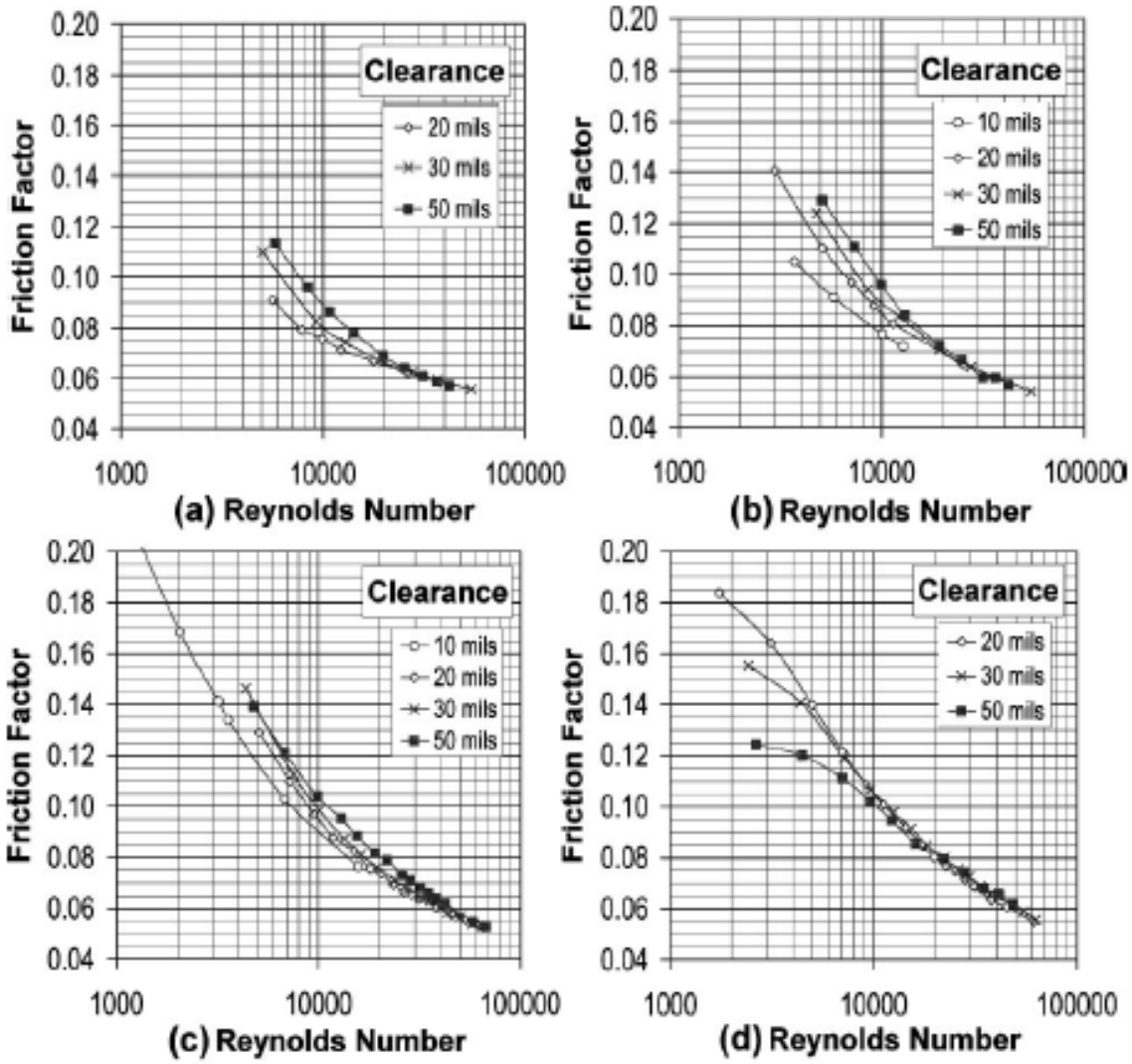

Figure 48. Numerical friction factor in recess geometries (a) big (b) large (c) small (d) tiny by Villasmil [17]

b) *"The big recess (BR) has the lowest friction factor for all clearances"*- The same is observed with the current tests. The plate with h_{φ} = 12.15 mm has maximum leakage at all the tested clearances.

c) *"The friction factor curves of the largest clearance (50 mils, 1.270 mm) in the small and tiny recesses are nearly equal for Reynolds number larger than 10,000"*- In the current tests also, at the tested maximum clearance of 0.681 mm (25 mils), the leakage with both the hole-pattern plates are comparable.(Here all the tests are higher than *Re* = 10,000).

Hence, the test results confirm the friction-factor-variation-trend with hole diameter and clearance, predicted by Villasmil. Note that the area ratio of the recess geometry in the current tests is considerably higher than the area ratios in Villasmil's analyses, and the flow considered in Villasmil's analyses was with water.

8. TEST RESULTS: DYNAMIC PRESSURE DATA

Dynamic pressure data were recorded at eight locations, four on the smooth side plate and four on the HP plate. Figure 49-Figure 50 present the dynamic pressure data for plates with h_d = 2.9 mm at C_{pl} = 0.254 mm and P_{in} = 84 bar at the maximum *Re*. The dominant frequency in all the cases is around 37 kHz.

Kheireddin explained non-friction-factor jump on his tests based on the absence of Helmholtz frequencies. Even in the current tests, Helmholtz frequency is not dominating. For a hole depth of 2.9 mm, considering a static temperature of about 295K, the Helmholtz frequency given by, (f_{res}= c_0/4*h_d), where c_0 is the local acoustic velocity , is found to be around 30kHz. The large diameter holes in the current study are very shallow considering the size of their diameter, while Kheireddin's smaller diameter holes have a higher depth to diameter ratio. Helmholtz's frequency may not be expected to dominate at these situations, as it is a characteristic of features that have a neck section with high depth to diameter ratio.

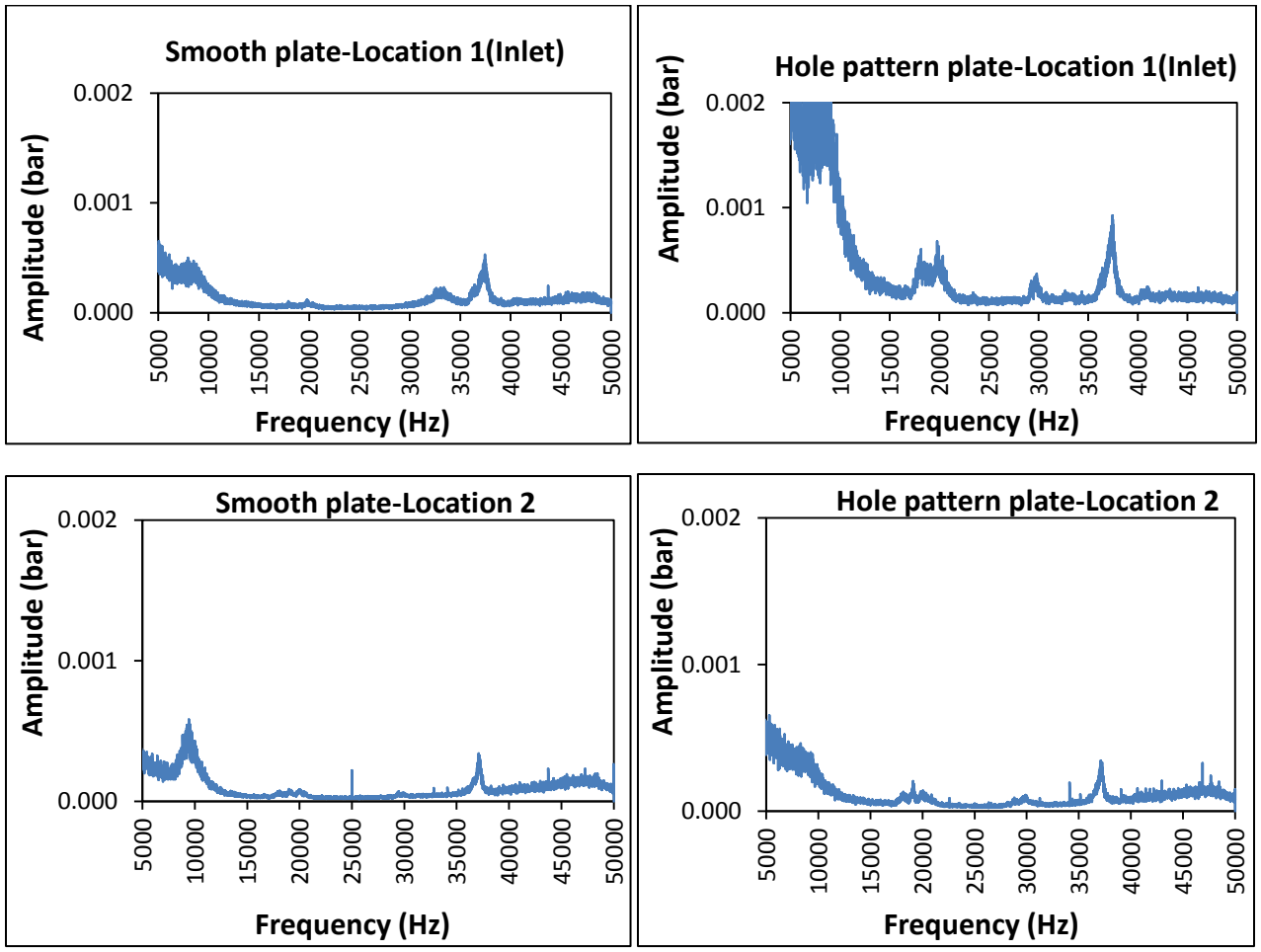

Figure 49. Dynamic pressure at locations 1 and 2 (h_d = 2.9 mm, C_{pl} = 0.254 mm, P_{in} = 84 bar, Re= 32500 (maximum))

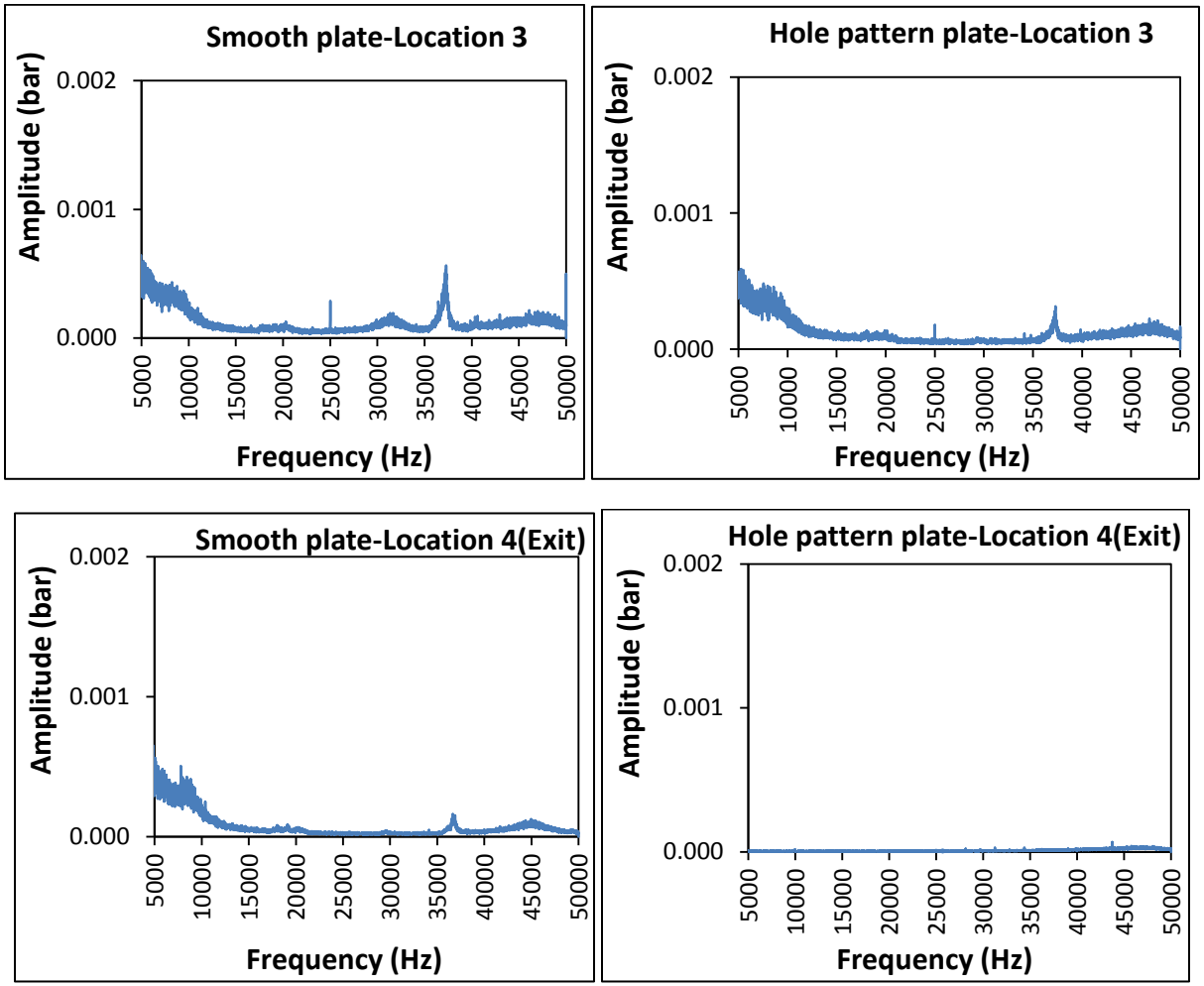

Figure 50. Dynamic pressure at locations 3 and 4 (h_d = 2.9 mm, C_{pl} = 0.254 mm, P_{in} = 84 bar, Re= 32500 (maximum))

Figure 51 compares the spectra from pressure measurements on the smooth plate side to corresponding measurements on HP plate. Both in the case of smooth plate and HP plate, the dominant frequency marginally decreases from inlet to exit; also the magnitude of pulsation is greater at the inlet and reduces gradually towards the exit.

Figure 52 and Figure 53 compare the smooth plate spectra to HP plate spectra on each location from inlet to exit. The dominant frequency coincides at a same location. The amplitude is greater on the HP side close to the inlet and then gradually decreases towards the exit.

The above discussions were found to be valid with the spectra captured in other plates. For the other two plates with h_d of 1.9 mm and 0.9 mm, the Helmholtz frequency is about 45kHz and well above 50kHz respectively. The data is captured at 100 kHz sampling rate, which would make anything beyond 50 kHz not valid. But, in the captured range, for plate with h_d = 1.9 mm, there is no dominant frequency close to 45kHz.

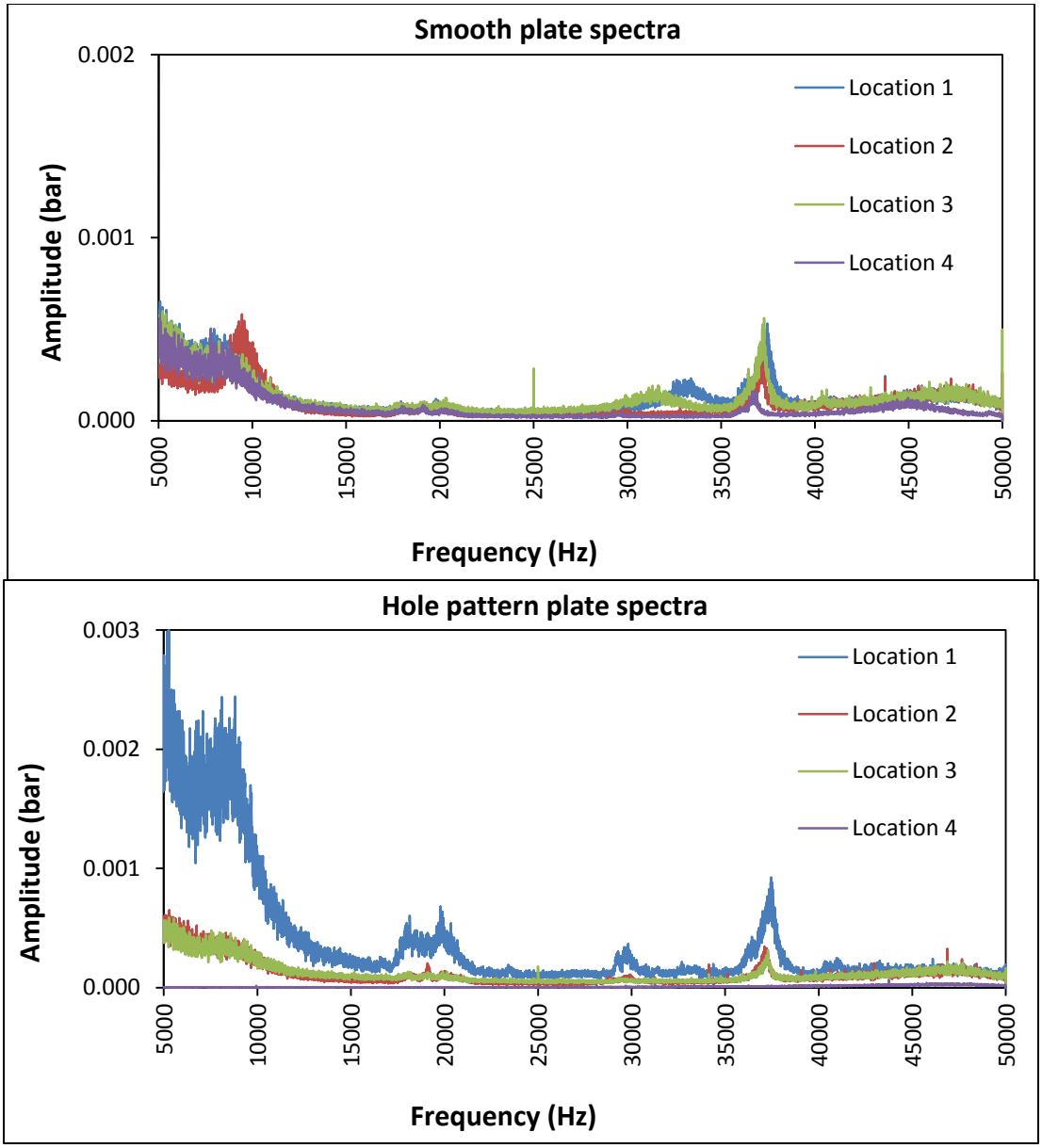

Figure 51. Dynamic pressure looked separately at smooth plate side and HP plate side (h_d = 2.9 mm, C_{pl} = 0.254 mm, P_{in} = 84 bar, Re= 32500 (maximum))

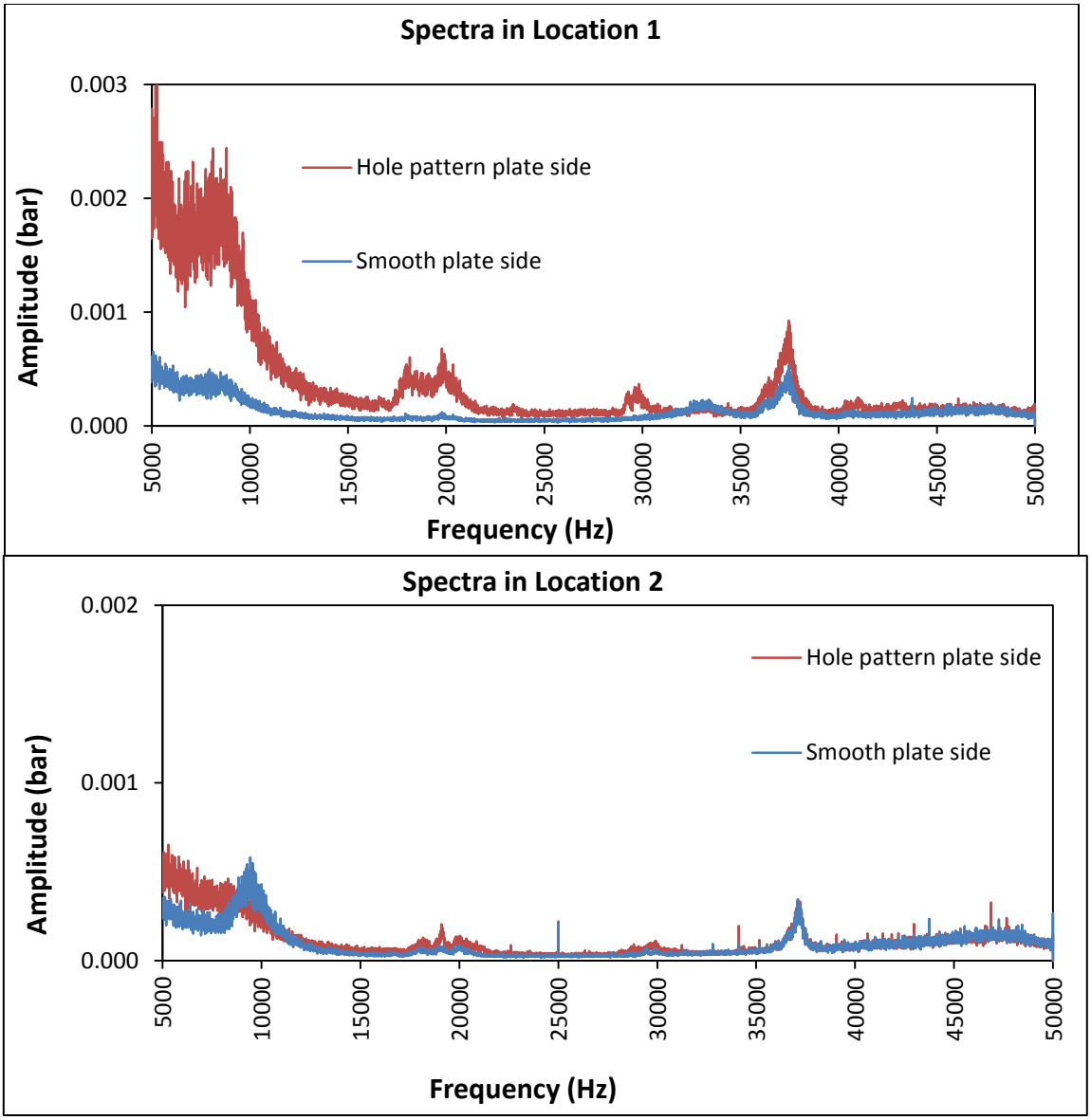

Figure 52. Dynamic pressure looked separately at location 1 and 2

(h_d = 2.9 mm, C_{pl} = 0.254 mm, P_{in} = 84 bar, Re= 32500 (maximum))

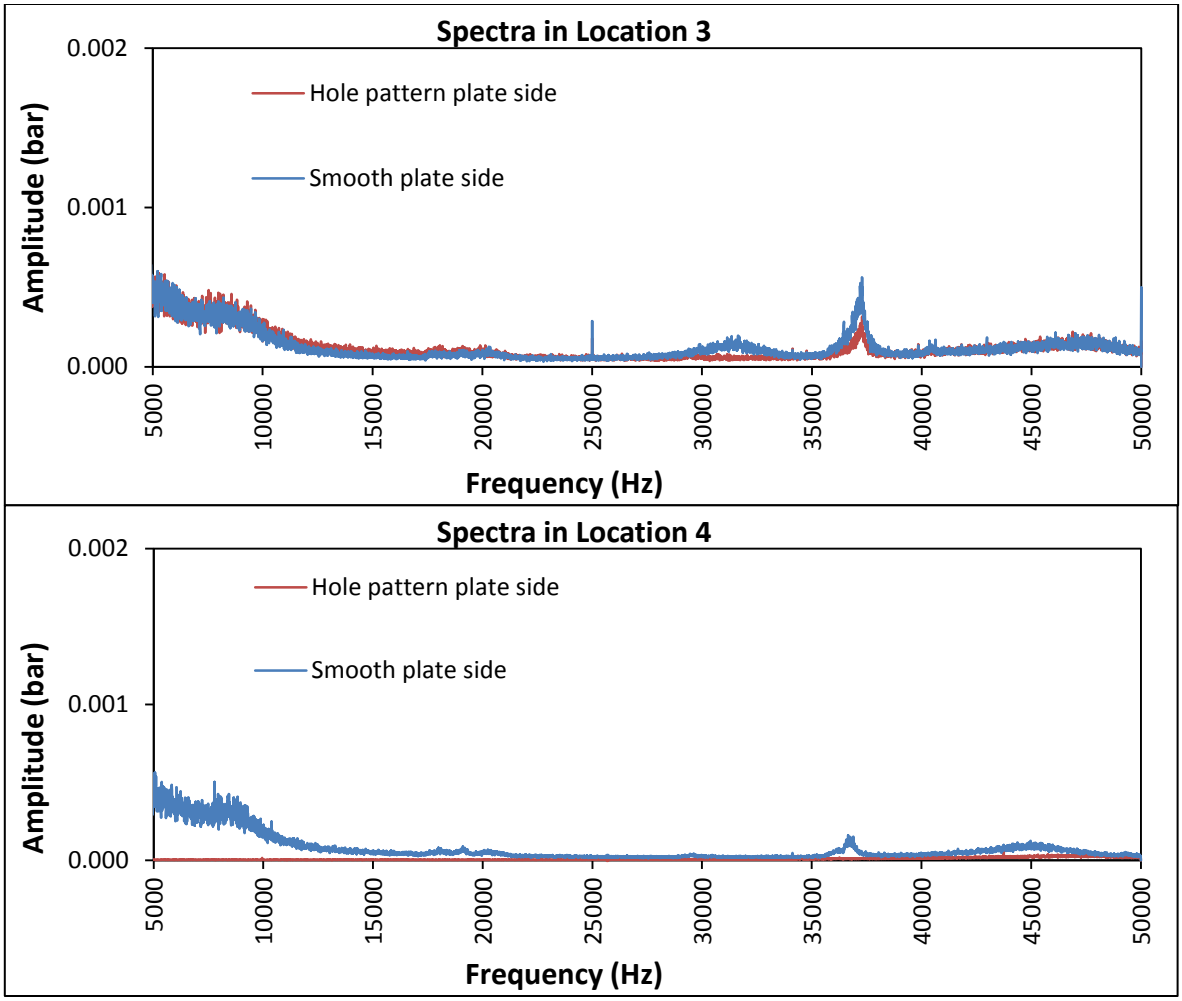

Figure 53. Dynamic pressure looked separately at location 3 and 4

(h_d = 2.9 mm, C_{pl} = 0.254 mm, P_{in} = 84 bar, *Re*= 32500 (maximum))

For establishing the data for any future reference, representative data from each plate tested at 84 bar inlet pressure at all clearances for the maximum *Re* is given in the following Figure 54-Figure 62.

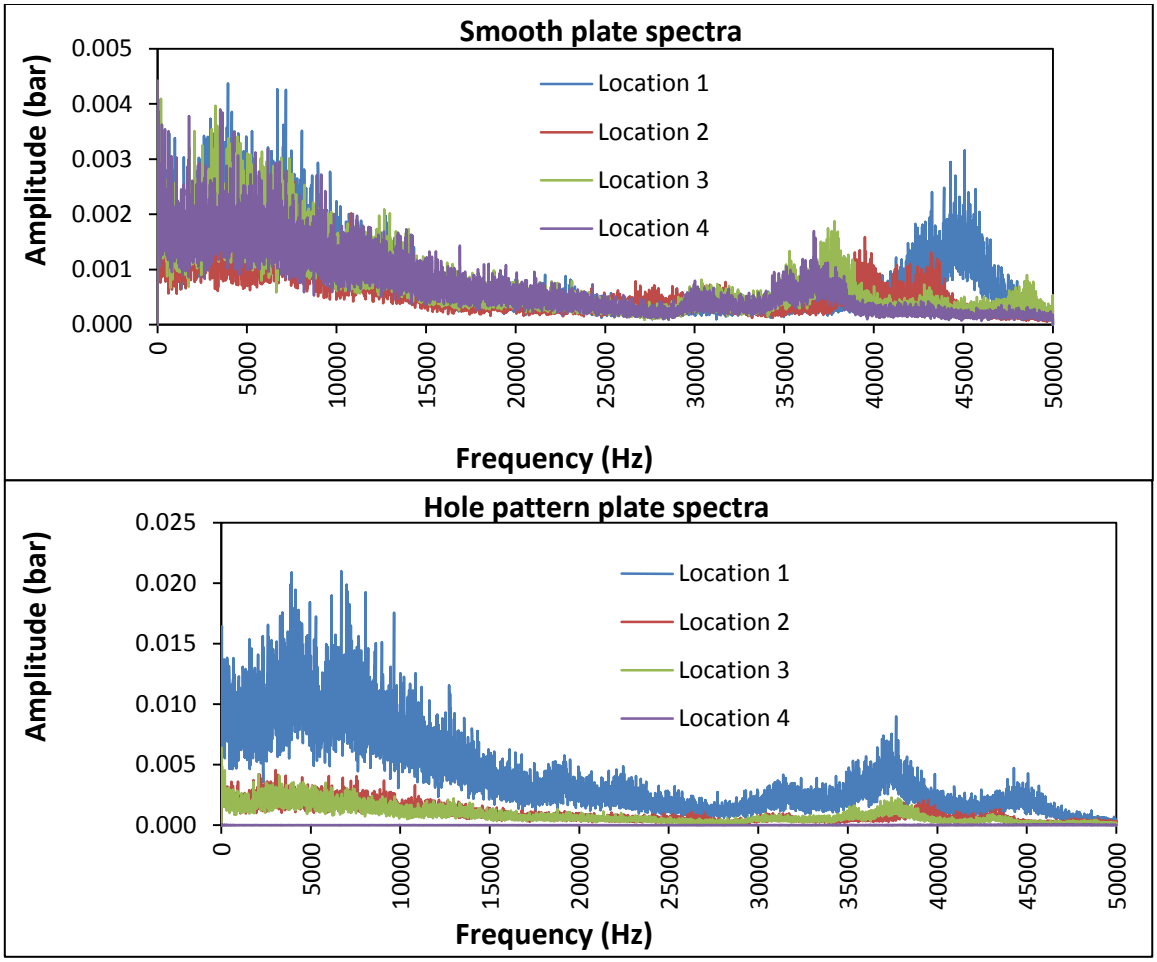

Figure 54. Dynamic pressure data (h_d = 0.9 mm, P_{in} = 84 bar, C_{pl} = 0.254 mm, *Re*=301000)

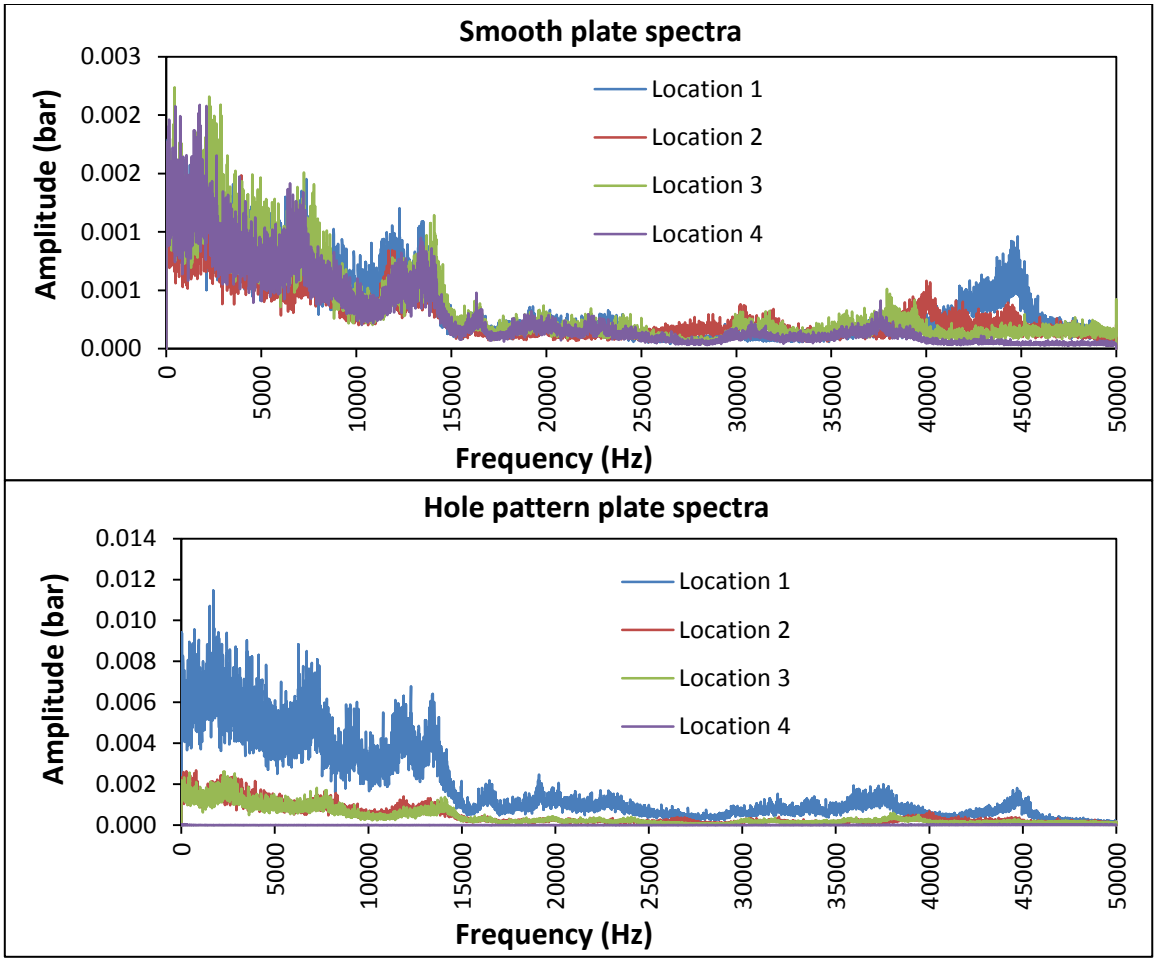

Figure 55. Dynamic pressure data (h_d = 0.9 mm, P_{in} = 84 bar, C_{pl} = 0.381 mm, Re=443000)

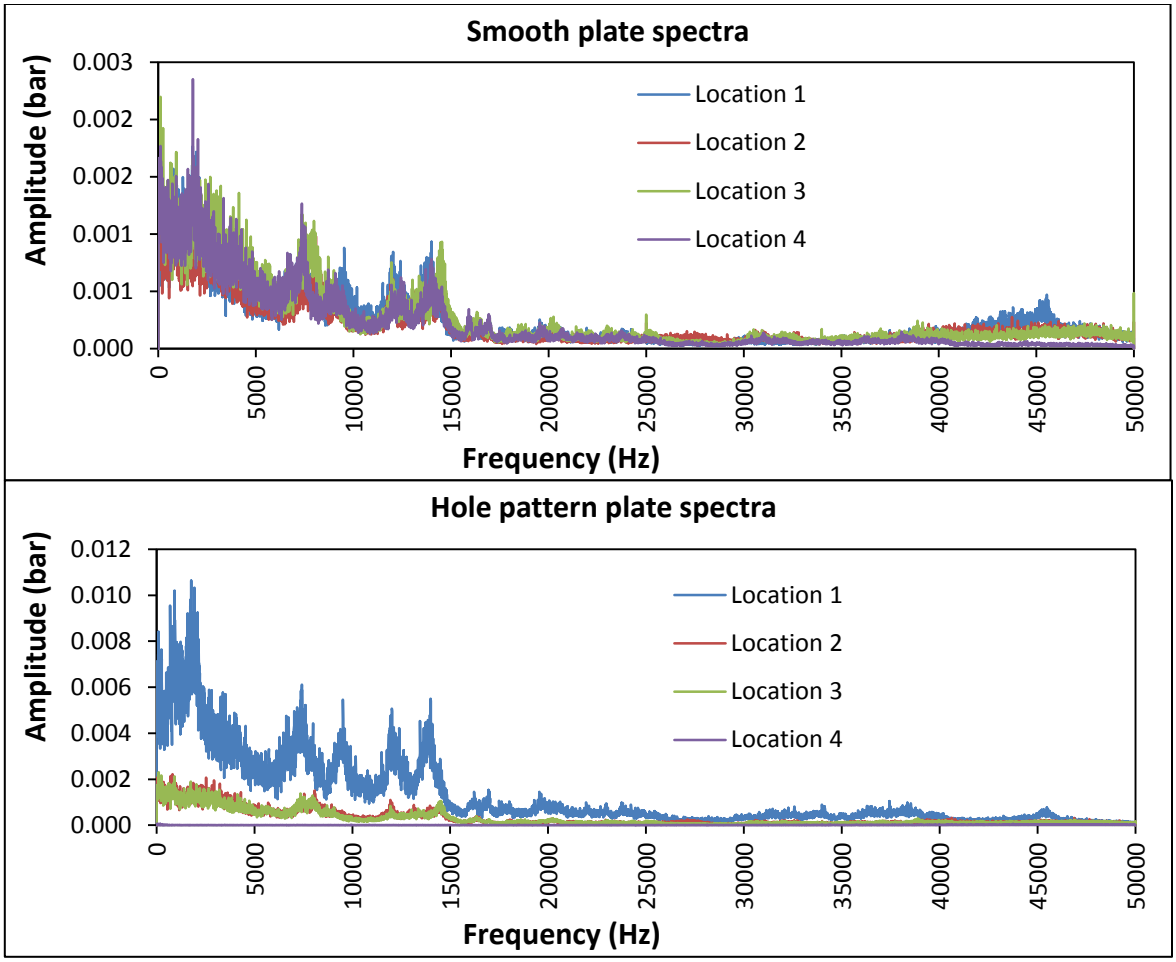

Figure 56. Dynamic pressure data (h_d = 0.9 mm, P_{in} = 84 bar, C_{pl} = 0.635 mm, Re=790000)

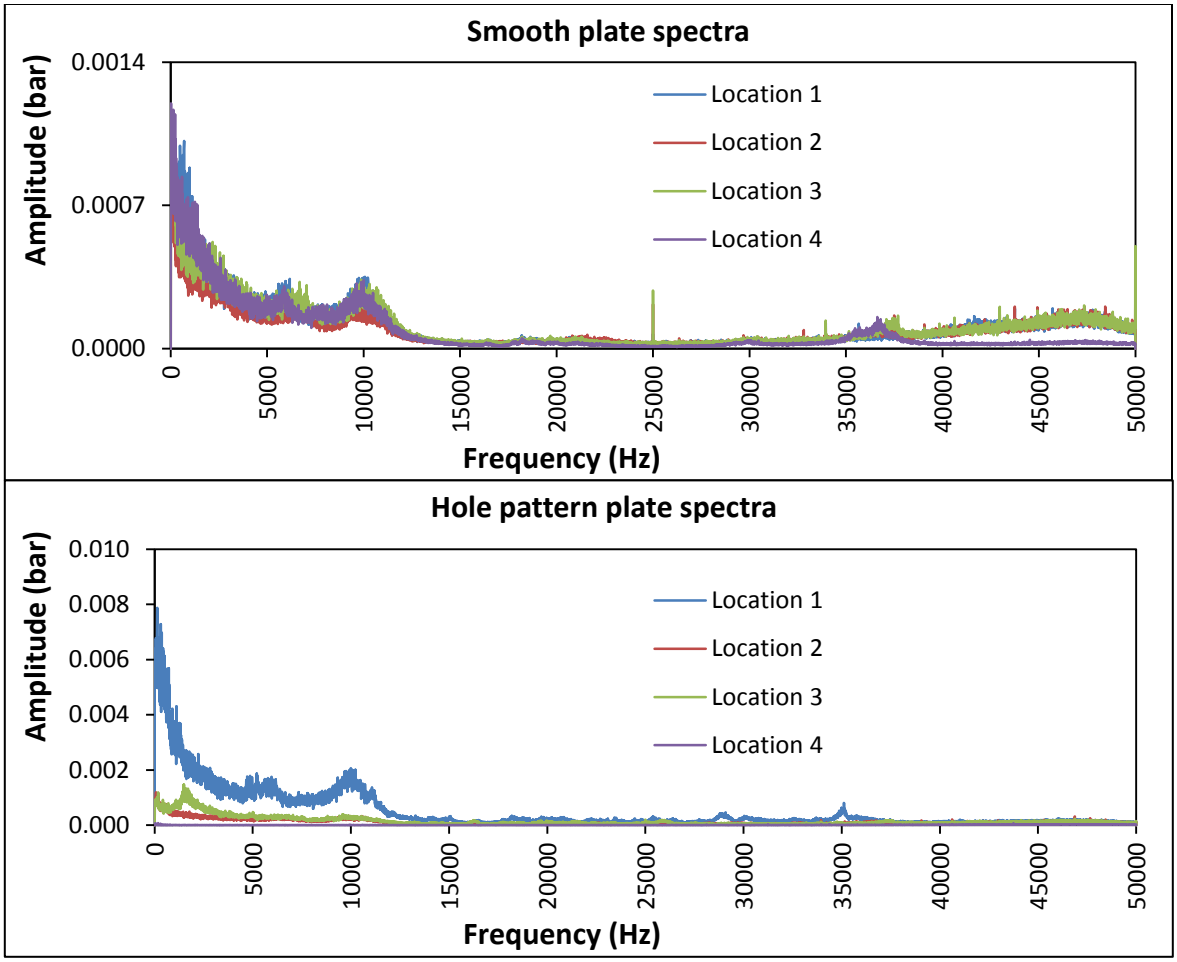

Figure 57. Dynamic pressure data (h_d = 1.9 mm, P_{in} = 84 bar, C_{pl} = 0.254 mm, Re=274000)

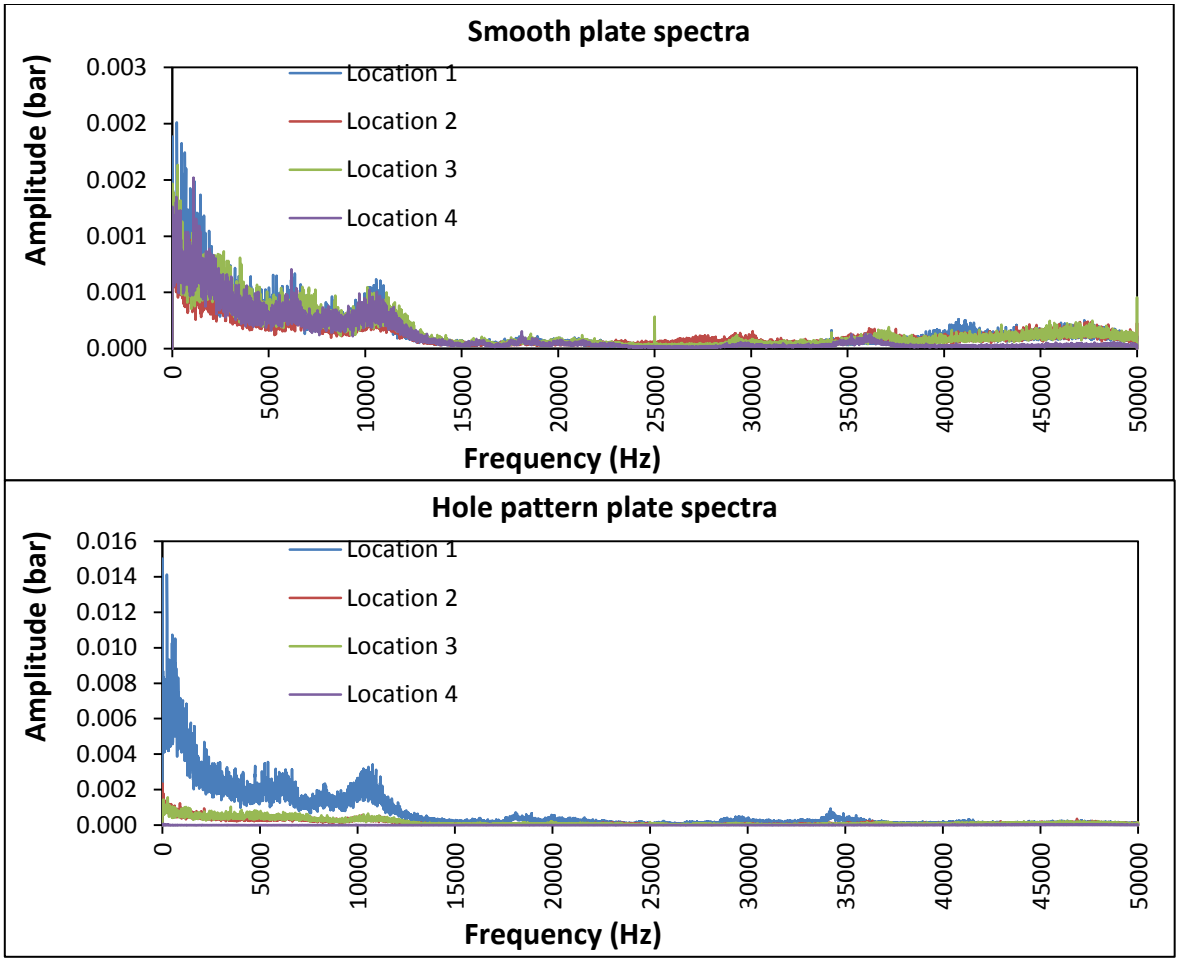

Figure 58. Dynamic pressure data (h_d = 1.9 mm, P_{in} = 84 bar, C_{pl} = 0.381 mm, Re=381000)

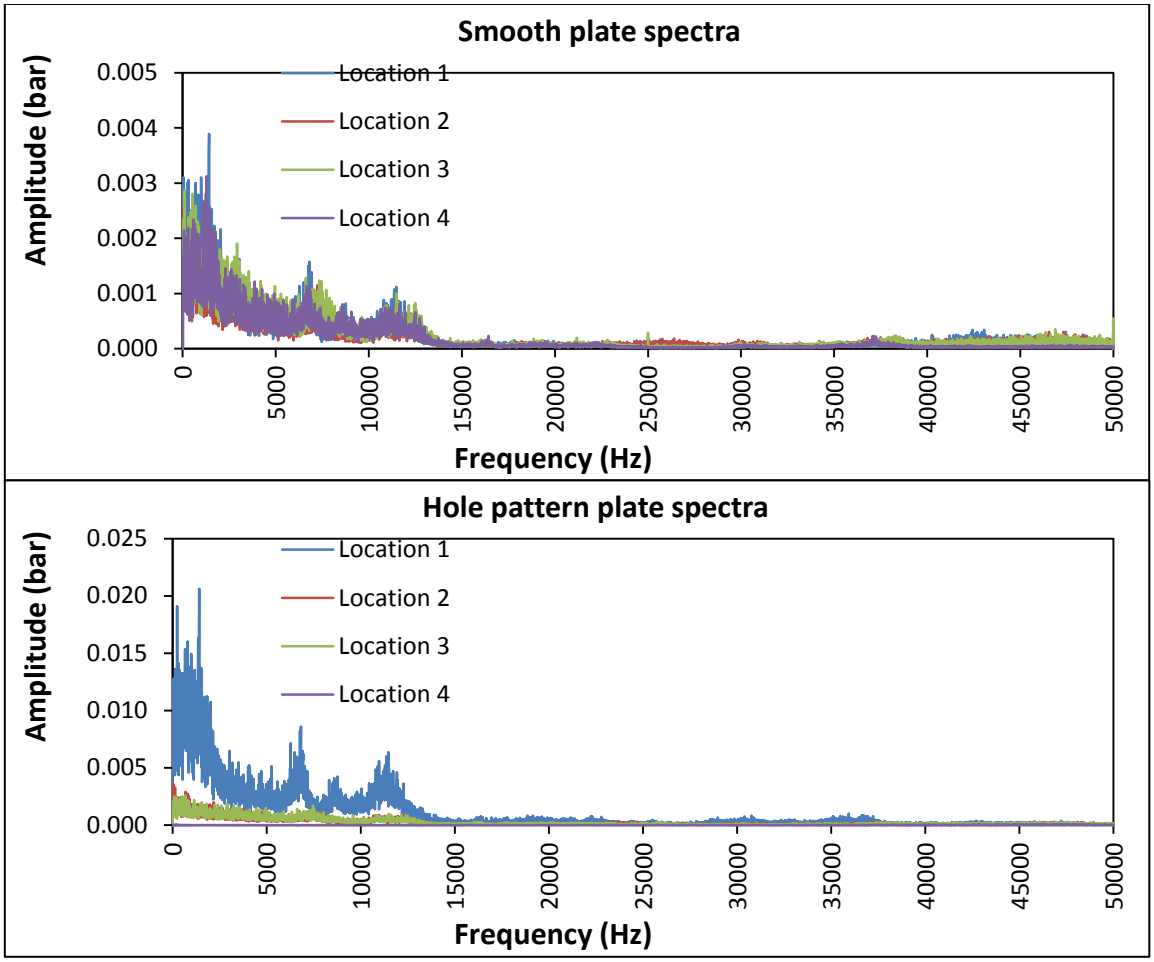

Figure 59. Dynamic pressure data (h_d = 1.9 mm, P_{in} = 84 bar, C_{pl} = 0.635 mm, Re=646000)

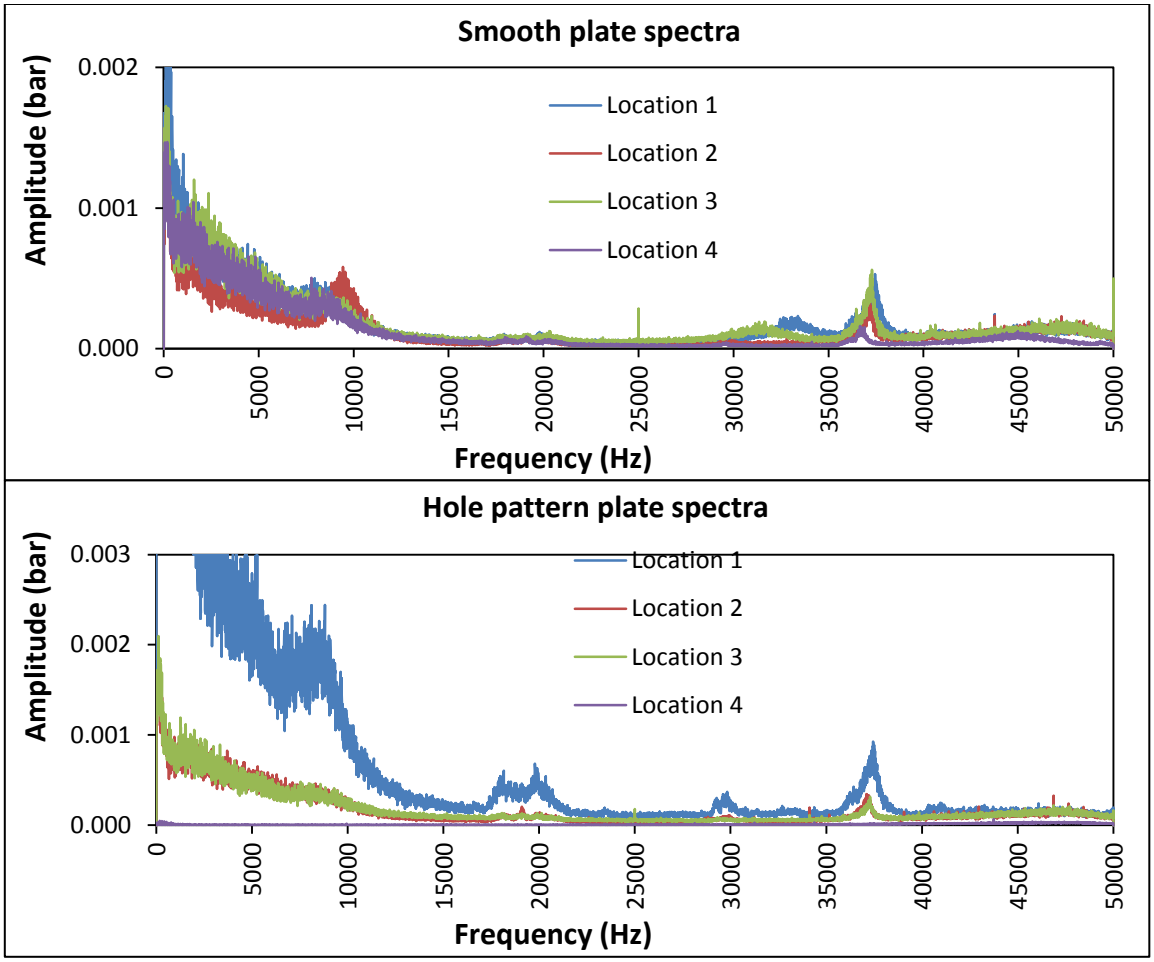

Figure 60. Dynamic pressure data (h_d = 2.9 mm, P_{in} = 84 bar, C_{pl} = 0.254 mm, Re=325000)

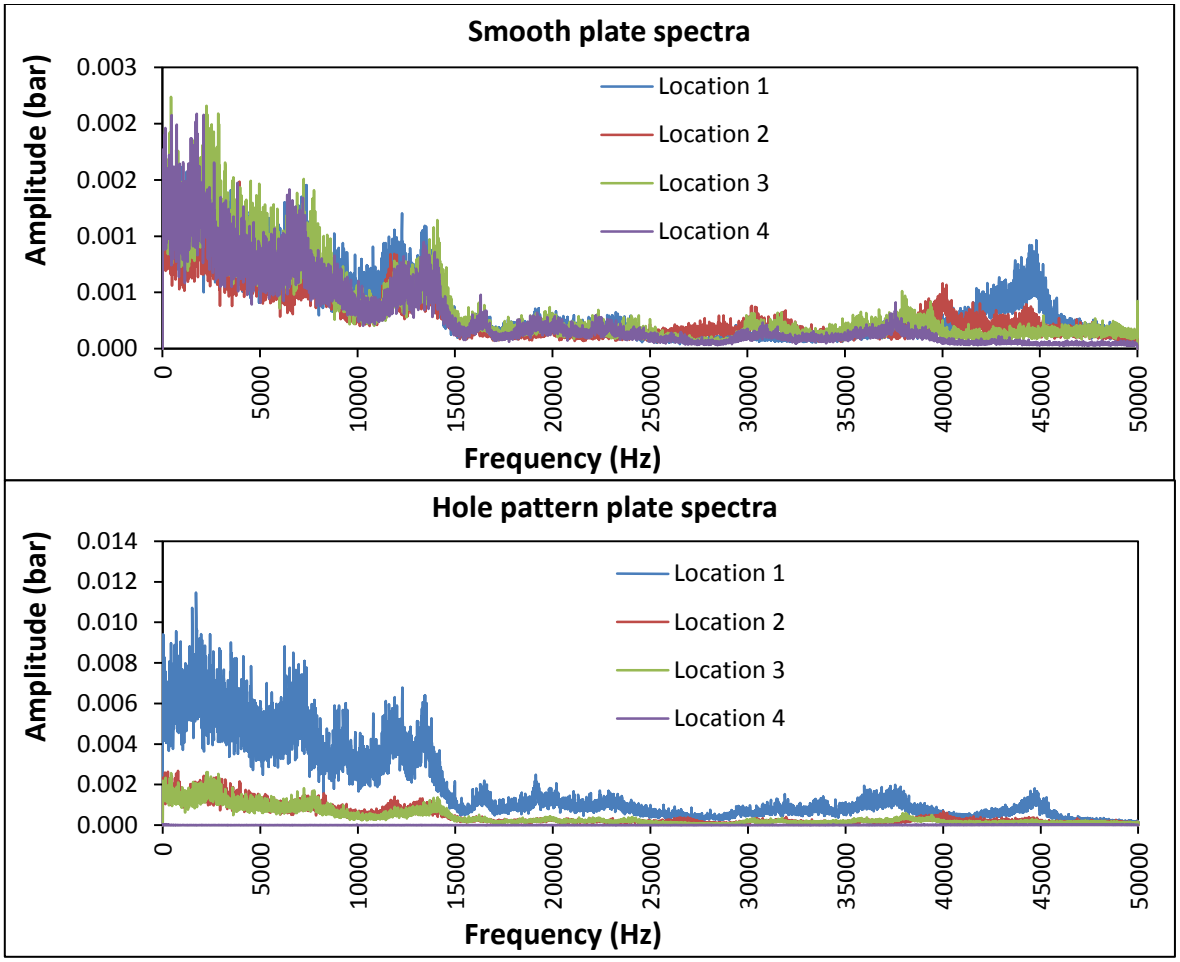

Figure 61. Dynamic pressure data (h_d = 2.9 mm, P_{in} = 84 bar, C_{pl} = 0.381 mm, Re=456000)

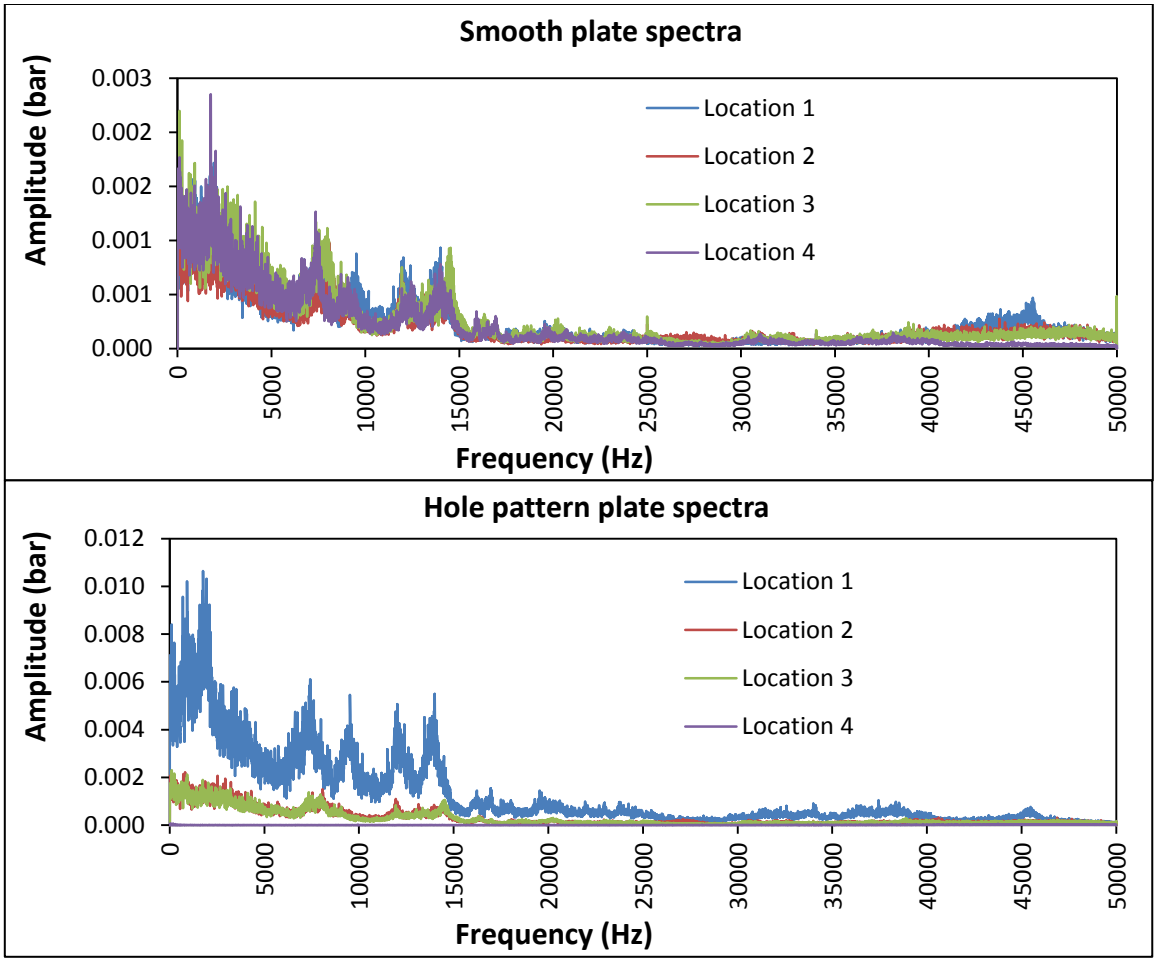

Figure 62. Dynamic pressure data (h_d = 2.9 mm, P_{in} = 84 bar, C_{pl} = 0.635 mm, Re=685000)

9. CONCLUSION

Friction-factor upset phenomenon was overcome and repeatable measurements were ensured in both forward and reveres processes of testing.

The three flat-plates selected for analysis with the HP diameter 12.15 mm and depths 0.9, 1.9, and 2.9 mm were tested with three clearance and three inlet pressure combinations, thereby making nine tests for each plate. Friction factor data in all the tested configurations are presented.

Friction-factor jump is not faced in any of the tests, and the dynamic pressure is found not to have Helmholtz frequency dominance, similar to previous experience with flat-plate test data.

At minimum clearance, plates with smaller hole-pattern have better leakage control than plates with larger hole size. When the clearance increases, this effect diminishes, and their leakage control performance is comparable.

Friction factor increases from plate with hole depth of 0.9 mm to plate with hole depth of 1.9 mm and then reduces towards the plate with hole depth of 2.9 mm. But, this wavy nature is retained in all test clearances and all inlet pressures. Similar observations have been made with honeycomb plates and plates with smaller diameter HP.

Friction factor is significantly affected by clearance. Friction factor increases for increasing clearance and within the tested range of clearances, the plateau clearance was not observed. Previously tested honeycomb plates and small diameter holed plates also exhibited similar behavior.

Reynolds number does not considerably affect friction factor. Still, in all test cases, friction factor either continuously decreases or remains almost constant with increasing Reynolds number. The effect is not random in any test configuration.

Inlet pressure does not significantly affect friction factor. At low clearances, tests at low input pressure results in higher values of friction factor.

The two friction factor models created based on the experimental data fit the data well and their incorporation into ISOTSEAL might improve the prediction of leakage and dynamic coefficients of a similar HP seal.

REFERENCES

[1] Sprowl,T.B.,2003 “A study of the effects of inlet preswirl on the dynamic coefficients of a straight-bore honeycomb gas damper seal” M.S. Thesis, Texas A&M University, College Station, TX.

[2] Childs, D.W., and Moyer, D.,1985, “Vibrations Characteristics of the HPOTP (High Pressure Oxygen Turbo Pump) for the SSME (Space Shuttle Main Engine),”ASME Journal of Engineering for Gas Turbine and Power, **107**, no.1, pp. 152-159.

[3] Zeidan, F., Perez, R., and Stephenson, E., 1993, “The Use of Honeycomb Seals in Stabilizing Two Centrifugal Compressors,” Proceedings of the Twenty-Second Turbomachinery Symposium, The Turbomachinery Laboratory, Texas A&M University, College Station, TX, pp. 3-15.

[4] Armstrong, J., and Perricone, F., 1996, “Turbine Instability Solution-Honeycomb Seals”, Proceedings of the 25th Turbomachinery Symposium, Turbomachinery Laboratory, Texas A&M University, College Station, TX, pp. 47-56.

[5] Ha, T.W., 1992, “Rotordynamic Analysis of Annular Honeycomb-Stator Turbulent Gas Seals Using Friction factor Model Based on Flat Plate Tests,” PhD. Dissertation, Department of Mechanical Engineering, Texas A&M University, College Station, TX.

[6] Childs, D.W., and Yu, Z., 1988, “A Comparison of Experimental Rotordynamic Coefficients and Leakage Characteristics Between Hole-Pattern Gas

Damper Seals and a Honeycomb Seal," Journal of Engineering for Gas Turbines and Power, **120**, pp. 778-783.

[7] Lomakin, A.A., 1958, "Calculation of Critical Speed and Securing of Dynamic Stability of Hydraulic High Pressure Pumps with Reference to the Forces Arising in the Gap Seals," Energomachinostroenie,**Vol.**4,no. 1,pp. 1-5.

[8] Childs, D.W., 1993, *Turbomachinery Rotordynamics: Phenomena, Modeling and Analysis*, John Wiley & Sons, Inc., New York.

[9] Hirs, G.A., 1973, "Bulk-flow Theory for Turbulence in Lubricant Films", ASME Journal of Lubrication Technology, **75**, pp. 137-146.

[10] Nelson, C. C., 1984, "Analysis for Leakage and Rotordynamic Coefficients of Surface-Roughened Tapered Annular Gas Seals," ASME Journal of Engineering for Gas Turbines and Power, **106**, pp. 927-934.

[11] Kleyhans,G., 1996, "A Two Control Volume Bulk Flow Rotordynamic Analysis for Smooth-rotor/Honeycomb-stator Gas Annular Seals," Ph.D. Dissertation, Texas A&M University, College Station,TX.

[12] Wade, J., 2004, "Test Versus Predictions for Rotordynamic Coefficients and Leakage Rates for Hole-Pattern Gas Seals at Two Clearances in Choked and Unchoked Conditions," M.S. Thesis, Department of Mechanical Engineering, Texas A&M University, College Station, TX.

[13] Moody, L.F., 1944, "Friction Factors for Pipe Flow," Trans. Am. Soc. Mech. Engrs. **66**, pp.671-684.

[14] Ha, T.W., 1989, “Friction Factor Data for Flat-Plate Tests of Smooth and Honeycomb Surfaces,” M.S. Thesis, Department of Mechanical Engineering, Texas A&M University, College Station, TX.

[15] Thomas, J., 1992, “Determination of Variation of Friction Factor with Reynolds number for Flow Between Two Closely Spaced Rough Plates,” Senior Thesis, Texas A&M University, College Station, TX.

[16] Nava, D.L., 1993, “Observations of Friction factors for Various Roughness Patterns in Channel Flow,” M.S. Thesis, Department of Mechanical Engineering, Texas A&M University, College Station, TX.

[17] Villasmil, L.A., 2002, “Understanding the Friction Factor Behavior in Liquid Annular Seals with Deliberately Roughened Surfaces, a CFD Approach,” M.S. Thesis, Department of Mechanical Engineering, Texas A&M University, College Station, TX.

[18] Villasmil, L.A., 2006, “Parameters Defining Flow Resistance and the Friction Factor Behavior in Liquid Annular Seals with Deliberately Roughened Surfaces,” Ph.D. Dissertation, Texas A&M University, College Station, TX.

[19] DeOtte, R., Morrison, G.L., Nava D.L., and Hess, J.C., 1994, “A Study of Friction factors in Channel Flow Between Plates with Highly Roughened Surfaces,” Fluid Machinery , U.S. Rohatgi and A. Ogut, eds, ASME, New York.

[20] Childs, D.W., and Fayolle, P., 1999, “Test Results for Liquid ‘Damper’ Seals Using a Round-Hole Roughness Pattern for the Stators,” ASME Journal of Tribology, **121**, pp. 42-49.

[21] Arghir, M., Billy, F.,Pineau, G., and Frêne, J., 2007, "Theoretical Analysis of Textured 'Damper' Annular Seals," ASME Journal of Tribology,**129**, pp.669-678.

[22] Kheireddin, B.A., 2009, " Investigation of the Friction Factor Behavior for Flat Plate Tests of Smooth and Roughened Surfaces with Supply Pressures up to 84 Bars" . M.S. Thesis, Texas A&M University, College Station, TX.

[23] Morrison, G.L., 2008, "Gas Dynamics Class Notes," Texas A&M University, College Station, TX.

[24] John, J.E.A., 2006, *Gas Dynamics,* Allyn and Bacon, Newton, MA.

[25] Hess, J.C., 1993, "Dynamic Pressure Response of Water Flow Between Closely Spaced Roughened Flat Plates," M.S. Thesis, Texas A&M University, College Station, TX.

[26] Schlichting, H., 1979, *Boundary-Layer Theory*, 7th Ed., McGraw-Hill, New York, NY,

[27] Coleman, H.W., 1989, *Experimentation and Uncertainty Analysis for Engineers*, John Wiley & Sons. Inc, New York.

APPENDIX A

FRICTION FACTOR VALUES FOR ALL CONFIGURATIONS

Table 3. Friction factor data: h_d = 0.9 mm, C_{pl} = 0.254 mm, P_{in} = 56 bar

h_d: 0.9 mm						C_{pl}: 0.254 mm					P_{in}: 56bar(800psi)				
Sl.No.	Flow	Static pressure (psi)											T_t	Re	f_f
	Kg/s	Inlet	1	2	3	4	5	6	7	8	9	Exit	K		
1	0.088	806.3	765.8	735.1	704.8	671.4	634.2	602.3	561.2	516.9	468.1	341.0	293.2	193000	0.00561
2	0.084	795.1	758.2	730.5	702.8	672.5	638.8	610.6	574.3	535.7	494.2	397.8	293.1	184000	0.00567
3	0.083	810.3	775.0	748.8	722.6	693.8	662.1	635.6	601.8	566.1	528.5	445.1	293.1	182000	0.00572
4	0.077	796.4	765.8	743.7	721.0	696.4	669.4	647.1	619.0	589.7	559.6	496.1	293.1	168000	0.00584
5	0.073	807.6	780.7	761.8	741.7	720.4	696.9	677.9	653.9	629.3	604.6	553.7	293.2	159000	0.00592
6	0.066	799.8	777.9	763.4	747.0	730.0	711.0	696.1	677.4	658.4	639.8	602.0	293.3	145000	0.00588
7	0.059	801.6	784.7	774.6	761.8	749.0	734.4	723.5	709.7	695.8	682.6	655.6	293.4	130000	0.00579
8	0.049	798.1	785.9	779.9	770.3	761.1	750.4	742.9	733.2	723.6	714.7	696.4	293.5	106000	0.00636

Table 4. Friction factor data: h_d = 0.9 mm, C_{pl} = 0.254 mm, P_{in} = 70 bar

h_d: 0.9 mm						C_{pl}: 0.254 mm					P_{in}: 70bar(1000psi)				
Sl.No.	Flow rate	Static pressure (psi)											T_t	Re	f_f
	Kg/s	Inlet	1	2	3	4	5	6	7	8	9	Exit	K		
1	0.114	1000.1	953.5	916.9	881.7	841.3	797.6	758.4	709.5	656.4	598.1	434.2	295.2	250000	0.00487
2	0.112	1004.8	960.0	925.4	891.7	853.5	812.1	775.4	729.8	680.7	627.5	488.7	295.3	245000	0.00492
3	0.108	1001.1	959.4	928.0	896.6	861.5	823.7	790.4	749.5	705.8	659.2	544.8	295.5	237000	0.00493
4	0.105	1005.1	967.2	938.5	909.3	877.3	842.8	812.8	776.1	737.4	696.6	600.2	295.7	229000	0.00498
5	0.102	1010.5	975.2	948.9	922.0	892.7	861.1	834.0	801.0	766.4	730.4	647.4	295.9	223000	0.00495
6	0.095	1004.1	973.1	950.8	927.1	901.7	874.4	851.4	823.5	794.4	764.6	697.7	296.1	208000	0.00505
7	0.088	996.6	970.1	951.9	931.6	910.8	887.4	868.5	845.7	822.1	798.2	745.6	296.2	191000	0.00508
8	0.080	999.4	977.4	963.0	945.7	928.6	908.6	893.1	874.6	855.5	836.4	794.6	296.4	174000	0.00529
9	0.069	997.7	981.4	972.1	959.1	946.6	931.5	920.5	907.3	893.6	880.5	851.3	296.6	151000	0.00536
10	0.060	1002.8	990.8	985.5	975.9	966.6	955.2	947.9	938.1	928.4	919.5	898.1	296.7	131000	0.00527
11	0.046	1005.3	998.7	998.3	992.4	987.6	981.2	977.4	972.5	967.0	963.1	952.3	296.9	101000	0.00488

Table 5. Friction factor data: h_d = 0.9 mm, C_{pl} = 0.254 mm, P_{in} = 84 bar

h_d: 0.9 mm						C_{pl}: 0.254 mm					P_{in}: 84bar(1200psi)				
Sl.No.	Flow	Static pressure (psi)											T_t	Re	f_f
	Kg/s	Inlet	1	2	3	4	5	6	7	8	9	Exit	K		
1	0.137	1192.2	1135.8	1092.4	1050.1	1001.9	950.2	903.3	845.4	781.6	711.3	513.9	296.6	301000	0.00470
2	0.133	1187.0	1132.1	1090.2	1049.4	1002.9	953.2	908.4	853.3	793.0	727.4	557.0	296.7	291000	0.00490
3	0.132	1187.3	1134.2	1094.2	1054.9	1010.4	962.9	920.3	868.2	811.5	750.4	600.2	296.8	290000	0.00478
4	0.129	1190.7	1140.1	1102.3	1065.0	1022.9	978.0	938.1	889.5	837.1	781.2	647.9	296.9	283000	0.00486
5	0.126	1194.6	1146.4	1111.0	1075.6	1035.9	993.7	956.4	911.2	863.0	812.1	692.9	297.1	276000	0.00489
6	0.123	1200.3	1155.0	1122.3	1089.2	1052.4	1013.3	979.0	937.7	894.0	848.7	746.0	297.3	269000	0.00493
7	0.119	1206.1	1163.9	1134.2	1103.5	1069.8	1033.7	1002.7	965.2	926.1	885.7	795.3	297.4	261000	0.00491
8	0.112	1202.7	1165.2	1139.7	1112.4	1082.9	1051.2	1024.4	992.2	958.9	924.8	848.6	297.6	245000	0.00501
9	0.106	1201.9	1168.2	1146.3	1121.8	1095.7	1067.7	1044.2	1016.1	987.2	958.0	892.7	297.7	231000	0.00509
10	0.098	1202.9	1174.2	1156.8	1135.9	1114.2	1090.5	1071.2	1048.2	1024.5	1001.1	948.8	297.9	215000	0.00506
11	0.089	1203.3	1179.3	1166.1	1148.2	1130.4	1110.7	1095.0	1076.3	1057.1	1038.7	996.6	298.0	196000	0.00516
12	0.080	1203.0	1184.1	1175.5	1160.7	1147.0	1131.5	1119.6	1105.5	1090.9	1077.4	1046.1	298.2	174000	0.00516
13	0.053	1201.9	1193.7	1193.6	1185.8	1180.5	1173.2	1168.7	1163.4	1157.3	1153.3	1141.3	298.4	115000	0.00510

Table 6. Friction factor data: h_d = 0.9 mm, C_{pl} = 0.381 mm, P_{in} = 56 bar

h_d: 0.9 mm						C_{pl}: 0.381 mm					P_{in}:56bar(800psi)				
Sl.No.	Flow rate	Static pressure (psi)											T_t	Re	f_f
	Kg/s	Inlet	1	2	3	4	5	6	7	8	9	Exit	K		
1	0.135	797.9	769.9	739.9	707.1	669.9	630.4	594.2	550.0	501.0	445.8	323.0	290.2	295000	0.00874
2	0.130	797.7	771.6	744.2	713.8	679.6	643.6	611.1	571.7	528.8	482.2	392.4	290.5	285000	0.00882
3	0.126	799.2	775.3	750.9	723.3	692.7	660.4	631.9	597.4	560.8	521.9	452.1	290.8	275000	0.00881
4	0.120	799.3	777.9	756.5	731.8	704.8	676.2	651.5	621.8	590.6	558.3	503.0	290.8	262000	0.00885
5	0.113	800.9	781.7	763.2	741.2	717.4	692.2	670.9	645.1	618.5	591.5	546.3	290.9	248000	0.00896
6	0.107	812.6	795.8	780.1	760.8	740.3	718.4	700.2	678.4	656.0	633.7	596.6	291.2	235000	0.00902
7	0.094	805.6	792.5	781.5	766.4	750.9	734.1	720.8	704.7	688.4	672.5	646.4	291.3	205000	0.00921
8	0.080	808.5	798.9	792.3	781.2	770.3	758.1	749.0	738.0	726.8	716.4	698.9	291.5	175000	0.00931
9	0.058	799.9	794.6	793.3	786.9	781.4	774.6	770.3	765.0	759.5	754.9	746.3	291.7	126000	0.00932

Table 7. Friction factor data: h_d = 0.9 mm, C_{pl} = 0.381 mm, P_{in} = 70 bar

h_d: 0.9 mm						C_{pl}: 0.381 mm					P_{in}:70bar(1000psi)				
Sl.No.	Flow rate	Static pressure (psi)											T_t	Re	f_f
	Kg/s	Inlet	1	2	3	4	5	6	7	8	9	Exit	K		
1	0.171	1005.4	970.0	932.3	891.8	845.5	796.1	750.5	694.8	633.2	563.9	411.5	291.9	373000	0.00853
2	0.169	1000.6	966.3	930.2	891.1	846.7	799.4	756.1	703.2	645.4	581.3	451.3	292.2	369000	0.00842
3	0.164	997.2	964.5	930.3	893.2	851.3	806.7	766.3	717.1	663.9	606.1	495.7	292.4	360000	0.00846
4	0.159	994.5	963.8	932.3	897.7	859.0	817.8	780.9	736.4	688.7	637.8	545.6	292.7	348000	0.00850
5	0.152	987.3	959.1	930.9	899.4	864.5	827.4	794.7	755.4	713.8	670.3	594.5	292.9	333000	0.00854
6	0.149	1008.8	982.8	957.5	928.6	896.9	863.4	834.2	799.3	762.8	725.3	661.5	293.2	325000	0.00850
7	0.141	1010.7	987.1	964.7	938.5	910.1	880.0	854.3	823.6	791.7	759.3	704.9	293.4	309000	0.00864
8	0.131	1005.0	984.3	965.4	942.5	918.1	892.0	870.2	844.3	817.5	790.7	746.6	293.5	287000	0.00884
9	0.120	1006.1	989.1	974.8	956.1	936.5	915.5	898.4	878.2	857.6	837.4	803.8	293.7	263000	0.00869
10	0.105	998.0	984.7	974.8	960.0	945.1	928.7	915.9	900.8	885.5	870.9	846.4	293.7	230000	0.00888
11	0.090	1007.8	997.8	992.0	980.8	970.1	957.9	948.9	938.2	927.5	917.6	900.8	293.9	197000	0.00906
12	0.068	1003.3	997.1	996.1	989.1	983.1	975.6	970.9	965.1	959.2	954.4	945.3	294.0	149000	0.00907

Table 8. Friction factor data: h_d = 0.9 mm, C_{pl} = 0.381 mm, P_{in} = 84 bar

h_d: 0.9 mm						C_{pl}: 0.381 mm					P_{in}:84bar(1200psi)				
Sl.No.	Flow rate	Static pressure (psi)											T_t	Re	f_f
	Kg/s	Inlet	1	2	3	4	5	6	7	8	9	Exit	K		
1	0.203	1192.9	1150.5	1106.2	1058.0	1003.4	945.1	891.6	825.7	752.9	670.5	484.0	295.0	443000	0.00832
2	0.200	1193.2	1151.9	1109.2	1062.7	1010.2	954.2	903.0	840.8	772.3	696.1	548.3	294.8	437000	0.00836
3	0.198	1200.2	1160.0	1118.9	1073.8	1023.1	969.0	920.1	860.8	796.0	724.9	592.9	295.0	433000	0.00839
4	0.191	1186.6	1149.5	1112.2	1070.7	1024.5	975.3	931.2	878.1	821.0	759.6	648.5	295.2	417000	0.00832
5	0.188	1196.7	1161.0	1125.7	1086.0	1042.0	995.3	953.8	904.1	851.0	794.7	690.7	295.4	411000	0.00834
6	0.180	1194.7	1161.7	1129.6	1093.1	1053.0	1010.4	972.9	928.4	881.4	832.3	749.1	295.6	393000	0.00849
7	0.177	1210.2	1178.8	1148.9	1114.4	1076.7	1036.6	1001.8	960.3	917.1	872.6	798.3	295.7	387000	0.00850
8	0.166	1199.8	1172.1	1146.6	1116.2	1083.4	1048.6	1018.8	983.5	947.0	910.1	849.9	295.8	362000	0.00858
9	0.156	1197.8	1172.8	1150.6	1123.3	1094.3	1063.3	1037.2	1006.4	974.7	943.1	891.3	295.9	342000	0.00870
10	0.144	1203.3	1182.0	1164.4	1141.0	1116.9	1090.9	1069.5	1044.2	1018.5	993.3	948.7	296.1	315000	0.00883
11	0.131	1206.0	1188.4	1175.3	1155.9	1136.4	1115.2	1098.3	1078.4	1058.3	1039.0	1003.9	296.2	286000	0.00887
12	0.114	1201.3	1187.3	1178.5	1163.0	1148.2	1131.5	1118.7	1103.6	1088.4	1074.2	1048.1	296.3	249000	0.00920
13	0.100	1202.1	1191.3	1186.5	1174.4	1163.6	1150.8	1141.6	1130.7	1119.8	1110.0	1091.5	296.3	219000	0.00897
14	0.078	1214.4	1207.2	1207.3	1198.7	1192.4	1184.0	1178.7	1172.4	1165.9	1160.9	1150.2	296.4	170000	0.00921

Table 9. Friction factor data: h_d = 0.9 mm, C_{pl} = 0.635 mm, P_{in} = 56 bar

h_d: 0.9 mm						C_{pl}: 0.635 mm					P_{in}:56bar(800psi)				
Sl.No.	Flow rate	Static pressure (psi)											T_t	Re	f_f
	Kg/s	Inlet	1	2	3	4	5	6	7	8	9	Exit	K		
1	0.241	796.5	776.8	753.1	718.2	677.7	635.8	594.6	549.7	494.6	435.3	482.6	295.2	527000	0.01320
2	0.233	799.9	781.7	760.4	728.4	691.7	653.8	617.4	578.2	531.4	483.2	556.6	295.8	509000	0.01327
3	0.227	802.8	785.7	766.2	736.3	702.2	667.2	633.9	598.1	556.3	514.1	602.6	296.0	495000	0.01336
4	0.219	809.2	793.5	776.1	748.8	718.0	686.3	656.8	625.2	588.9	553.3	649.1	296.3	478000	0.01340
5	0.204	807.0	793.3	779.0	755.4	729.2	702.3	677.8	651.6	622.2	594.0	698.5	296.6	446000	0.01359
6	0.188	801.8	790.1	778.7	758.6	736.7	714.2	694.2	672.9	649.0	626.9	748.8	296.8	411000	0.01373
7	0.169	807.3	797.9	789.9	773.8	756.9	739.2	724.0	707.8	689.9	673.8	804.5	297.0	369000	0.01391
8	0.146	809.1	802.0	797.1	784.9	772.6	759.3	748.6	737.0	724.4	713.2	852.1	297.2	320000	0.01426
9	0.103	800.0	796.1	795.7	788.7	782.6	775.2	770.2	764.5	758.3	753.5	895.2	297.3	226000	0.01544

Table 10. Friction factor data: h_d = 0.9 mm, C_{pl} = 0.635 mm, P_{in} = 70 bar

h_d: 0.9 mm						C_{pl}: 0.635 mm					P_{in}:70bar(1000psi)				
Sl.No.	Flow rate	Static pressure (psi)											T_t	Re	f_f
	Kg/s	Inlet	1	2	3	4	5	6	7	8	9	Exit	K		
1	0.305	1004.9	980.7	951.4	908.2	858.5	805.8	753.7	697.5	628.6	555.0	403.8	293.8	668000	0.01277
2	0.303	1007.6	984.0	955.4	913.4	865.1	814.1	764.0	710.2	644.9	576.0	447.4	294.5	664000	0.01266
3	0.293	998.8	976.5	949.7	910.3	865.1	817.4	771.4	722.2	663.4	602.7	500.0	295.0	641000	0.01281
4	0.287	1001.5	980.1	954.9	917.5	874.5	829.6	786.6	740.8	686.8	631.9	544.1	295.4	628000	0.01287
5	0.277	1005.8	985.7	962.9	928.6	889.4	848.6	810.5	769.5	722.3	675.3	603.2	295.9	606000	0.01294
6	0.264	1001.5	982.9	962.7	931.5	896.3	859.6	825.9	789.7	748.7	708.5	648.3	296.2	578000	0.01303
7	0.251	1008.2	991.5	974.4	946.7	916.0	884.3	855.3	824.6	789.9	756.8	708.0	296.4	548000	0.01310
8	0.233	997.8	983.2	969.0	944.9	918.5	891.2	866.7	841.0	811.8	784.5	744.8	296.6	510000	0.01321
9	0.216	1011.6	999.2	988.5	968.3	946.8	924.3	904.6	884.3	861.3	840.1	809.2	296.9	472000	0.01314
10	0.195	1003.5	993.3	985.5	968.8	951.5	933.1	917.5	901.4	883.6	867.3	842.9	297.0	426000	0.01323
11	0.165	1002.3	994.6	990.6	978.3	966.2	952.8	942.1	931.0	918.9	908.1	891.5	297.1	360000	0.01341
12	0.110	994.9	991.1	992.0	985.7	980.4	973.7	969.4	964.6	959.6	955.6	948.8	297.5	240000	0.01370

Table 11. Friction factor data: h_d = 0.9 mm, C_{pl} = 0.635 mm, P_{in} = 84 bar

h_d: 0.9 mm						C_{pl}: 0.635 mm					P_{in}:84bar(1200psi)				
Sl.No.	Flow rate	Static pressure (psi)											T_t	Re	f_f
	Kg/s	Inlet	1	2	3	4	5	6	7	8	9	Exit	K		
1	0.361	1204.0	1174.1	1139.2	1087.5	1027.5	965.8	903.6	837.2	755.4	667.2	482.6	295.1	790000	0.01294
2	0.358	1207.3	1179.1	1146.0	1096.6	1039.0	980.8	922.4	860.3	784.8	705.2	556.6	295.7	783000	0.01276
3	0.349	1199.8	1172.8	1141.5	1094.3	1040.3	984.6	929.8	871.9	802.3	729.9	602.6	296.0	764000	0.01279
4	0.341	1193.5	1168.0	1138.6	1093.9	1043.1	990.9	940.0	886.5	823.1	758.1	649.1	296.3	746000	0.01273
5	0.334	1197.4	1173.1	1145.7	1103.2	1055.1	1006.3	958.9	909.5	851.6	793.1	698.5	296.6	732000	0.01270
6	0.324	1197.9	1175.2	1150.1	1110.3	1066.1	1020.8	977.7	932.8	881.1	829.5	748.8	296.9	708000	0.01278
7	0.309	1196.0	1175.2	1153.2	1117.1	1077.7	1037.0	999.1	959.7	915.0	871.2	804.5	297.1	675000	0.01287
8	0.300	1206.3	1187.0	1167.1	1133.5	1097.7	1059.8	1025.2	989.5	949.2	910.3	852.1	297.4	656000	0.01289
9	0.284	1203.2	1185.8	1168.7	1138.5	1107.0	1073.3	1043.1	1012.0	977.2	944.1	895.2	297.6	20000	0.01300
10	0.261	1200.4	1185.6	1172.4	1146.7	1120.7	1092.4	1067.7	1042.4	1014.4	988.2	949.8	297.8	571000	0.01309
11	0.238	1196.4	1184.0	1174.1	1152.7	1131.3	1107.7	1087.8	1067.3	1044.8	1024.3	994.0	297.9	521000	0.01318
12	0.214	1201.1	1191.0	1184.4	1167.1	1149.9	1130.7	1115.6	1099.2	1081.7	1066.1	1042.8	298.1	468000	0.01333
13	0.184	1207.3	1199.7	1196.6	1183.5	1171.1	1156.6	1146.3	1134.3	1121.9	1111.4	1094.9	298.2	402000	0.01346
14	0.131	1208.3	1203.8	1204.9	1196.8	1190.3	1181.9	1176.5	1170.4	1163.4	1158.5	1149.8	298.4	287000	0.01468

Table 12. Friction factor data: h_d = 1.9 mm, C_{pl} = 0.254 mm, P_{in} = 56 bar

h_d: 1.9 mm						C_{pl}: 0.254 mm					P_{in}:56 bar(800psi)				
Sl.No.	Flow rate	Static pressure (psi)											T_t	Re	f_f
	Kg/s	Inlet	1	2	3	4	5	6	7	8	9	Exit	K		
1	0.084	813.6	775.1	760.0	726.4	690.1	654.2	616.6	574.2	524.6	467.3	334.8	296.8	183000	0.00666
2	0.083	809.7	771.8	757.0	724.0	688.3	653.1	616.3	574.9	526.6	471.1	351.8	296.6	181000	0.00670
3	0.080	805.1	770.0	756.6	726.1	693.4	661.1	627.9	590.7	547.9	499.8	404.8	296.7	175000	0.00665
4	0.077	805.9	773.6	761.7	733.6	703.9	674.5	644.6	611.3	573.6	532.0	454.4	296.9	168000	0.00675
5	0.073	799.9	771.6	761.6	737.0	711.2	685.7	660.3	632.1	600.6	566.6	506.0	297.1	159000	0.00670
6	0.068	801.4	775.7	767.1	744.6	721.5	698.6	675.9	651.0	623.2	593.7	542.1	297.2	149000	0.00698
7	0.063	802.7	781.3	774.9	756.2	737.3	718.4	700.2	680.3	658.3	635.4	596.3	297.3	137000	0.00699
8	0.056	797.7	780.8	776.7	761.8	747.2	732.4	718.5	703.4	686.9	669.9	641.3	297.4	123000	0.00690
9	0.047	809.9	797.9	796.3	785.5	775.5	764.9	755.7	745.5	734.5	723.4	704.8	297.7	103000	0.00717

Table 13. Friction factor data: h_d = 1.9 mm, C_{pl} = 0.254 mm, P_{in} = 70 bar

h_d: 1.9 mm						C_{pl}: 0.254 mm					P_{in}:70 bar(1000psi)				
Sl.No.	Flow rate	Static pressure (psi)											T_t	Re	f_f
	Kg/s	Inlet	1	2	3	4	5	6	7	8	9	Exit	K		
1	0.103	996.8	951.2	932.6	893.1	850.1	806.5	761.1	708.9	649.0	578.9	416.5	297.4	225000	0.00648
2	0.101	993.0	947.7	929.6	891.3	849.8	808.2	764.6	715.3	658.5	593.6	454.5	297.5	221000	0.00647
3	0.098	994.2	950.2	932.8	896.1	856.4	816.6	775.2	728.8	675.5	615.2	492.8	297.7	214000	0.00669
4	0.097	998.1	956.6	940.8	906.2	869.3	832.4	794.4	752.0	703.8	650.2	549.8	297.9	211000	0.00653
5	0.093	1004.3	965.6	951.5	919.4	885.6	851.8	817.3	779.2	736.3	689.1	605.1	298.2	204000	0.00658
6	0.089	1002.1	966.4	953.8	924.2	893.4	862.7	831.4	797.4	759.3	717.8	645.9	298.4	194000	0.00676
7	0.085	1005.4	973.8	963.4	937.1	910.3	883.5	856.5	827.4	795.1	760.5	701.4	298.6	185000	0.00668
8	0.078	1005.9	978.5	970.4	947.6	924.7	901.7	879.0	854.7	828.0	799.6	752.6	298.8	171000	0.00683
9	0.073	1005.8	982.5	976.6	956.9	937.8	918.3	899.5	879.5	857.8	834.9	797.0	298.9	159000	0.00681
10	0.062	998.3	980.9	977.8	962.8	948.8	934.2	920.8	906.4	891.0	875.1	848.2	299.1	135000	0.00702
11	0.053	1007.5	994.6	994.0	982.4	972.5	961.5	952.1	942.0	931.1	920.2	901.2	299.2	116000	0.00710
12	0.041	1005.0	996.6	998.4	990.5	984.8	977.5	972.1	966.2	959.8	953.8	942.5	299.3	90000	0.00737

Table 14. Friction factor data: h_d = 1.9 mm, C_{pl} = 0.254 mm, P_{in} = 84 bar

h_d: 1.9 mm						C_{pl}: 0.254 mm					P_{in}:84 bar(1200psi)				
Sl.No.	Flow rate	Static pressure (psi)											T_t	Re	f_f
	Kg/s	Inlet	1	2	3	4	5	6	7	8	9	Exit	K		
1	0.125	1205.0	1143.7	1119.2	1068.5	1014.5	959.9	903.4	839.7	766.1	682.5	501.1	295.2	274000	0.00651
2	0.124	1205.1	1145.8	1122.4	1073.4	1021.7	969.3	915.7	855.6	786.5	709.5	557.1	295.0	271000	0.00645
3	0.121	1211.7	1153.7	1131.1	1083.8	1034.1	983.7	932.3	875.2	810.0	737.8	601.9	295.1	266000	0.00659
4	0.119	1207.5	1153.0	1132.0	1087.5	1040.5	993.4	945.4	892.4	832.6	767.4	648.9	295.2	260000	0.00655
5	0.115	1197.6	1147.6	1129.0	1088.3	1045.8	1003.3	960.4	913.0	860.6	804.2	706.2	295.3	251000	0.00646
6	0.110	1198.2	1150.2	1132.9	1094.7	1055.1	1015.4	975.9	931.9	884.0	832.9	746.1	295.3	241000	0.00665
7	0.108	1210.3	1165.6	1150.0	1114.5	1077.9	1041.6	1005.2	965.3	921.4	876.0	799.6	295.4	236000	0.00657
8	0.099	1194.8	1155.1	1142.4	1112.1	1081.2	1050.2	1019.8	987.0	950.7	914.0	853.7	295.5	216000	0.00678
9	0.094	1201.3	1166.9	1156.4	1128.8	1101.3	1073.7	1046.7	1017.8	986.1	954.3	901.9	295.6	206000	0.00677
10	0.086	1191.9	1162.4	1154.5	1131.1	1108.1	1084.9	1062.6	1038.9	1013.2	987.7	945.2	295.7	189000	0.00684
11	0.081	1204.4	1178.7	1172.8	1152.1	1132.3	1112.0	1092.9	1072.6	1050.9	1029.4	993.3	295.9	177000	0.00691
12	0.073	1206.7	1186.4	1183.0	1166.5	1151.3	1135.2	1120.6	1105.3	1088.8	1072.9	1045.8	296.0	159000	0.00683
13	0.063	1213.0	1197.8	1197.0	1184.2	1173.2	1160.9	1150.5	1139.5	1127.8	1116.7	1097.7	296.2	138000	0.00681

Table 15. Friction factor data: h_d = 1.9 mm, C_{pl} = 0.381 mm, P_{in} = 56 bar

h_d: 1.9 mm						C_{pl}: 0.381 mm					P_{in}:56 bar(800psi)				
Sl.No.	Flow rate	Static pressure (psi)											T_t	Re	f_f
	Kg/s	Inlet	1	2	3	4	5	6	7	8	9	Exit	K		
1	0.117	809.1	777.8	764.1	725.4	682.5	640.9	598.6	546.4	487.2	417.5	297.9	294.0	256000	0.01347
2	0.115	807.1	777.1	764.3	727.2	686.5	646.9	607.2	558.3	503.6	440.7	343.2	293.9	251000	0.01344
3	0.112	814.1	785.8	774.0	739.2	701.1	664.1	627.6	583.0	533.8	478.9	400.1	294.1	245000	0.01358
4	0.104	795.9	770.9	760.8	730.2	697.1	665.0	633.9	596.2	555.4	511.2	451.9	294.4	228000	0.01370
5	0.101	798.9	776.0	767.2	739.2	709.2	680.2	652.4	619.1	583.1	545.1	495.9	294.5	220000	0.01361
6	0.095	809.3	789.0	781.6	756.8	730.5	705.1	681.0	652.5	622.0	590.7	551.2	294.8	208000	0.01387
7	0.085	804.4	787.8	782.7	762.6	741.6	721.4	702.6	680.6	657.2	634.0	605.3	295.0	186000	0.01417
8	0.076	798.3	785.0	781.7	765.5	749.0	732.9	718.4	701.4	683.7	666.3	644.8	295.1	166000	0.01425
9	0.066	809.6	799.5	798.0	785.5	773.3	761.0	750.5	738.2	725.4	713.2	698.0	295.3	145000	0.01448
10	0.049	807.5	801.8	802.9	795.5	789.0	781.8	776.6	770.2	763.7	757.8	750.0	295.5	107000	0.01450

Table 16. Friction factor data: h_d = 1.9 mm, C_{pl} = 0.381 mm, P_{in} = 70 bar

h_d: 1.9 mm						C_{pl}: 0.381 mm					P_{in}:70 bar(1000psi)				
Sl.No.	Flow rate	Static pressure (psi)											T_t	Re	f_f
	Kg/s	Inlet	1	2	3	4	5	6	7	8	9	Exit	K		
1	0.145	999.4	961.4	944.0	897.4	844.8	793.9	741.7	676.9	604.2	518.8	371.8	295.6	318000	0.01307
2	0.144	1004.3	967.8	951.3	906.7	856.8	808.4	759.2	699.0	631.7	554.9	437.1	295.7	314000	0.01299
3	0.140	1005.1	970.8	955.7	913.8	867.4	822.7	777.4	722.7	662.2	595.0	499.3	296.0	306000	0.01297
4	0.135	1008.5	976.4	962.4	923.4	880.3	839.0	797.4	747.6	693.1	633.8	553.5	296.2	296000	0.01314
5	0.130	1009.8	980.1	967.7	931.8	892.5	855.0	817.5	773.1	725.0	673.6	606.5	296.4	284000	0.01329
6	0.123	998.8	971.9	961.2	928.7	893.6	860.1	827.0	788.0	746.1	702.2	646.2	296.5	269000	0.01334
7	0.116	999.5	975.6	966.6	937.8	907.0	877.6	849.0	815.5	780.1	743.3	697.2	296.7	253000	0.01348
8	0.106	1000.6	980.6	974.0	949.9	924.7	900.4	877.4	850.8	822.9	794.4	759.1	296.9	232000	0.01350
9	0.099	1010.8	993.4	988.3	967.4	945.8	924.8	905.3	882.9	859.8	836.2	807.2	297.1	217000	0.01362
10	0.086	999.4	985.9	983.1	966.8	950.4	934.2	919.7	903.1	886.0	869.1	848.2	297.2	188000	0.01391
11	0.074	1006.7	996.6	995.9	983.4	971.6	959.4	949.0	937.2	925.0	913.3	898.8	297.3	162000	0.01411
12	0.058	1002.4	995.9	997.4	989.2	982.1	974.2	968.2	961.3	954.2	947.8	939.2	297.4	126000	0.01424

Table 17. Friction factor data: h_d = 1.9 mm, C_{pl} = 0.381 mm, P_{in} = 84 bar

h_d: 1.9 mm		C_{pl}: 0.381 mm						P_{in}:84 bar(1200psi)							
Sl.No.	Flow rate	Static pressure (psi)											T_t	Re	f_f
	Kg/s	Inlet	1	2	3	4	5	6	7	8	9	Exit	K		
1	0.174	1200.3	1156.4	1138.6	1082.5	1020.4	960.7	896.9	821.1	733.3	629.6	443.3	296.4	381000	0.01294
2	0.171	1196.7	1153.9	1135.7	1082.0	1022.1	964.8	905.8	832.8	751.0	656.5	504.8	296.9	375000	0.01294
3	0.169	1194.9	1152.9	1134.9	1083.3	1025.7	971.1	914.6	845.9	769.4	682.5	551.1	297.1	369000	0.01288
4	0.165	1195.8	1155.1	1137.3	1088.3	1033.7	982.0	929.1	864.8	794.1	715.0	600.3	297.3	361000	0.01288
5	0.161	1197.0	1158.1	1141.2	1094.9	1043.5	995.0	945.7	886.2	821.6	750.3	654.8	297.5	352000	0.01294
6	0.156	1198.4	1161.2	1145.7	1102.0	1053.9	1008.5	962.8	908.1	849.4	785.1	696.3	297.8	342000	0.01302
7	0.151	1202.6	1168.3	1154.8	1114.4	1070.8	1029.4	988.6	939.8	888.5	833.0	755.6	298.0	329000	0.01303
8	0.146	1204.8	1172.7	1160.5	1122.9	1082.8	1044.5	1007.2	962.9	916.5	867.1	798.3	298.2	320000	0.01293
9	0.138	1198.0	1169.0	1158.7	1125.1	1089.6	1055.6	1023.1	984.4	944.4	902.5	844.1	298.3	301000	0.01309
10	0.127	1195.6	1170.3	1162.1	1132.9	1102.5	1073.1	1045.7	1013.1	979.7	945.3	897.5	298.5	277000	0.01351
11	0.119	1198.4	1176.4	1170.2	1144.7	1118.6	1093.2	1069.9	1042.3	1014.4	985.9	946.5	298.6	259000	0.01353
12	0.107	1191.3	1173.2	1169.1	1147.9	1126.7	1105.7	1086.9	1064.8	1042.5	1020.3	990.8	298.7	235000	0.01362
13	0.096	1205.2	1190.7	1188.8	1171.4	1154.6	1137.5	1122.8	1105.5	1088.1	1071.0	1047.5	298.9	210000	0.01393
14	0.080	1204.6	1194.3	1194.8	1182.1	1170.6	1158.3	1148.3	1136.8	1125.2	1114.2	1098.9	299.0	175000	0.01416
15	0.059	1209.1	1202.8	1205.8	1197.7	1191.5	1183.9	1178.6	1172.6	1166.3	1160.9	1153.4	299.2	130000	0.01450

Table 18. Friction factor data: h_d = 1.9 mm, C_{pl} = 0.635 mm, P_{in} = 56 bar

h_d: 1.9 mm						C_{pl}: 0.635 mm					P_{in}:56 bar(800psi)				
Sl.No.	Flow rate	Static pressure (psi)											T_t	Re	f_f
	Kg/s	Inlet	1	2	3	4	5	6	7	8	9	Exit	K		
1	0.203	801.9	780.2	771.7	733.2	688.2	643.8	598.1	544.0	479.6	404.5	275.9	290.3	444000	0.02171
2	0.201	811.0	790.4	782.5	745.9	703.3	661.2	618.7	568.5	510.2	444.2	346.1	290.4	439000	0.02156
3	0.190	807.0	787.7	780.6	746.5	707.0	668.2	629.4	583.8	532.0	474.7	395.3	290.4	415000	0.02269
4	0.178	795.3	778.1	772.3	741.9	707.1	673.0	639.5	600.5	557.1	510.3	449.6	290.4	389000	0.02299
5	0.170	803.5	788.0	783.3	756.2	725.6	695.5	666.5	632.9	596.2	557.6	509.7	290.6	372000	0.02300
6	0.158	801.7	788.1	784.6	761.0	734.7	708.8	684.3	656.0	625.7	594.4	556.5	290.7	346000	0.02323
7	0.148	802.4	790.5	788.0	767.4	744.7	722.4	701.6	677.7	652.2	626.4	595.7	290.8	323000	0.02342
8	0.134	807.5	797.8	796.7	779.9	761.9	743.9	727.8	709.2	689.6	670.1	647.2	291.0	293000	0.02346
9	0.115	811.1	803.9	804.3	791.8	779.1	766.0	754.8	741.9	728.4	715.3	700.1	291.2	251000	0.02347
10	0.087	810.5	806.2	808.2	800.5	793.3	785.3	779.3	772.3	765.0	758.2	750.1	291.4	189000	0.02388

Table 19. Friction factor data: h_d = 1.9 mm, C_{pl} = 0.635 mm, P_{in} = 70 bar

h_d: 1.9 mm						C_{pl}: 0.635 mm					P_{in}:70 bar(1000psi)				
Sl.No.	Flow rate	Static pressure (psi)											T_t	Re	f_f
	Kg/s	Inlet	1	2	3	4	5	6	7	8	9	Exit	K		
1	0.252	998.9	971.9	961.0	914.1	858.7	803.6	746.7	679.0	599.0	506.0	346.5	291.9	552000	0.02143
2	0.248	1002.4	976.2	965.9	920.6	867.5	814.7	760.6	696.6	621.9	537.0	405.7	292.1	543000	0.02156
3	0.246	1005.2	979.8	970.0	926.3	875.0	824.3	772.5	711.6	641.2	562.6	449.0	292.3	539000	0.02136
4	0.240	999.1	975.1	966.0	924.6	876.3	828.6	780.4	723.9	659.4	588.5	491.4	292.4	524000	0.02136
5	0.235	1009.7	987.0	978.8	939.8	894.6	850.1	805.6	753.8	695.6	632.6	550.6	292.6	514000	0.02131
6	0.215	1009.2	990.3	984.6	952.4	916.0	880.1	845.3	805.2	761.4	715.5	659.6	293.0	470000	0.02134
7	0.204	999.6	982.4	977.7	948.6	916.0	883.8	853.0	817.6	779.3	739.6	692.1	293.0	445000	0.02148
8	0.190	1004.7	989.8	986.6	961.6	934.1	906.7	881.1	852.0	820.6	788.8	751.2	293.2	417000	0.02130
9	0.170	996.9	984.8	983.3	963.3	941.6	919.8	900.0	877.7	854.0	830.2	802.1	293.3	372000	0.02135
10	0.154	1004.0	994.1	993.9	977.5	960.3	942.8	927.2	909.8	891.4	873.4	852.0	293.5	338000	0.02119
11	0.102	1008.1	1003.4	1006.2	998.5	991.6	983.5	977.6	970.9	963.8	957.5	949.5	293.9	223000	0.02076

Table 20. Friction factor data: h_d = 1.9 mm, C_{pl} = 0.635 mm, P_{in} = 84 bar

h_d: 1.9 mm						C_{pl}: 0.635 mm					P_{in}:84 bar(1200psi)				
Sl.No.	Flow rate	Static pressure (psi)											T_t	Re	f_f
	Kg/s	Inlet	1	2	3	4	5	6	7	8	9	Exit	K		
1	0.295	1191.7	1159.0	1146.3	1090.4	1024.1	958.8	891.0	810.1	713.6	601.2	411.7	293.9	646000	0.02214
2	0.291	1188.6	1156.5	1144.2	1089.8	1025.4	962.3	896.7	819.2	727.7	622.4	461.7	294.2	636000	0.02225
3	0.290	1199.7	1168.1	1156.2	1102.6	1039.4	977.6	913.8	838.6	750.5	650.3	505.5	294.3	633000	0.02236
4	0.286	1200.6	1169.8	1158.4	1106.4	1045.4	985.8	924.4	852.7	769.3	675.6	546.6	294.5	625000	0.02239
5	0.280	1203.7	1174.3	1163.8	1114.3	1056.6	1000.3	943.0	876.2	799.8	715.4	604.4	294.8	612000	0.02237
6	0.274	1207.2	1179.0	1169.4	1122.4	1067.8	1014.7	961.0	898.8	828.8	752.2	651.3	295.0	599000	0.02236
7	0.266	1201.8	1175.2	1166.5	1122.3	1071.3	1021.6	971.8	914.5	850.6	781.7	693.2	295.2	582000	0.02232
8	0.256	1201.8	1177.2	1169.9	1129.2	1082.8	1037.7	992.9	941.7	885.5	825.8	751.7	295.4	560000	0.02231
9	0.247	1209.1	1186.1	1179.7	1141.8	1098.9	1057.2	1016.1	969.3	918.6	865.4	799.8	295.5	540000	0.02260
10	0.236	1204.3	1183.4	1178.3	1144.1	1105.7	1068.3	1032.0	990.8	946.6	900.8	844.7	295.7	516000	0.02247
11	0.217	1198.4	1180.5	1177.1	1148.0	1115.9	1084.4	1054.3	1020.6	984.7	948.1	903.9	295.9	474000	0.02270
12	0.202	1197.0	1181.2	1179.0	1153.5	1125.8	1098.3	1072.6	1043.8	1013.4	982.7	945.9	296.0	441000	0.02295
13	0.182	1196.8	1183.8	1183.3	1162.4	1140.3	1118.0	1097.7	1075.2	1051.5	1028.1	999.9	296.1	398000	0.02301
14	0.167	1204.9	1193.6	1194.2	1176.2	1157.7	1138.7	1121.9	1103.1	1083.6	1064.4	1041.4	296.3	366000	0.02331
15	0.140	1205.2	1196.9	1199.1	1185.9	1173.2	1159.4	1148.0	1135.2	1122.0	1109.4	1093.8	296.4	306000	0.02359
16	0.103	1201.2	1195.7	1199.5	1190.9	1183.5	1174.8	1168.3	1161.1	1153.6	1146.9	1137.9	296.5	226000	0.02589

Table 21. Friction factor data: h_d = 2.9 mm, C_{pl} = 0.254 mm, P_{in} = 56 bar

h_d: 2.9 mm						C_{pl}: 0.254 mm					P_{in}:56 bar(800psi)				
Sl.No.	Flow rate	Static pressure (psi)											T_t	Re	f_f
	Kg/s	Inlet	1	2	3	4	5	6	7	8	9	Exit	K		
1	0.087	803.9	762.0	740.9	707.6	671.1	634.2	595.3	550.3	503.8	450.7	314.8	290.9	191000	0.00605
2	0.088	812.6	771.8	751.4	719.0	683.7	648.2	610.9	567.7	524.0	474.3	355.5	291.1	191000	0.00597
3	0.084	802.1	764.8	746.6	717.1	685.2	653.2	620.1	581.9	544.0	501.6	406.9	291.3	184000	0.00587
4	0.081	807.5	772.8	756.3	729.0	699.8	670.5	640.5	606.0	572.5	535.4	456.2	291.5	178000	0.00601
5	0.077	807.0	775.9	761.6	737.1	711.3	685.3	659.2	629.0	600.4	569.1	504.7	291.7	168000	0.00612
6	0.072	802.5	775.7	763.9	742.8	720.9	698.7	677.0	651.7	628.3	603.0	552.2	292.0	158000	0.00606
7	0.066	801.7	779.7	771.0	753.6	735.9	717.9	700.8	680.8	662.7	643.3	605.2	292.3	145000	0.00603
8	0.061	806.5	788.5	782.2	767.8	753.6	738.9	725.4	709.5	695.4	680.4	651.2	292.6	134000	0.00586
9	0.050	797.9	785.0	781.9	771.3	761.3	750.7	741.6	730.6	721.1	711.2	691.7	292.8	109000	0.00632

Table 22. Friction factor data: h_d = 2.9 mm, C_{pl} = 0.254 mm, P_{in} = 70 bar

h_d: 2.9 mm						C_{pl}: 0.254 mm					P_{in}:70 bar(1000psi)				
Sl.No.	Flow rate	Static pressure (psi)											T_t	Re	f_f
	Kg/s	Inlet	1	2	3	4	5	6	7	8	9	Exit	K		
1	0.123	1006.9	954.5	927.4	886.7	841.2	795.3	746.2	689.3	631.2	564.7	395.8	292.3	269000	0.00451
2	0.120	997.6	948.1	922.8	884.3	841.5	798.6	753.2	700.5	647.5	587.6	447.4	292.4	262000	0.00451
3	0.118	1003.5	956.3	932.6	896.0	855.7	815.3	772.9	723.9	675.3	620.9	500.5	292.7	258000	0.00451
4	0.114	999.4	955.5	933.9	900.1	863.1	826.0	787.5	743.2	700.1	652.1	550.6	292.9	249000	0.00454
5	0.111	1006.3	965.8	946.2	914.9	881.1	847.1	812.5	772.3	734.3	692.0	605.6	293.2	243000	0.00455
6	0.107	1001.3	964.4	947.3	918.9	888.7	858.3	827.6	792.3	759.2	722.8	649.9	293.4	234000	0.00444
7	0.101	993.6	961.2	946.8	921.9	895.7	869.3	843.0	812.9	785.0	754.7	695.2	293.7	220000	0.00447
8	0.096	1002.7	973.7	961.5	939.4	916.3	892.9	870.1	843.9	820.0	794.1	743.7	293.9	210000	0.00448
9	0.086	999.5	976.6	968.4	950.6	932.8	914.5	897.3	877.3	859.8	840.8	803.9	294.3	189000	0.00445
10	0.081	1004.9	985.5	979.8	964.1	949.3	933.8	919.5	903.0	888.7	873.4	843.4	294.5	176000	0.00440
11	0.068	1005.6	992.3	990.3	979.0	969.1	958.3	949.0	938.0	929.0	919.3	900.2	294.8	149000	0.00430
12	0.052	1006.3	998.6	1000.1	992.9	987.9	981.0	976.3	970.1	965.9	961.1	951.0	295.1	114000	0.00416

Table 23. Friction factor data: h_d = 2.9 mm, C_{pl} = 0.254 mm, P_{in} = 84 bar

h_d: 2.9 mm						C_{pl}: 0.254 mm					P_{in}:84 bar(1200psi)				
Sl.No.	Flow rate	Static pressure (psi)											T_t	Re	f_f
	Kg/s	Inlet	1	2	3	4	5	6	7	8	9	Exit	K		
1	0.149	1201.5	1140.5	1109.9	1061.7	1009.1	955.9	899.3	831.4	762.4	681.1	479.3	294.4	325000	0.00426
2	0.148	1201.8	1140.8	1110.2	1062.3	1009.8	957.3	901.0	834.9	767.1	688.3	500.4	294.3	324000	0.00427
3	0.146	1204.1	1145.0	1115.5	1069.4	1019.0	968.8	915.0	852.6	789.2	716.7	554.7	294.5	320000	0.00428
4	0.144	1205.3	1148.3	1119.9	1075.4	1027.1	978.9	927.6	868.8	809.4	742.2	597.6	294.7	315000	0.00430
5	0.139	1193.9	1141.1	1115.0	1073.8	1029.2	984.6	937.8	884.2	831.4	772.1	650.4	294.9	303000	0.00435
6	0.137	1200.5	1150.3	1125.9	1086.8	1045.0	1003.2	959.6	909.9	861.7	807.8	698.8	295.2	299000	0.00431
7	0.131	1193.3	1147.3	1125.5	1089.6	1051.6	1013.5	974.4	929.7	887.2	840.2	746.1	295.4	287000	0.00434
8	0.127	1199.2	1157.7	1138.7	1105.6	1071.6	1037.5	1003.0	963.3	926.3	885.8	805.2	295.6	277000	0.00433
9	0.121	1197.3	1160.6	1144.1	1114.3	1084.7	1053.5	1022.9	988.0	956.0	921.0	852.4	295.9	265000	0.00432
10	0.115	1192.5	1159.4	1145.6	1119.6	1093.2	1065.7	1039.3	1009.2	981.8	952.4	895.8	296.2	251000	0.00430
11	0.109	1200.4	1170.9	1159.9	1137.4	1114.9	1091.7	1069.4	1043.7	1020.8	996.5	949.8	296.5	238000	0.00419
12	0.099	1201.2	1176.5	1168.3	1149.3	1130.7	1111.3	1093.2	1072.3	1054.2	1034.7	997.3	296.7	216000	0.00430
13	0.089	1202.4	1183.0	1178.2	1163.0	1148.8	1133.7	1120.1	1104.1	1090.8	1076.6	1049.1	297.0	195000	0.00416
14	0.074	1200.3	1186.9	1185.6	1174.8	1165.4	1154.8	1145.9	1135.2	1126.9	1118.0	1100.0	297.3	162000	0.00413
15	0.060	1198.3	1189.4	1191.6	1183.3	1177.5	1170.3	1165.0	1158.1	1153.6	1148.5	1137.5	297.5	132000	0.00402

Table 24. Friction factor data: h_d = 2.9 mm, C_{pl} = 0.381 mm, P_{in} = 56 bar

h_d: 2.9 mm						C_{pl}: 0.381 mm					P_{in}:56 bar(800psi)				
Sl.No.	Flow rate	Static pressure (psi)											T_t	Re	f_f
	Kg/s	Inlet	1	2	3	4	5	6	7	8	9	Exit	K		
1	0.139	805.5	774.8	755.9	720.9	677.5	637.0	590.6	537.3	482.4	417.1	278.0	291.0	303000	0.00908
2	0.134	808.1	779.3	761.9	729.2	689.0	651.5	609.3	560.8	512.7	456.6	352.6	291.9	292000	0.00935
3	0.130	804.9	777.8	761.8	731.2	693.9	659.1	620.4	575.8	533.0	483.5	397.0	292.1	283000	0.00939
4	0.124	803.3	779.0	765.1	737.6	704.5	673.7	640.0	601.1	565.2	524.2	456.4	292.3	271000	0.00941
5	0.118	803.7	781.9	770.2	745.3	716.1	688.8	659.6	625.6	595.4	561.1	506.2	292.5	258000	0.00942
6	0.110	800.5	781.8	772.8	751.2	726.8	703.6	679.5	651.2	627.1	599.9	557.4	292.5	241000	0.00940
7	0.102	798.1	782.2	775.1	756.5	736.2	716.4	696.4	672.8	653.4	631.4	597.8	292.6	223000	0.00947
8	0.092	800.4	787.6	782.6	767.6	751.8	735.8	720.8	701.9	687.5	671.0	646.1	292.8	200000	0.00960
9	0.079	805.5	795.9	793.4	782.2	770.6	758.7	748.3	734.7	724.8	713.7	696.3	293.1	174000	0.00960
10	0.062	813.6	808.0	808.4	801.6	795.1	788.1	782.5	774.3	770.0	764.3	755.0	293.4	135000	0.00933

Table 25. Friction factor data: h_d = 2.9 mm, C_{pl} = 0.381 mm, P_{in} = 70 bar

h_d: 2.9 mm						C_{pl}: 0.381 mm					P_{in}:70 bar(1000psi)				
Sl.No.	Flow rate	Static pressure (psi)											T_t	Re	f_f
	Kg/s	Inlet	1	2	3	4	5	6	7	8	9	Exit	K		
1	0.171	1003.9	966.0	942.5	899.2	845.6	795.4	737.6	671.0	602.5	521.6	349.0	293.6	374000	0.00911
2	0.168	1000.5	963.8	941.2	899.7	848.6	800.7	746.0	683.2	620.0	546.1	402.8	294.0	366000	0.00916
3	0.167	1006.4	971.3	949.8	909.8	861.1	815.4	763.7	704.3	645.8	578.2	455.5	294.3	366000	0.00895
4	0.162	1002.2	969.0	948.8	910.8	865.2	821.8	773.5	718.0	664.4	602.9	496.9	294.5	354000	0.00917
5	0.158	1003.2	972.2	953.5	917.8	875.4	834.8	790.2	739.0	690.7	635.5	544.1	294.7	346000	0.00916
6	0.151	1003.0	973.8	957.2	925.0	886.2	849.5	809.9	763.9	722.0	674.4	598.1	294.9	331000	0.00929
7	0.145	1003.6	976.9	962.2	933.1	898.1	865.2	830.2	789.0	752.8	711.7	647.3	295.0	317000	0.00929
8	0.136	998.5	974.8	962.6	936.8	906.5	878.1	847.9	812.8	782.1	748.0	695.4	295.1	297000	0.00942
9	0.128	1001.3	980.9	971.2	949.1	923.4	899.2	874.1	844.8	820.2	792.5	750.1	295.2	279000	0.00930
10	0.115	999.6	983.0	976.2	958.1	937.7	918.2	898.6	875.5	857.1	836.1	804.0	295.3	251000	0.00944
11	0.105	1007.2	993.3	988.6	973.4	956.8	940.6	924.7	905.8	891.4	874.9	849.5	295.4	229000	0.00960
12	0.088	1007.3	997.2	995.4	984.4	972.8	961.2	950.5	937.0	928.1	917.2	900.3	295.6	193000	0.00966
13	0.069	1012.6	1006.5	1007.6	1000.6	994.2	987.1	981.3	972.7	969.2	963.6	954.4	295.7	150000	0.00930

Table 26. Friction factor data: h_d = 2.9 mm, C_{pl} = 0.381 mm, P_{in} = 84 bar

h_d: 2.9 mm		C_{pl}: 0.381 mm						P_{in}:84 bar(1200psi)							
Sl.No.	Flow rate	Static pressure (psi)											T_t	Re	f_f
	Kg/s	Inlet	1	2	3	4	5	6	7	8	9	Exit	K		
1	0.208	1206.3	1161.4	1132.7	1081.1	1016.3	956.1	885.7	805.9	721.7	622.2	421.8	295.7	456000	0.00875
2	0.205	1202.6	1158.2	1130.4	1079.6	1016.6	957.4	889.6	811.9	731.6	636.5	454.9	296.0	449000	0.00882
3	0.202	1200.1	1156.9	1130.2	1081.2	1020.5	963.5	898.7	824.9	749.5	661.0	503.6	296.3	442000	0.00887
4	0.200	1202.3	1160.3	1134.8	1087.6	1029.3	974.4	912.8	842.8	772.4	690.7	551.1	296.5	437000	0.00883
5	0.195	1202.9	1162.6	1138.6	1093.7	1038.7	986.7	928.9	863.7	799.1	724.9	602.3	296.8	426000	0.00896
6	0.190	1201.8	1163.6	1141.2	1098.8	1047.0	998.2	944.5	883.7	825.1	758.1	650.3	296.9	416000	0.00897
7	0.185	1202.0	1165.9	1145.4	1105.5	1057.4	1011.9	962.4	906.3	853.8	793.5	699.2	297.1	404000	0.00902
8	0.178	1199.8	1166.2	1147.7	1110.7	1066.5	1024.8	979.8	928.3	881.7	828.5	746.1	297.3	390000	0.00907
9	0.171	1195.8	1164.8	1148.5	1114.7	1074.8	1037.5	997.3	950.8	910.1	864.0	793.0	297.4	374000	0.00905
10	0.160	1196.5	1168.6	1155.1	1125.4	1090.9	1058.5	1024.0	984.4	950.2	911.9	854.0	297.5	351000	0.00919
11	0.153	1201.2	1175.9	1164.3	1137.2	1106.1	1076.8	1046.0	1010.5	980.5	946.9	896.8	297.6	335000	0.00928
12	0.140	1197.3	1175.7	1166.7	1143.6	1117.6	1092.9	1067.5	1037.8	1014.0	986.6	945.8	297.7	307000	0.00947
13	0.130	1199.8	1181.6	1175.1	1155.3	1133.5	1112.6	1091.5	1066.5	1047.6	1025.5	991.9	297.8	284000	0.00951
14	0.113	1194.4	1180.4	1176.9	1161.6	1145.5	1129.5	1114.2	1095.3	1082.2	1066.5	1042.3	297.9	247000	0.00959
15	0.075	1205.3	1198.7	1200.9	1193.4	1187.1	1179.8	1174.0	1164.7	1161.8	1156.4	1147.1	298.1	165000	0.00926

Table 27. Friction factor data: h_d = 2.9 mm, C_{pl} = 0.635 mm, P_{in} = 56 bar

h_d: 2.9 mm						C_{pl}: 0.635 mm					P_{in}:56 bar(800psi)				
Sl.No.	Flow rate	Static pressure (psi)											T_t	Re	f_f
	Kg/s	Inlet	1	2	3	4	5	6	7	8	9	Exit	K		
1	0.210	797.4	775.5	760.7	729.3	683.3	640.8	589.3	536.1	469.9	398.5	259.7	290.5	458000	0.01982
2	0.208	801.6	780.3	766.0	735.5	691.0	649.9	600.6	549.9	487.5	421.6	305.1	290.5	456000	0.01974
3	0.206	805.1	784.5	771.0	741.7	699.3	660.2	613.5	565.8	508.0	448.1	349.6	290.8	450000	0.01961
4	0.200	801.5	782.2	769.9	742.6	703.3	667.1	624.5	581.2	529.6	477.4	396.5	291.1	436000	0.01957
5	0.194	802.3	784.5	773.5	748.4	712.5	679.6	641.2	602.6	557.3	512.5	446.3	291.5	424000	0.01931
6	0.185	803.8	787.6	778.1	755.4	723.2	693.7	659.8	625.9	586.7	548.8	494.7	291.8	405000	0.01940
7	0.174	804.9	790.8	783.2	763.3	735.7	710.4	681.8	653.4	621.0	590.5	548.1	292.2	381000	0.01938
8	0.157	799.8	788.2	782.7	766.3	744.0	723.5	700.9	678.5	653.3	630.1	598.4	292.6	344000	0.01966
9	0.141	803.3	794.0	790.7	777.6	760.4	744.3	727.3	710.5	691.7	674.7	651.6	293.0	309000	0.01940
10	0.120	799.7	792.9	792.2	782.1	770.1	758.5	747.0	735.4	722.7	711.5	696.1	293.4	263000	0.01924
11	0.092	807.3	803.1	804.8	798.2	791.6	784.6	778.5	772.4	765.5	759.8	751.6	293.7	200000	0.01919

Table 28. Friction factor data: h_d = 2.9 mm, C_{pl} = 0.635 mm, P_{in} = 70 bar

h_d: 2.9 mm						C_{pl}: 0.635 mm					P_{in}:70 bar(1000psi)				
Sl.No.	Flow rate	Static pressure (psi)											T_t	Re	f_f
	Kg/s	Inlet	1	2	3	4	5	6	7	8	9	Exit	K		
1	0.263	999.0	971.7	952.7	913.5	856.5	803.5	738.7	672.0	589.2	500.2	327.4	290.9	574000	0.01965
2	0.260	993.7	967.2	948.7	910.1	854.6	802.5	739.4	674.5	594.4	509.1	352.3	291.2	569000	0.01954
3	0.258	998.7	972.8	954.9	917.8	863.7	813.1	752.2	689.9	613.7	534.2	397.2	291.6	563000	0.01967
4	0.253	999.8	975.1	958.3	922.9	871.4	823.5	766.2	708.0	637.7	565.8	449.7	292.0	554000	0.01960
5	0.248	1000.9	977.3	961.5	928.0	879.3	834.1	780.5	726.4	661.6	596.7	496.7	292.5	543000	0.01953
6	0.243	1004.5	982.1	967.5	936.0	890.4	848.2	798.6	748.8	690.0	631.9	545.6	292.9	531000	0.01942
7	0.231	998.9	978.1	965.3	936.5	895.2	857.1	813.1	768.6	717.1	667.1	595.1	293.4	506000	0.01959
8	0.225	1005.7	986.4	975.1	948.6	910.9	876.4	836.6	796.6	750.9	707.1	645.3	293.7	492000	0.01938
9	0.212	1003.7	986.7	977.4	954.2	921.6	891.7	857.7	824.1	785.4	749.4	699.4	294.1	463000	0.01935
10	0.199	1005.1	990.1	982.8	962.6	934.6	908.9	880.1	852.0	819.6	790.1	749.3	294.5	434000	0.01924
11	0.182	1002.8	990.2	984.9	967.8	944.7	923.3	899.8	877.0	851.5	828.0	795.4	294.7	398000	0.01931
12	0.159	997.6	987.7	984.9	971.6	954.3	938.0	920.7	904.0	885.5	868.8	845.8	295.1	349000	0.01922
13	0.135	1001.0	993.7	993.3	983.5	971.5	959.8	948.2	936.9	924.5	913.6	898.2	295.4	295000	0.01902
14	0.103	1005.4	1000.7	1002.7	996.4	989.8	982.6	976.3	970.2	963.5	957.9	949.4	295.7	225000	0.01887

Table 29. Friction factor data: h_d = 2.9 mm, C_{pl} = 0.635 mm, P_{in} = 84 bar

h_d: 2.9 mm						C_{pl}: 0.635 mm					P_{in}:84 bar(1200psi)				
Sl.No.	Flow	Static pressure (psi)											T_t	Re	f_f
	Kg/s	Inlet	1	2	3	4	5	6	7	8	9	Exit	K		
1	0.313	1205.0	1171.8	1149.8	1103.4	1035.5	972.7	894.9	813.7	715.1	607.8	395.7	290.3	685000	0.01997
2	0.307	1197.2	1165.0	1143.9	1098.7	1033.0	972.6	898.2	822.1	728.1	628.9	450.8	291.2	672000	0.02000
3	0.305	1203.9	1172.6	1152.1	1107.8	1043.7	985.1	913.3	840.3	751.2	657.9	501.0	292.0	666000	0.02005
4	0.298	1202.6	1172.7	1153.3	1110.7	1049.8	994.0	926.0	857.4	774.5	689.2	550.9	292.5	651000	0.02024
5	0.292	1199.5	1171.0	1152.5	1111.6	1053.6	1000.4	936.2	871.7	794.6	716.3	594.1	293.1	638000	0.02021
6	0.285	1200.0	1173.0	1155.8	1117.0	1062.3	1012.4	952.6	893.0	822.5	751.9	645.3	293.6	623000	0.02015
7	0.276	1200.2	1174.9	1159.0	1122.6	1071.6	1025.1	969.8	915.3	851.1	788.0	694.9	294.0	604000	0.02028
8	0.267	1200.1	1176.6	1162.4	1128.5	1081.6	1038.8	988.5	939.1	881.7	826.1	745.5	294.5	584000	0.02030
9	0.257	1203.1	1181.5	1169.0	1137.7	1095.0	1056.0	1010.6	966.3	915.5	866.9	797.8	294.9	562000	0.02032
10	0.242	1195.0	1175.5	1165.0	1136.9	1099.0	1064.2	1024.3	985.6	941.7	900.2	841.9	295.3	528000	0.02063
11	0.227	1194.8	1177.5	1169.1	1144.1	1111.2	1080.8	1046.4	1013.3	976.0	941.2	892.8	295.7	497000	0.02070
12	0.208	1193.6	1179.0	1172.9	1151.6	1124.6	1099.0	1070.9	1043.9	1013.7	986.1	947.7	296.1	456000	0.02079
13	0.198	1203.9	1191.1	1186.6	1167.7	1144.5	1121.7	1097.5	1074.3	1048.6	1025.3	992.9	296.3	433000	0.02044
14	0.169	1196.8	1187.2	1185.6	1171.2	1154.8	1137.7	1120.6	1104.4	1086.4	1070.4	1047.8	296.7	369000	0.02067
15	0.143	1199.7	1192.7	1193.4	1183.0	1171.5	1159.0	1147.6	1136.5	1124.4	1114.0	1098.8	297.1	313000	0.02033
16	0.116	1199.0	1194.1	1196.7	1189.4	1182.1	1173.3	1167.0	1159.4	1152.0	1145.9	1136.3	297.3	253000	0.02020

APPENDIX B

FRICTION FACTOR MODELING

Factors need to be considered

As discussed earlier, for flat plates with circular HP, the f_f is affected by the following factors.

Plate geometry

h_φ and h_d affect f_f. There is not enough data available to include h_φ as one of the functions to model f_f (Kheireddin tested plates with 3.175 mm diameter holes and in the current case 12.15 mm diameter holes. Friction factor cannot be generalized with these data for hole diameter between these two values). So, f_f model will be established for plates of 12.15 mm diameter holes individually and it may not be considered for any other plate.

As seen, in the current tests with h_φ= 12.15 mm, h_d definitely affects the f_f, but its effect is not linear. Friction factor increases initially with increasing h_d and then decreases. So, it may not be appropriate to include h_d as a parameter. Hence, the modeling is established individually for each plate with distinct h_d.

Reynolds number

In flat-plate testing, *Re* is defined in terms of the mean axial velocity across the plates, U_m. The effect of *Re* follows either decreasing or being constant trend in any test performed with all the three plates. Hence friction factors dependence on *Re* can be modeled with a function.

Clearance

Clearance is the dominant factor in changing f_f, and among the tested clearances, the f_f increases with increasing C_{pl} in all the tested cases. Hence, C_{pl} would be one of the major parameters in modeling f_f.

Inlet pressure

Inlet pressure hardly affects the f_f. However for h_d = 2.9 mm, C_{pl} = 0.254 mm case, f_f with P_{in} = 56 bar was higher than tests with P_{in}= 70 bar and 84 bar. So, either inlet pressure can be included as a variable or the models can be established individually for each inlet pressure.

Existing models for friction factor

There have been attempts to model honeycomb annular gas or liquid seals in the past from experimental data. Most of the analyses, Childs [20], and Nelson [10] used a Blasius Model for f_f to be used in predicting the rotordynamic coefficients. The main models proposed are discussed below.

Blasius model

Blasius model is the customary model. Here, f_f is modeled only as a function of *Re*.

The model is,

$$f_f = n\,(Re)^m \tag{24}$$

Here, the definition of *Re* is $\mathrm{Re} = \dfrac{\rho\,(2C_{pl})\,U_m}{\mu}$

Where U_m is the mean flow velocity relative to the surface and C_{pl} is the film thickness. The two coefficients *n* and *m* are found empirically from experimental data.

Ha model

Ha's f_f model is based on his tests using flat-plates representing honeycomb HP. Ha's tests showed that the f_f is nearly constant or slightly increase as the *Re* increases, for the tests where friction-factor jump was not experienced.

Ha felt that f_f for the honeycomb surfaces had a better correlation with *M* than *Re*. Also, f_f was sensitive to change in clearance [14].

Ha's model is,

$$f_f = 1 + \frac{C_{pl}}{b}\left[\frac{c2}{\frac{P}{Pc}} + c3(M)^{c4}\right] \tag{26}$$

where, c1,c2,c3 and c4 are constants for each honeycomb geometry.

b = Honeycomb cell width (mm)

C_{pl} = clearance (mm)

P = Inlet pressure (bar)

P_c = Critical pressure of air (37.7 bar)

Even though, Ha had included seal geometry parameters in the model, the constants c1 to c4 had to be found individually for each geometry using experimental data.

For cases with friction-factor jump, Ha's model was

$$f_f = \text{c1} + \frac{c2}{(\frac{P}{Pc})} + \text{c3}\ (M) + \text{c4}\ (M)^2 + \text{c5}\ (M)^3 \quad (27)$$

Again, the constants c1 to c5 are determined on a case-to-case basis.

Childs and Fayolle model

In the discussion of the paper of liquid seals with a hole-patterned roughened stator, the authors [20] set out to develop a f_f model that would improve or reasonably predict the rotordynamic coefficients. Estimates of the stator (roughened surface) f_f were obtained from delta Pressure/ leakage rate data. A least square curve fit was used to calculate Blasius type coefficients for each clearance. The f_f model is

$$f_s = n_s\ (\text{C}_r)\ (\text{Re})^{\text{m}_s(\text{C}_r)} \quad (28)$$

The co-efficients n_s and m_s were then curve fit as quadratic functions of C_r using

$$n_s = \text{a0} + \text{a1}\ C_r + \text{a2}\ C_r^2 \quad (29)$$

$$m_s = \text{b0} + \text{b1}\ C_r + \text{b2}\ C_r^2 \quad (30)$$

where C_r is the radial clearance.

Expressing the coefficients as functions of the C_{pl} instead of keeping them constants greatly improved the prediction of the cross-coupled stiffness coefficient but only modestly improved predictions for the direct stiffness coefficient. No great change resulted for the direct and cross-coupled damping coefficients.

Models from current data

Blasius model

The Blasius model, $f_f = n\ (\mathrm{Re})^{m}$ is used in ISOTSEAL. Friction factor data at from each test is fit as a function of *Re*.

Figure 63 shows a typical curve fit.

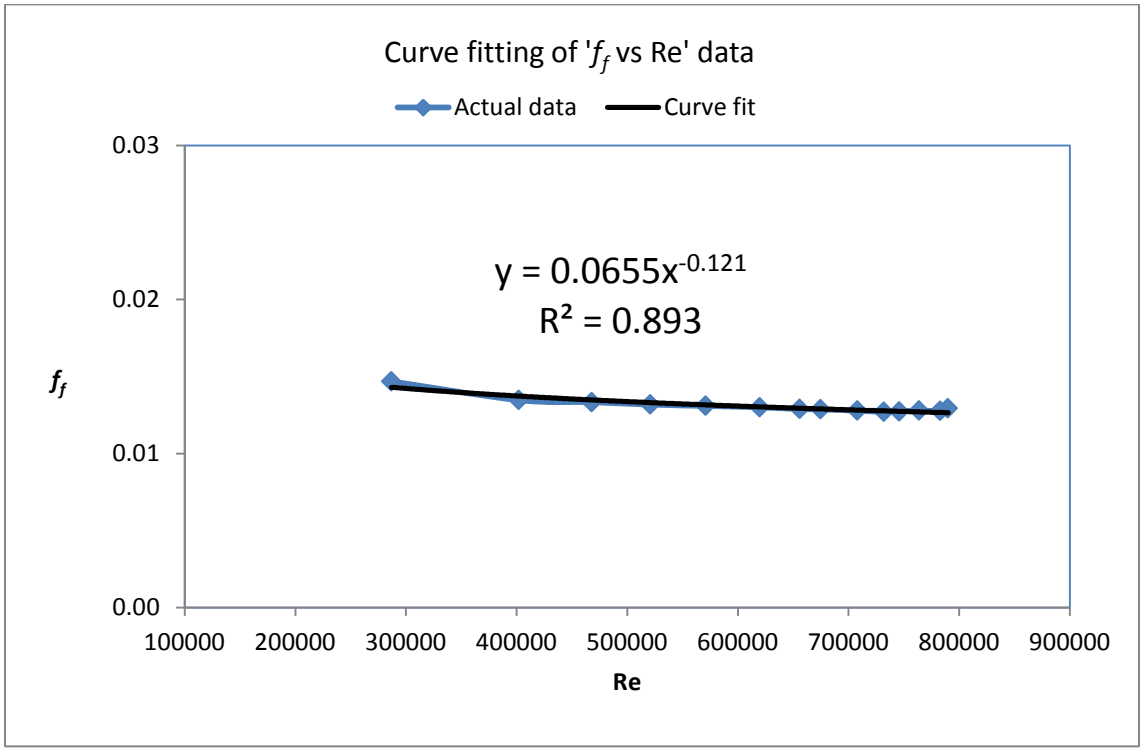

Figure 63. Curve fit of Blasius equation (h_d = 0.9 mm, C_{pl} = 0.254 mm, P_{in} = 84 bar)

Desired *m* and *n* values are given in Table 30-Table 32. As has been observed, f_f and hence *n* and *m* are strong functions of the clearance, *n* and *m* (at a particular inlet

pressure for a plate) are expressed as functions of the clearance, following Childs and Fayolle [20]. The relationship is as follows.

$$n = a + b\,C_{pl} + c\,C_{pl}^2 \quad (32)$$

$$m = d + e\,C_{pl} + f\,C_{pl}^2 \quad (33)$$

where C_{pl} is the clearance in mm.

Figure 64 shows a typical curve fit of n and m versus C_{pl}. The R^2 value for these graphs will be 1, as the quadratic curve fit always passes through all the three data points. Table 30-Table 32 present the coefficients n and m and their curve fit coefficients for the tested plates.

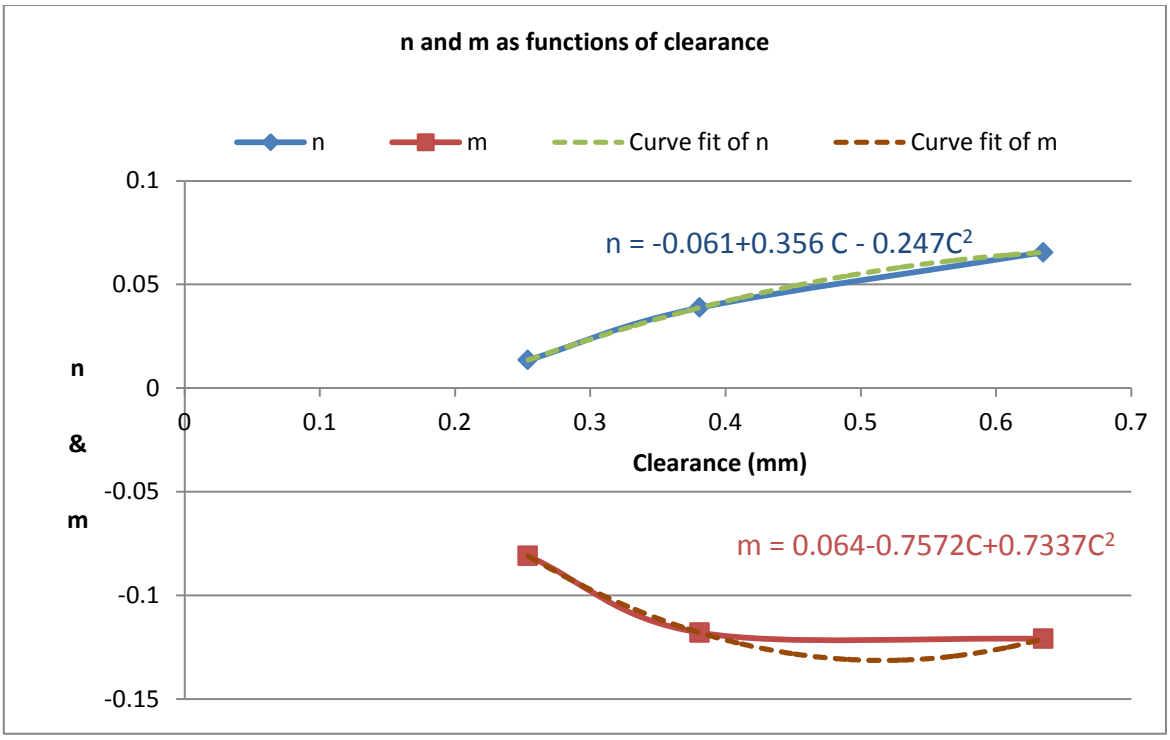

Figure 64. Expressing Blasius coefficients as functions of C_{pl}

(h_d = 0.9 mm, C_{pl} = 0.254 mm, P_{in} = 84 bar)

Table 30. Blasius coefficients for the plate with h_d = 0.9 mm

h_d (mm)	P_{in} (bar)	C_{pl} (mm)	Blasius coefficients $f_f = n*Re^m$			Coefficients for n $n = a + b\,C_{pl} + c\,C_{pl}^2$			Coefficients for $m = d + e\,C_{pl} + f\,C_{pl}^2$		
			R^2 value of regression	n	m	a	b	c	d	e	f
0.9	56	0.254	0.7661	0.043	-0.167	0.2277	-1.1175	1.5366	-0.598	2.3871	-2.7177
		0.381	0.8551	0.025	-0.083						
		0.635	0.987	0.1377	-0.178						
	70	0.254	0.1503	0.0088	-0.045	-0.0516	0.3076	-0.2749	0.14	-0.9934	1.0437
		0.381	0.8768	0.0257	-0.087						
		0.635	0.9166	0.0329	-0.07						
	84	0.254	0.5716	0.0135	-0.081	-0.061	0.356	-0.247	0.064	-0.7572	0.7337
		0.381	0.8935	0.0388	-0.118						
		0.635	0.893	0.0655	-0.121						

Table 31. Blasius coefficients for the plate with h_d = 1.9 mm

h_d (mm)	P_{in} (bar)	C_{pl} (mm)	Blasius coefficients $f_f = n*Re^m$			Coefficients for n $n = a + b\,C_{pl} + c\,C_{pl}^2$			Coefficients for $m = d + e\,C_{pl} + f\,C_{pl}^2$		
			R^2 value of regression	n	m	a	b	c	a	b	c
1.9	56	0.254	0.8264	0.0301	-0.124	0.004	0.0883	0.0568	-0.231	0.5656	-0.5683
		0.381	0.8824	0.0459	-0.098						
		0.635	0.6615	0.083	-0.101						
	70	0.254	0.9437	0.0337	-0.133	-0.0663	0.5717	-0.7006	-0.1036	-0.3346	0.8618
		0.381	0.9554	0.0498	-0.106						
		0.635	0.7773	0.0142	0.0314						
	84	0.254	0.7099	0.0204	-0.091	-0.0912	0.5234	-0.3307	0.026	-0.6155	0.6097
		0.381	0.9643	0.0602	-0.12						
		0.635	0.8782	0.1078	-0.119						

Table 32. Blasius coefficients for the plate with h_d = 2.9 mm

h_d (mm)	P_{in} (bar)	C_{pl} (mm)	Blasius coefficients $f_f = n*Re^m$			Coefficients for n $n = a + b\,C_{pl} + c\,C_{pl}^2$			Coefficients for $m = d + e\,C_{pl} + f\,C_{pl}^2$		
			R^2 value of regression	n	m	a	b	c	a	b	c
2.9	56	0.254	0.2751	0.0129	-0.063	0.013	-0.0012	0.0031	-0.1566	0.4199	-0.2025
		0.381	0.1829	0.013	-0.026						
		0.635	0.5039	0.0135	0.0284						
	70	0.254	0.8976	0.0014	0.0928	-0.0698	0.3822	-0.4009	0.7611	-3.6303	3.9339
		0.381	0.4595	0.0176	-0.051						
		0.635	0.9102	0.0112	0.0421						
	84	0.254	0.7339	0.0018	0.0694	-0.0896	0.479	-0.4691	0.72	-3.4953	3.6766
		0.381	0.5716	0.0248	-0.078						
		0.635	0.1658	0.0254	-0.017						

Custom model incorporating clearance, Reynolds number and inlet pressure

The previous model does not include inlet pressure as a parameter to model f_f. An attempt is made to model f_f as a function of *Re*, C_{pl} and P_{in}, fitting them simultaneously. As, there are three independent variables, simultaneous fitting with them will be cumbersome and hence they are reduced into two variables.

One variable is formed combining C_{pl} and P_{in} as, $C_{pl} - \frac{P_{in}}{1000 C_{pl}}$ and the other variable is *Re*. The surface fitting tool from Matlab is used to fit the data with the following equation of fit that gave the best fit.

$$f_f = \frac{[C1*(C_{pl} - \frac{P_{in}}{10000C_{pl}})^2 + C2*(C_{pl} - \frac{P_{in}}{10000C_{pl}}) + C3]*[(\frac{Re}{10^5})^{(C4*(Cpl-\frac{Pin}{10000Cpl})^2 + C5*(Cpl-\frac{Pin}{10000Cpl}) + C6)}]}{1000} \quad (33)$$

C_{pl} is the clearance in mm

P_{in} is the inlet pressure in bar

C1, C2, C3 and C4 are coefficients particular to a plate

Figure 65 below shows a typical fit in Matlab® with surface fit tool.

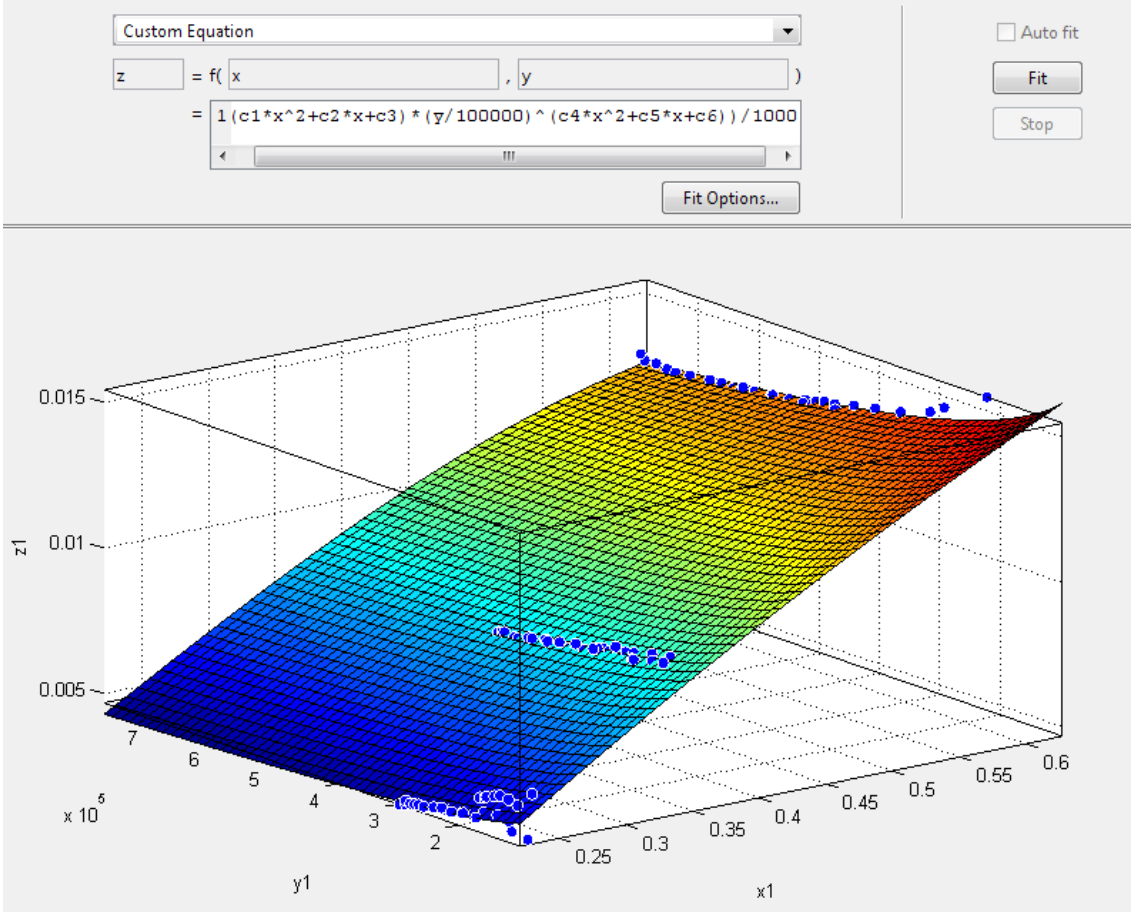

Figure 65.Typical curve fit for f_f vs. C_{pl}, Re, and P_{in}

Table 33 presents the coefficients C1 to C6 for the three plates with the regression measures R^2 and SSE (Error Sum of Squares)

Table 33.Coefficients C1, C2, C3, C4 , C5, C6 and measures of fit for the custom f_f model

h_d (mm)	Coefficients of the curve fit						R^2	SSE
	C1	C2	C3	C4	C5	C6		
0.9	-11.27	35.84	-1.883	-0.7376	0.6172	-0.2164	0.9957	4.76E-06
1.9	-53.5	87.38	-10.02	1.077	-0.8801	0.08959	0.994	2.58E-05
2.9	10.22	24.18	-0.4132	-2.454	2.721	-0.7035	0.9953	2.20E-05

The *Re* in equation is defined in terms of U_m as, $\mathrm{Re} = \frac{\rho (2\mathrm{H})\, \mathrm{U_m}}{\mu}$, where $\mathrm{U_m}$ is defined in terms of control volume axial and circumferential velocities as, $U_m = \sqrt{W^2 + U^2}$. Substituting all these in equation (33), the model for f_f is given by,

$$f_f = \frac{[C1*(C_{pl} - \frac{P_{in}}{10000C_{pl}})^2 + C2*(C_{pl} - \frac{P_{in}}{10000C_{pl}}) + C3]*[(\frac{\rho(2C_{pl})\sqrt{W^2+U^2}}{10^5\mu})^{(C4*(Cpl-\frac{Pin}{10000Cpl})^2 + C5*(Cpl-\frac{Pin}{10000Cpl}) + C6)}]}{1000} \quad (34)$$

Equations (33) is a model for f_f in terms of C_{pl}, *Re* and P_{in} and (34) is a model with *Re* replaced by the control volume velocities from equation (33).

Comparison of model data with the actual data

Test data is compared with the values obtained by the two curve fits.

Comparison is done for all the three plates in all the clearances with P_{in} = 84 bar. Figure 66 - Figure 68 compare the data for each plate.

From the graphs, it is seen that Blasius model fits better in most cases than the custom model and both the models fit the actual data reasonably well.

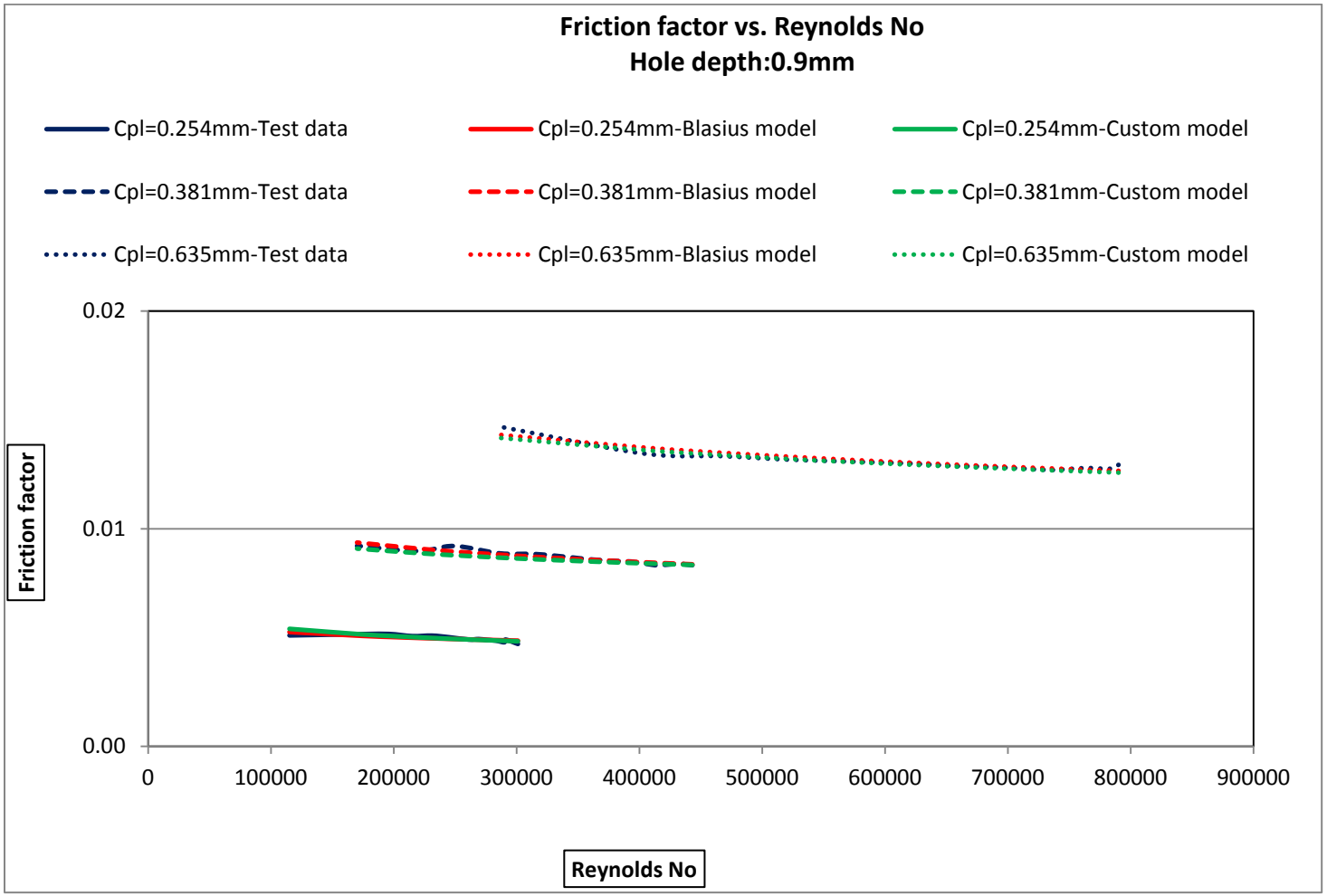

Figure 66. Comparison of model data with the actual data (h_d = 0.9 mm, P_{in} = 84 bar)

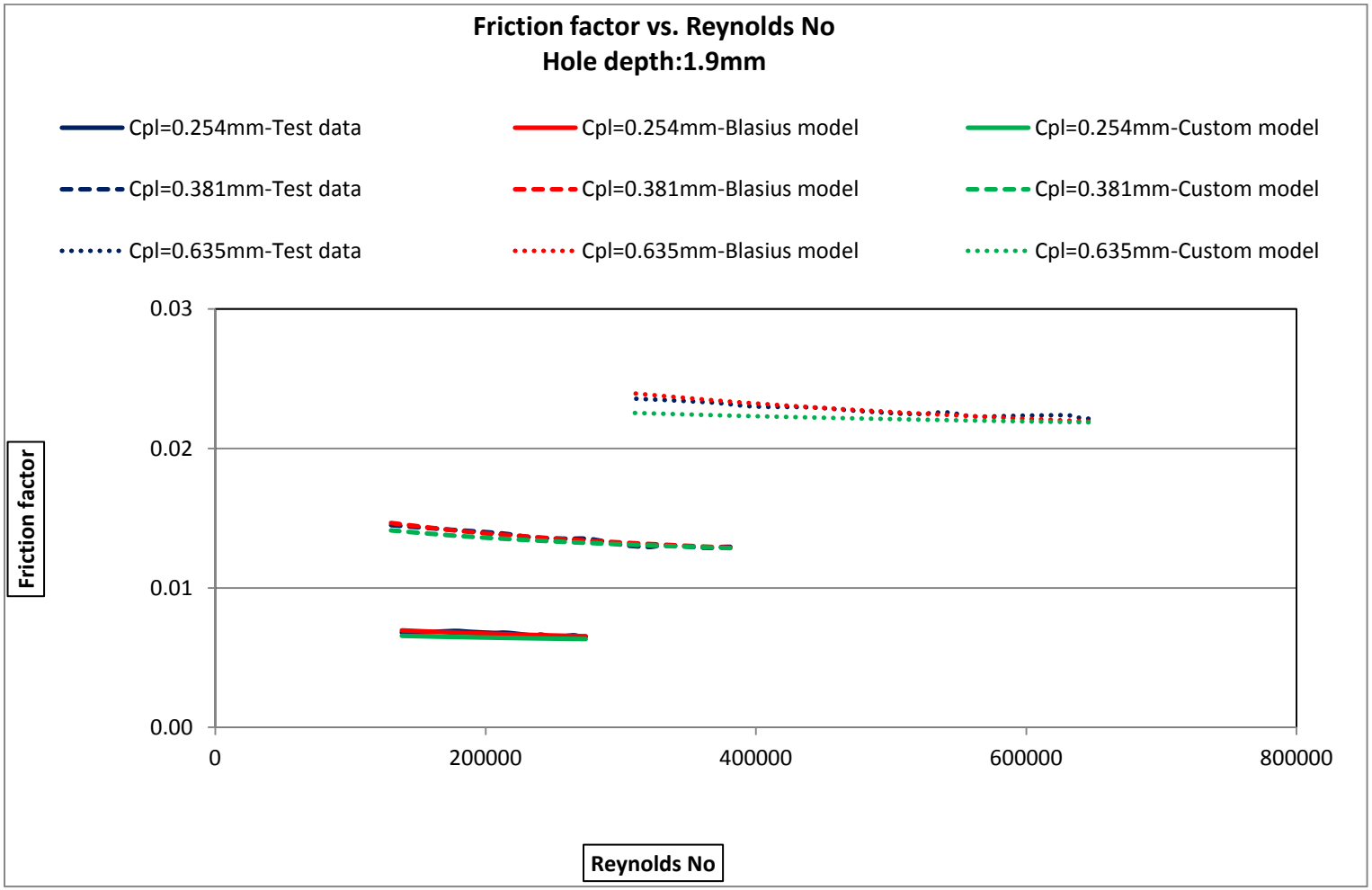

Figure 67. Comparison of model data with the actual data (h_d = 1.9 mm , P_{in} = 84 bar)

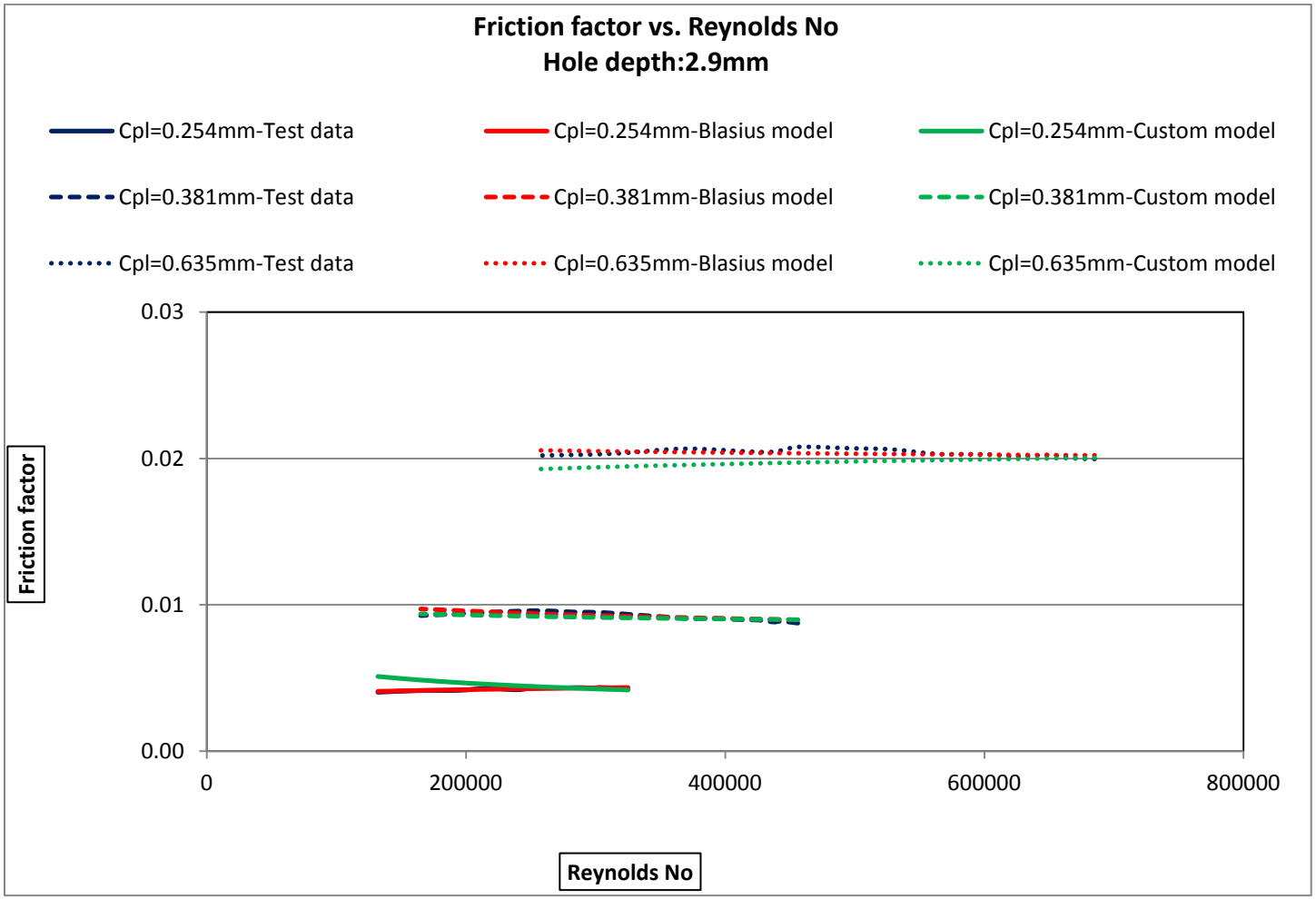

Figure 68. Comparison of model data with the actual data (h_d = 2.9 mm, P_{in} = 84 bar)

APPENDIX C

UNCERTAINTY ANALYSIS

The general uncertainty analysis is based on the method described by Coleman [27]. The uncertainty in a variable r which is a function of J variables is given by the following formula:

$$U_r = \left[\left(\frac{\partial r}{\partial X_1} U_{X_1}\right)^2 + \left(\frac{\partial r}{\partial X_2} U_{X_2}\right)^2 + \ldots \left(\frac{\partial r}{\partial X_J} U_{X_J}\right)^2 \right]^{\frac{1}{2}}$$

The calculations followed are referred from Kheireddin [22]. In the case of the Mach number in Equation (22), the primary variables are $\dot{m}, P, A$ and T_t. The uncertainties in these variables are 1.7 x 10^{-5} Kg/sec, 0.008 bar, 1.29 x 10^-6 m^2, and 1°K respectively.

Differentiating the Mach number with respect to each of the primary variables yields the following partial derivatives terms:

$$\frac{\partial M}{\partial P} = \frac{\frac{-1}{P}\left(\frac{\dot{m}}{PA}\right)^2 \left(\frac{RT_t}{\gamma}\right)}{M\sqrt{1+0.8\beta}}$$

$$\frac{\partial M}{\partial A} = \frac{\frac{-1}{A}\left(\frac{\dot{m}}{PA}\right)^2 \left(\frac{RT_t}{\gamma}\right)}{M\sqrt{1+0.8\beta}}$$

$$\frac{\partial M}{\partial \dot{m}} = \frac{\dot{m}\left(\frac{\dot{m}}{PA}\right)^2 \left(\frac{RT_t}{\gamma}\right)}{M\sqrt{1+0.8\beta}}$$

$$\frac{\partial M}{\partial T_t} = \frac{(\frac{\dot{m}}{PA})^2(\frac{R}{\gamma})}{2M\sqrt{1+0.8\beta}}$$

Where $\beta = \left(\frac{\dot{m}}{PA}\right)^2\left(\frac{RT_t}{\gamma}\right)$

Differentiating the f_f with respect to the primary variables in Equation (23) yields the following partial derivatives.

$$\frac{\partial f_f}{\partial H} = \frac{4(1-M^2)}{\alpha}\frac{dM}{dx}$$

$$\frac{\partial f_f}{\partial (dx)} = \frac{-4H(1-M^2)}{\alpha}\frac{dM}{(dx)^2}$$

$$\frac{\partial f_f}{\partial M} = \frac{8C_P(3M^4\gamma - 3M^4 - 5M^2\gamma + 7M^2 - 6)}{M^4\gamma(M^2\gamma - M^2 + 2)^2}\frac{dM}{dx}$$

Where $\alpha = 1.4M^3(1+0.2M^2)$

The estimated maximum uncertainty in f_f is 2.5%.

APPENDIX D

FRICTION FACTOR UPSET

Friction-factor upset is an undesirable phenomenon encountered during the course of testing. This section describes the phenomenon and how it created discrepancies in the measurement; also the procedure for eliminating the problem is described.

Forward process

Forward process is defined as, test done by increasing the pressure difference across the plate (ΔP) from minimum to maximum.

Reverse process

Reverse process is defined as, test done by decreasing ΔP from maximum to minimum.

Friction factor upset

In the initial stages of this test program using high pressure air, a strange flow behavior was met that made the readings non-repeatable and unreliable. The phenomenon was characterized by a sudden rise in $\dot{q}$ while reducing ΔP in case of a reverse process, or a sudden fall in $\dot{q}$ while increasing ΔP in case of a forward process. Kheireddin [22] observed that this upset occurred only for the forward process, and all his data were recorded using the reverse process. Subsequently, after the rig was moved internally to a different location, this behavior was observed in both forward and reverse methods, and it became impossible to establish repeatable data for any plate

configuration over the entire *Re* range. Friction factor-upset is explained in detail below with a particular test case. This behavior is different from Ha's friction-factor jump, which is a repeatable characteristic of a configuration where f_f increases suddenly with increasing *Re*.

Test with a HP plate with hole diameter of 3.175 mm, hole depth of 0.9 mm at a clearance of 0.254 mm at an inlet pressure of 84 bar with reveres process

A plate with h_φ = 3.175 mm, h_d = 0.9 mm (other than the three mentioned in this document) was used to analyze the friction-factor upset phenomenon.

For a test P_{in} = 84 bar, an inlet pressure of 84 bar will be maintained using the inlet valves with the exit valve completely open representing the maximum ΔP condition and then the exit valve will be closed step by step (usually this step will be around 50 psi~3.5 bar) thereby reducing the ΔP till a minimum value of ΔP is achieved. At each step, data will be recorded and the f_f will be calculated.

Figure 49 shows $\dot{m}$ versus ΔP for an initial test with the above configuration. Note that, at a ΔP~ 15 bar, there is a sudden jump in $\dot{m}$ that causes the f_f to drop. Figure 70 shows this drop in f_f. Figure 71 shows this upset versus *Re*. As seen, after the increase, then again $\dot{m}$ starts reducing for further reductions in ΔP. This sudden rise in $\dot{m}$ makes the *Re* increase and the f_f drop, thereby making a different series of data as seen in Figure 71 (a top series in the f_f range of about 0.017 and a series around 0.005). Hence two different f_f values are predicted for two close Reynolds numbers.

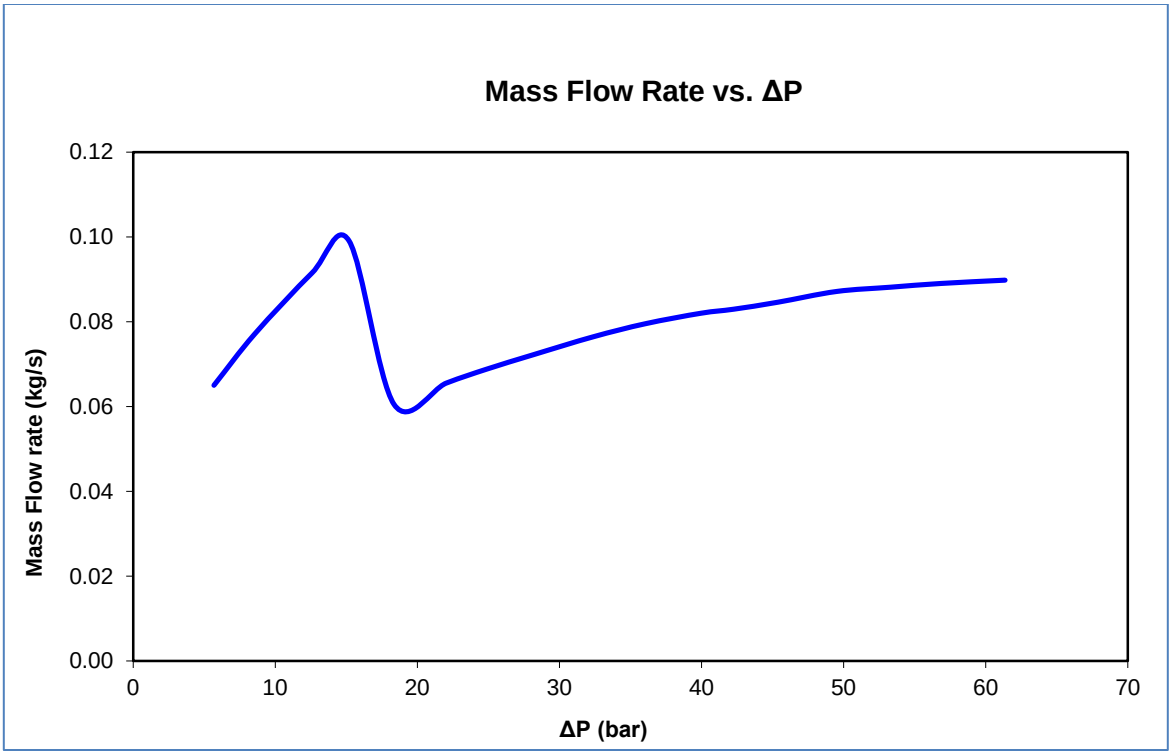

Figure 69. Mass flow rate vs. delta pressure, showing upset in the reverse process (C_{pl} = 0.254 mm, P_{in} = 84 bar)

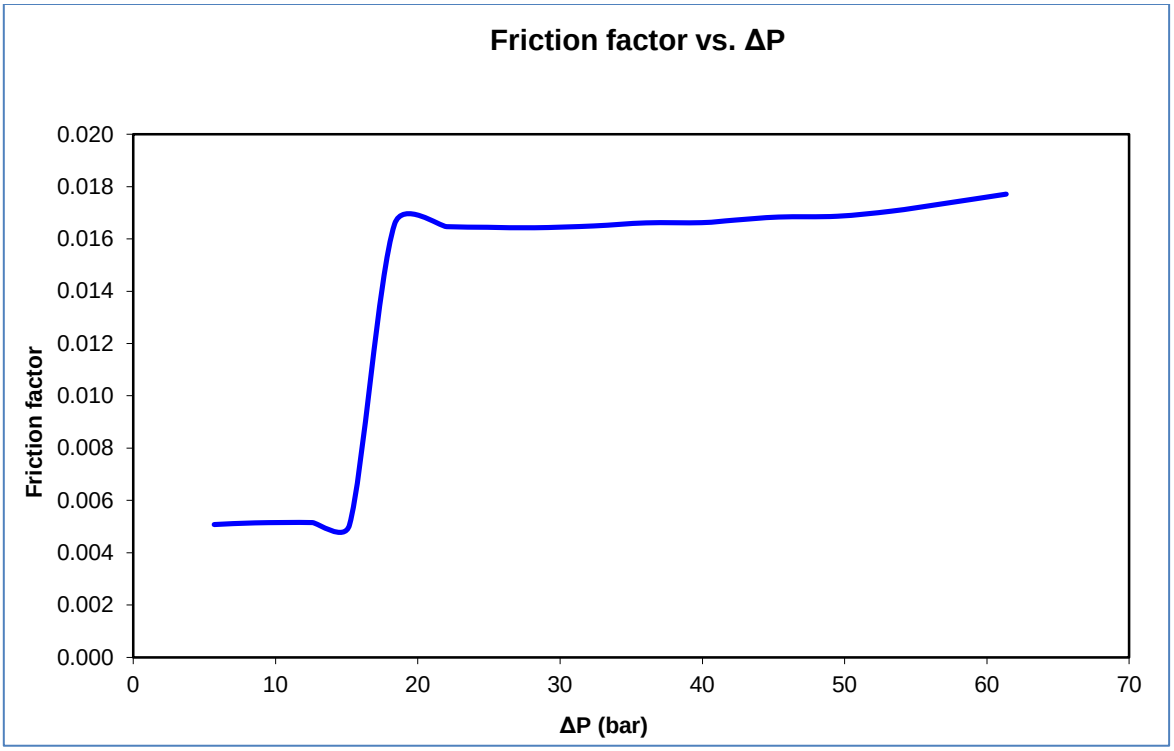

Figure 70. Friction factor vs. delta pressure, showing upset in the reverse process (C_{pl} = 0.254 mm, P_{in} = 84 bar)

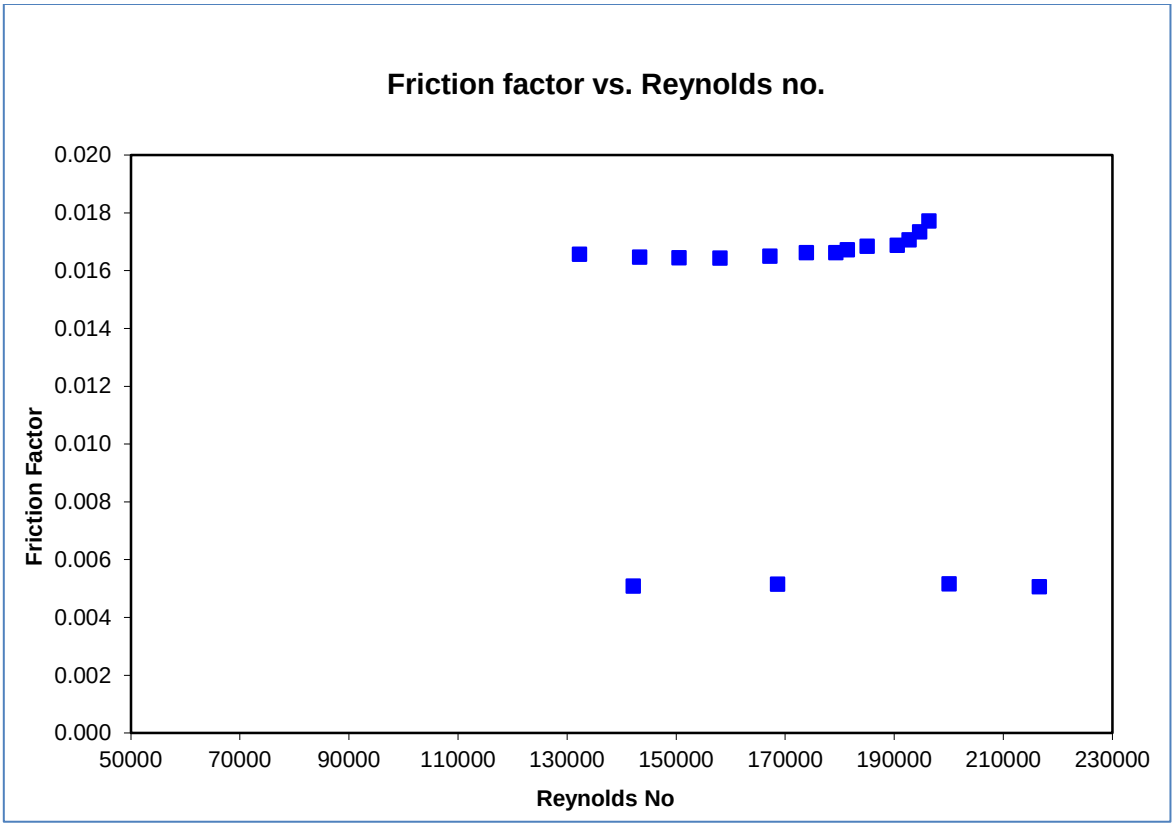

Figure 71. Friction factor vs. Reynolds No, showing upset in the reverse process (C_{pl} = 0.254 mm, P_{in} = 84 bar)

Observations

Friction-factor upset was initially believed to be caused by any flow discrepancy in the test section, like choking of flow at the exit or excitation of any cavity flow related frequencies, etc. Later observations showed that the upset-point was not repeatable for a same configuration. Each time while repeating the same test, the upset-point moved forward, backward or sometimes did not even occur at all giving a single series of f_f values.

It was also observed that the person who is physically adjusting the control valves had a control on deciding the upset-point based on how fast or how slow they rotate the potentiometer of the current source to the control valves.

Through continuous tests and observations, it was confirmed that the upset was related the control valves or somewhere else in the system induced by the control valves. i.e. Some particular position of the opening of the valves (the throat area) was observed to cause this upset. During the course of the test, the back pressure valve will be closed in steps to increase the back pressure. This increase in back pressure will create an increase in the inlet pressure even without adjusting the inlet valve. Inlet valve has to be closed a little bit to reduce the inlet pressure value back to 84 bar. Therefore, during the course of the test, the exit valve also is closed and the inlet valve is also closed, but very slightly. The upset phenomenon was observed, if the inlet valve throat area reaches some minimum value. i.e. If the throat area of the inlet valve is not allowed to go below a certain value, the upset was not faced.

Therefore it became important to maintain a minimum throat area of the inlet valve throughout the test to avoid this upset. This could have been achieved by any one or combination of the following.

1. Arranging the stagnation pressure of the flow (the tank pressure at the source) to be not so larger than the test inlet pressure so that the inlet valve will be needed to be closed only a little bit initially while starting the test to adjust from the tank-pressure to the inlet pressure. This will help in maintaining the throat area larger throughout the test.

2. Adding another inlet valve in series, so that the tank pressure can be reduced in two steps to reach the inlet pressure which will ensure larger throat area of the inlet valves, even if the tank pressure is much higher than the required inlet pressure.

For the test with 84 bar (1200 psi), it was observed that, the tank pressure had to be between 1500-1300 psi to maintain an upset free testing. If the tank pressure exceeded 1500 psi, upset was expected and if the tank pressure goes down, it may not be able to complete the test at all ΔP values, as the pressure will not be enough to maintain required pressure values.

It was decided to employ another inlet control valve which can maintain upset free testing irrespective of the tank pressure, as having control on the tank pressure took lot of time for each test to be completed. The test was repeated with two control valves and the same plots as seen above are shown in Figure 72-Figure 74. The usage of two inlet valves ensured repeatable f_f values without any upset for any number of tests.

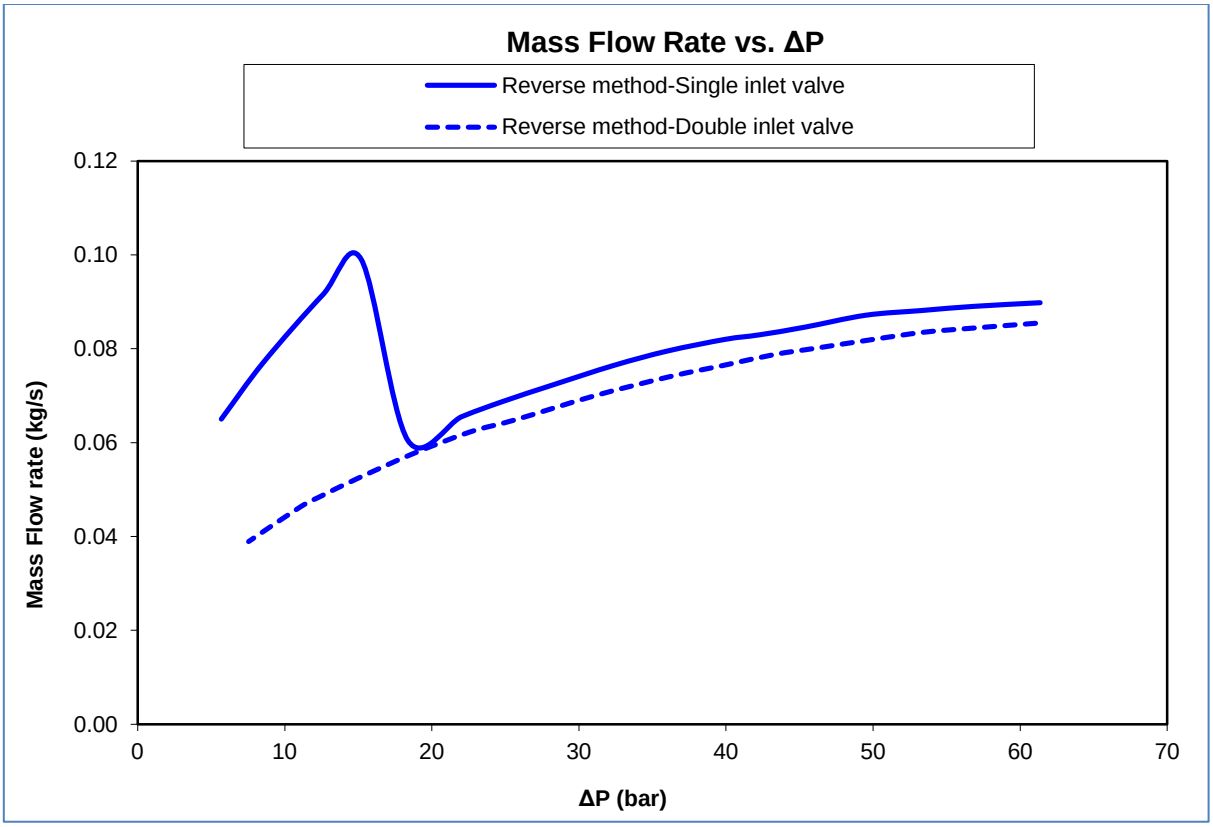

Figure 72. Mass flow rate vs. delta pressure, with and without upset in the reverse process (C_{pl} = 0.254 mm, P_{in} = 84 bar)

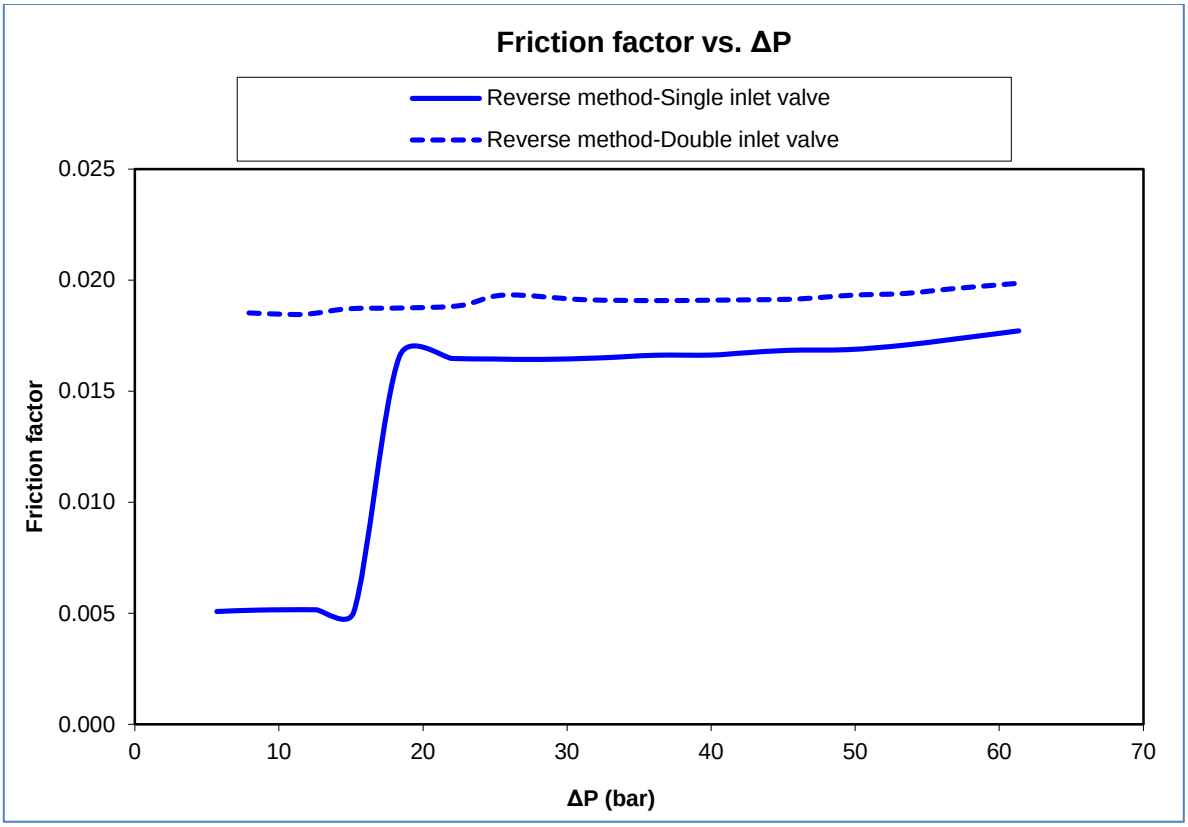

Figure 73. Friction factor vs. delta pressure, with and without upset in the reverse process (C_{pl} = 0.254 mm, P_{in} = 84 bar)

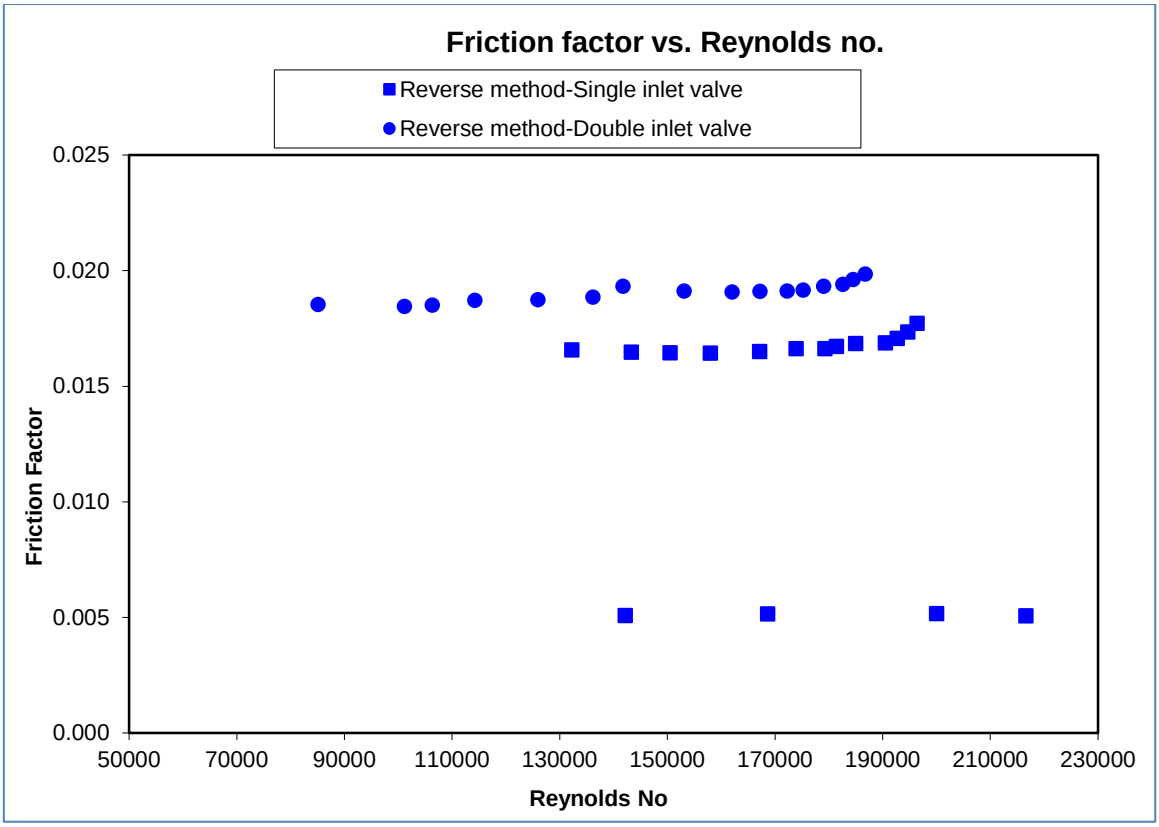

Figure 74. Friction factor vs. Reynolds No, with and without upset in the reverse process (C_{pl} = 0.254 mm, P_{in} = 84 bar)

Test with forward process

While doing the test with the same configuration in the forward process with a single inlet valve, it showed multiple upsets in a single test. Figure 75-Figure 77 show the plots of f_f values obtained in forward method as well as reverse process using a single inlet valve.

This multiple upset was also solved and repeatable readings could be taken with the double inlet valve. i.e. With the two inlet valves, irrespective of the method followed,

repeatable, upset free data could be taken and forward and reverse processes yield the same results (as one normally would expect). Figure 78-Figure 80 show the test results with two inlet valves.

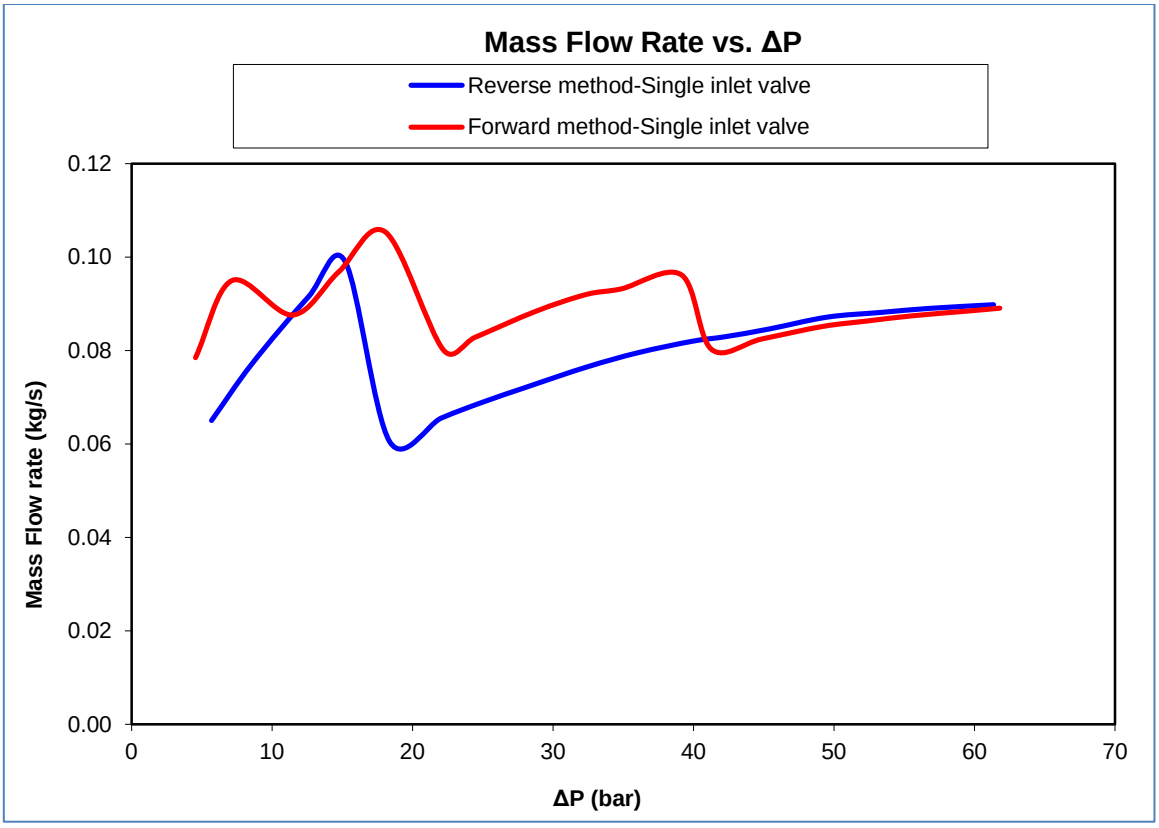

Figure 75. Mass flow rate vs. delta pressure, showing upset in forward and reverse processes (C_{pl} = 0.254 mm, P_{in} = 84 bar)

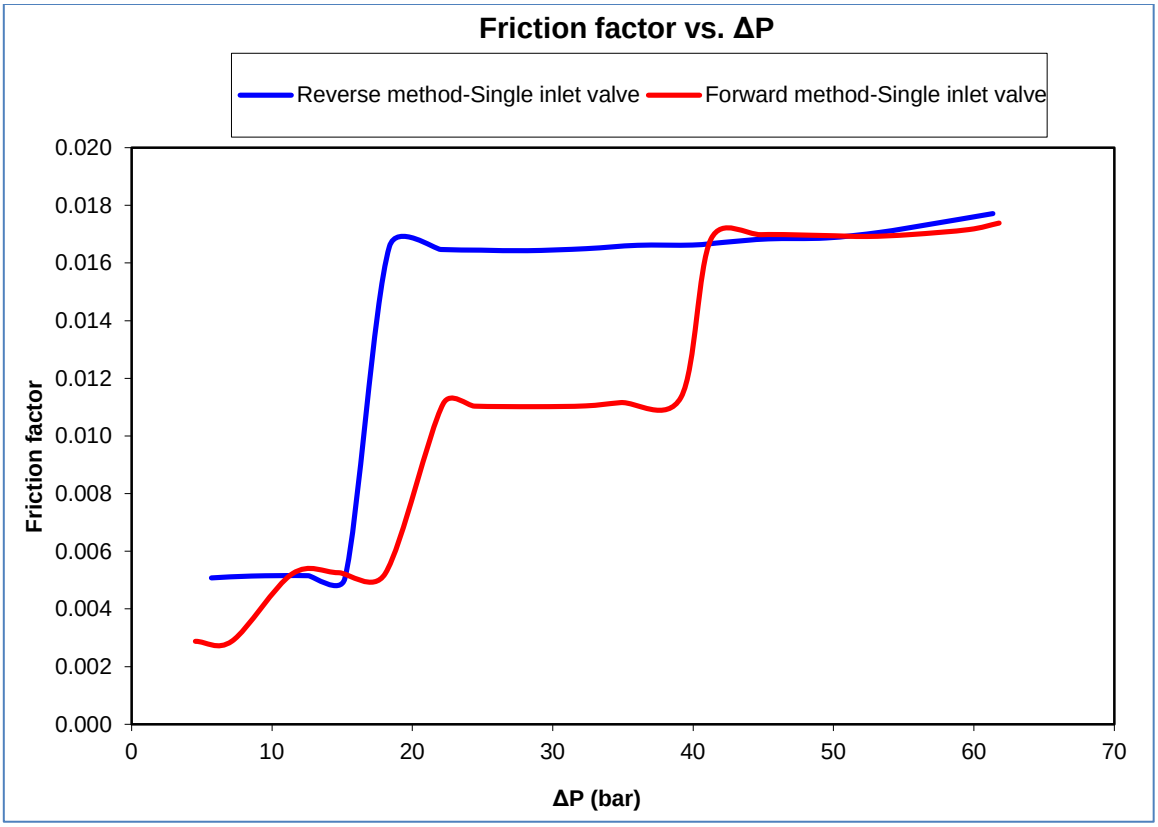

Figure 76. Friction factor vs. delta pressure, showing upset in forward and reverse processes (C_{pl} = 0.254 mm, P_{in} = 84 bar)

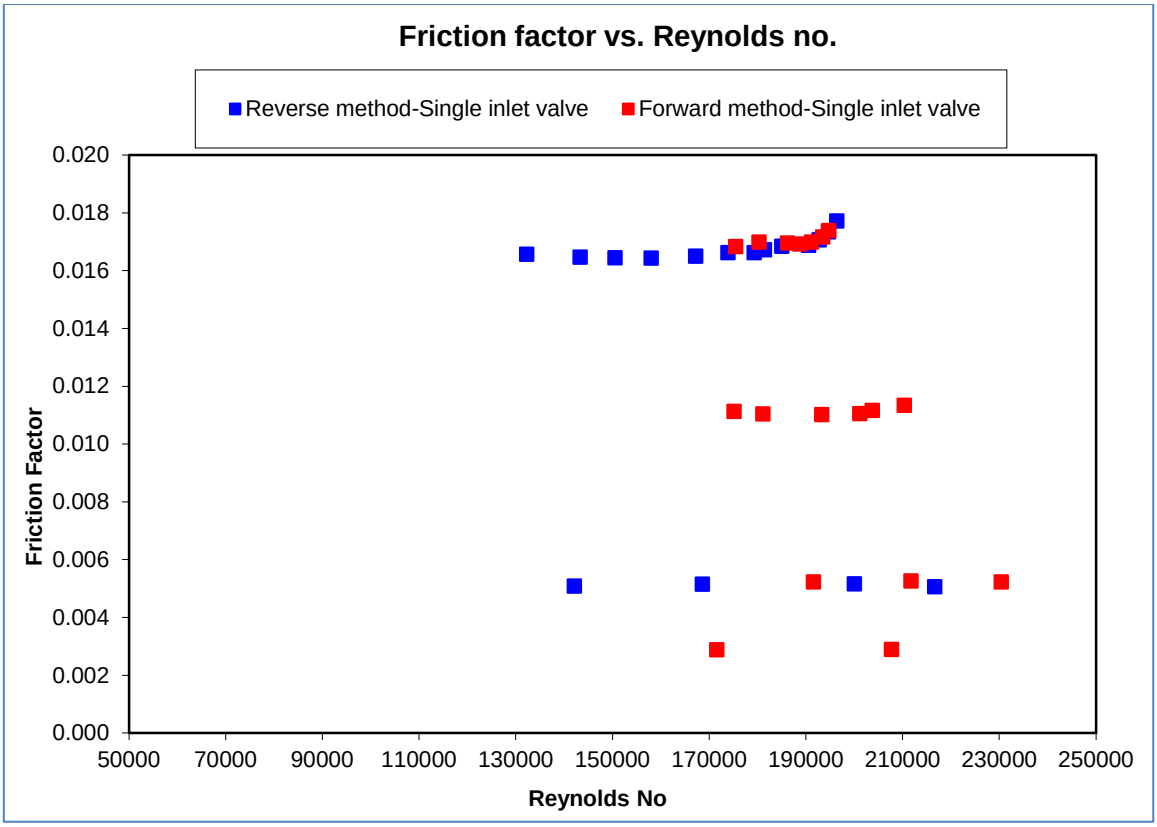

Figure 77. Friction factor vs. Reynolds No, showing upset in forward and reverse processes (C_{pl} = 0.254 mm, P_{in} = 84 bar)

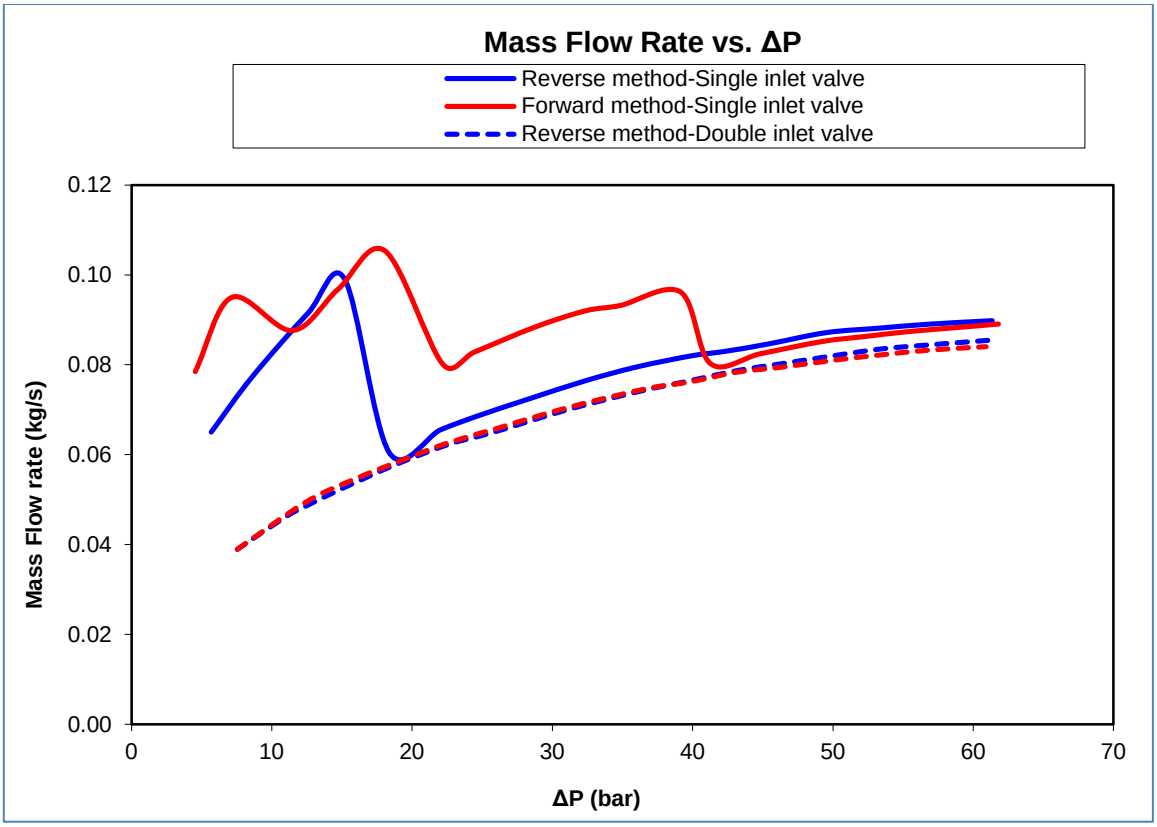

Figure 78. Mass flow rate vs. delta pressure, with and without upset in forward and reverse processes (C_{pl} = 0.254 mm, P_{in} = 84 bar)

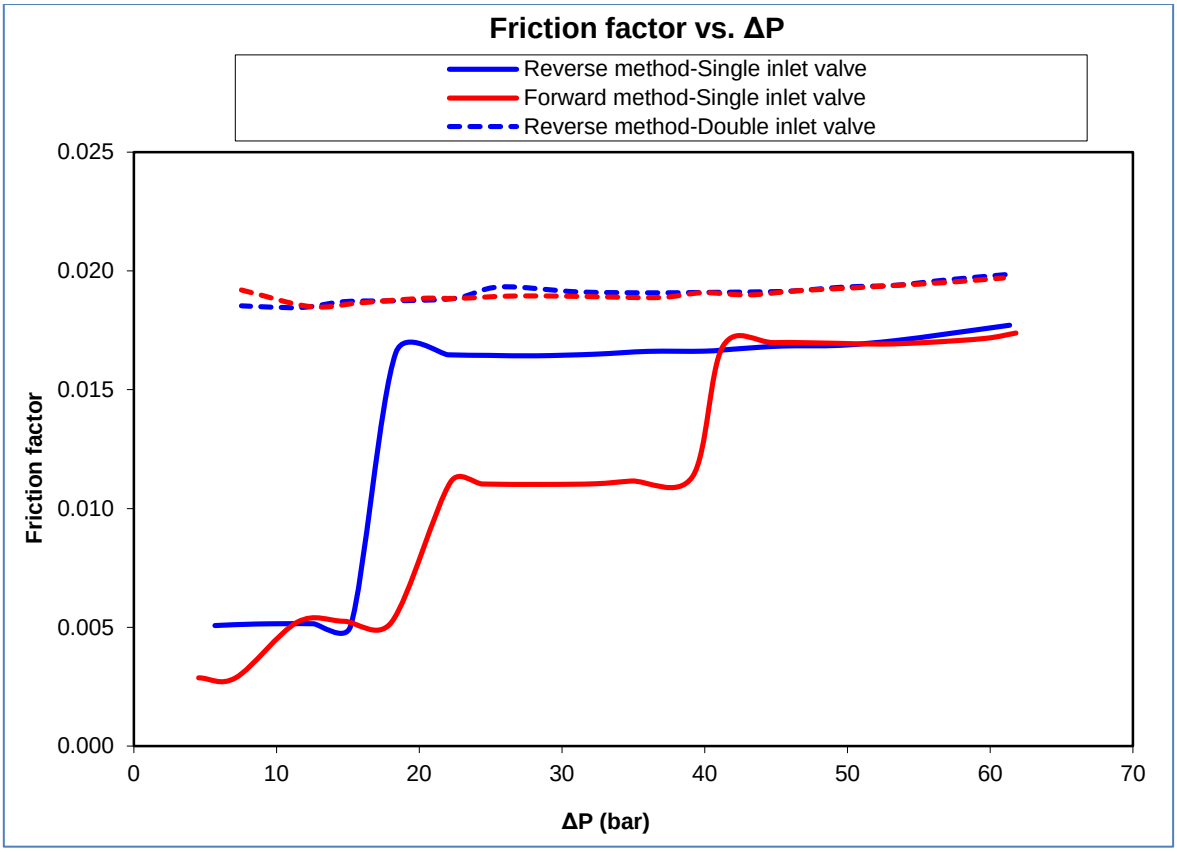

Figure 79. Friction factor vs. delta pressure, with and without upset in forward and reverse processes (C_{pl} = 0.254 mm, P_{in} = 84 bar)

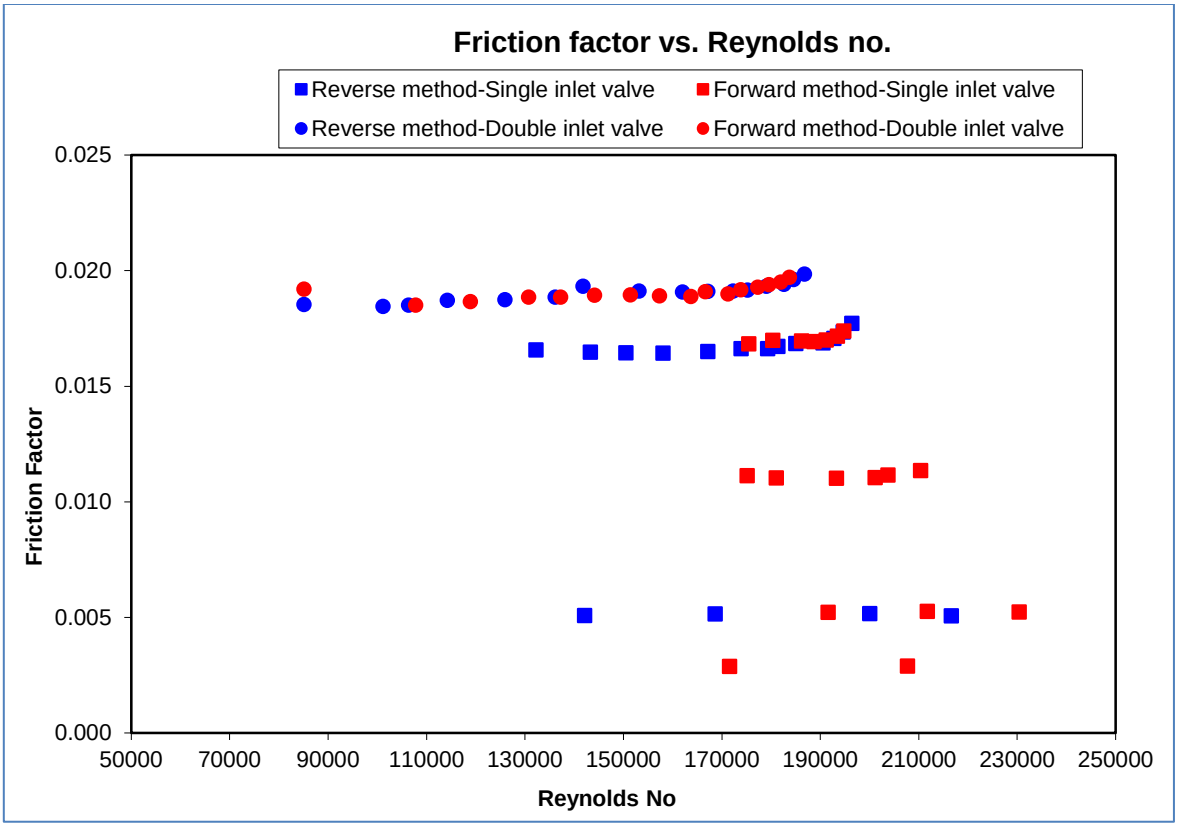

Figure 80. Friction factor vs. Reynolds No, with and without upset in forward and reverse processes (C_{pl} = 0.254 mm, P_{in} = 84 bar)

Test at other inlet pressures

Tests done at other inlet pressures also showed the upset behavior with the single inlet valve and upset free readings in double inlet valve methods. A new observation in 56 bar test was that, there would be a possibility of the upset to occur even at the very first reading of the test.(Because in 56 bar test, the pressure drop across the inlet valve is very high and even at the start of the test, the throat will be smaller in area that might cause the upset even in the very early stages of the test, even at the first point).In these

tests, one might say by seeing the graph that there is no upset as seen, but actually there was an upset which is not visible. With the two valves installed, even this problem was solved and repeatable readings were ensured. Figure 81 and Figure 82 show test results at 70 and 56 bar with single inlet valve as well as double inlet valve.

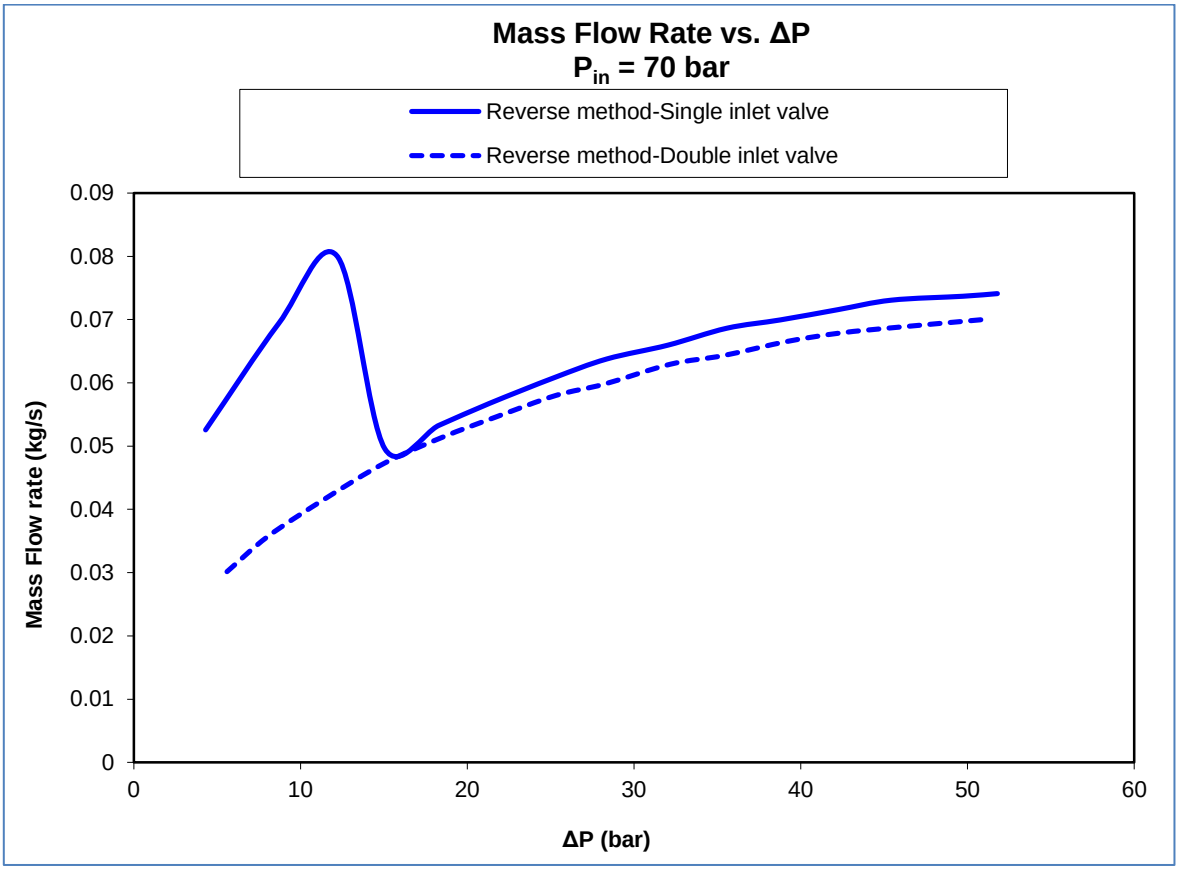

Figure 81. Mass flow rate vs. delta pressure, with and without upset in the reverse process (C_{pl} = 0.254 mm, P_{in} = 70 bar)

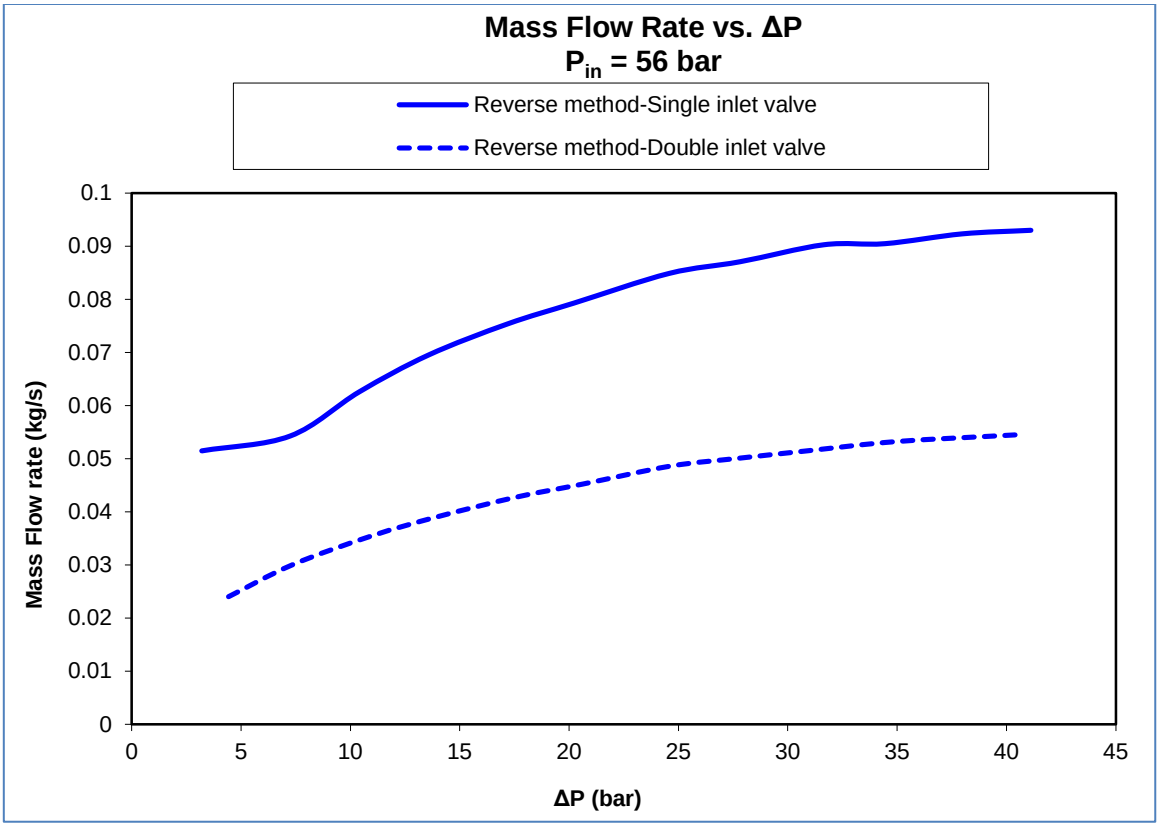

Figure 82. Mass flow rate vs. delta pressure, with and without upset in the reverse process (C_{pl} = 0.254 mm, P_{in} = 56 bar)

Through this double valve method, proper data could be taken with all the plates. Irrespective of the process, either forward or reverse, same data were obtained. The data presented in this report correspond to the readings taken by reverse process.

VITA

Name:	Thanesh Deva Asirvatham
Education:	B.E. in Mechanical Engineering (with Distinction) Government College of Technology, Coimbatore, India *May 2004* M.S. in Mechanical Engineering Texas A&M University, College Station, USA *December 2010*
Work experience:	Brakes India Ltd, Chennai, India from *May 2004* to *April 2007* Product development related to NVH (Noise, Vibration and Harshness) of automobile braking system Tata Motors Ltd, Pune, India from *May 2007* to *July 2008* NVH refinement of passenger cars
To contact:	2/110, Middle Street, Jacobpuram & Post, Tirunelveli District, Tamilnadu, India. Pin Code-627114 Email: thaneshda@gmail.com